# THE MAXIMUM SIGNIFICANT WAVE HEIGHT IN THE SOUTHERN NORTH SEA

FINAL REPORT

Report No. 14 - 94

February 1995

**Commissioned by Rijkswaterstaat**

**Work carried out by :**


| | | |
|---|---|---|
| *Delft University of Technology (DUT)* | : | L.H. Holthuijsen<br>Y. Eldeberky<br>N. Booij<br>P. Ferier |

**Assisted by :**

| | | |
|---|---|---|
| *Royal Netherlands Meteorological Institute (KNMI)* | : | E. Bouws |
| *National Oceanic and Atmospheric Administration (NOAA, USA), University Corporation for Atmospheric Research (UCAR)* | : | H.L. Tolman |

## Summary

The maximum possible wave conditions along the Dutch coast, which seem to be dominated by the limited water depth, have been estimated in the present study with numerical simulations.

These wave conditions are controlled by the physical regime of the air-sea interface and the sea-bottom interface. Both are not well known in limiting conditions in the sense of maximum wave generation. The present study has used state-of-the-art information to estimate these wave conditions, supplemented with an uncertainty analysis.

The computations to estimate the wave conditions have been carried out with the third-generation wave model WAVEWATCH-II (this implies that the wave spectrum evolves without a priori constraints). This type of model represents the state-of-the-art in wave modelling which has been shown elsewhere to accurately compute wave conditions in deep water hurricane conditions. It has been extended to shallow water by incorporating depth induced breaking in the shallow regions of the southern North Sea. The available freedom in the state-of-the-art formulations of the physical processes has been investigated and those formulations have been chosen that maximize the generation of the waves and minimize the dissipation of the waves partly based on a calibration in two historic storms. The uncertainty of the coefficients of these chosen formulations determines the uncertainty of the computed maximum significant wave height in the southern North Sea. This uncertainty appears to be about 5% upwards and 25% downwards. The model has been verified and calibrated against observations in two historic storms (Dec 1990 and Feb 1993). The results of the calibrated model are generally good (errors less than 10% in the significant wave height at the peak of the storm) except at one location (SON) where the error is 18%. The source of this error at SON is not clear. These storms were not sufficiently severe to verify shallow water wave dissipation, in particular depth induced wave breaking.

Discussions with meteorologists suggest that the maximum possible sustained wind speed in North Sea conditions is between 40 and 50 m/s (roughly equal to the wind speed in hurricanes but under different meteorological conditions). The extreme wave conditions in the southern North Sea have consequently been computed for a uniform wind field with a wind speed of 50 m/s. The results of a sensitivity analysis show that the results of these computations are not very sensitive for this choice of wind speed. The wave conditions in this uniform wind field (uniform 5 m storm surge assumed) are at a maximum for a wind direction of 330° N (i.e., from NNW). The significant wave height varies from 9.7 m at station BBR (near the Belgian border) and 14.2 m at station EUR. More information is available in tables and maps generated in this study. These values are approximately 25% higher than obtained with the second-generation wave model HISWA (default settings).

To verify that the computed extreme wave conditions in the southern North Sea for the uniform wind field are physically realizable (even if the generating uniform wind field is not), a large number of computations has also been carried out with the second-generation wave model DOLPHIN-B for synthetic, extreme but realistic storms (800 storms in which the wind speed does not exceed 50 m/s). It was found with an additional computation with the WAVEWATCH-II model that the maximum significant wave height in the most severe of these storms (a relatively small, intense storm with a slight overshoot in wind speed to 51.8 m/s due to the incremental nature of the search procedures) are almost identical to those computed with WAVEWATCH-II model in the uniform wind field of 50 m/s wind speed.

In the southern North sea (water depth less than 40 m), the ratio of significant wave height over local water depth, in the above extreme conditions is fairly constant and about 0.4. This ratio is maintained when a uniform storm surge is increased from 5 m to 6 m in the computations. The insensitivity of this ratio to variations in wind speed, wind field structure and storm surge level supports the notion that the maximum possible wave conditions in the southern North Sea are mainly controlled by the local water depth.

# CONTENTS

## List of tables

## List of figures

# 1. Introduction

This report describes the numerical modelling of maximum wave conditions along the Dutch coast. The study is carried out by the group of Hydraulic Engineering of the Delft University of Technology (DUT) assisted by the Royal Netherlands Meteorological Institute (KNMI) and the National Oceanic and Atmospheric Administration (NOAA, USA).

## 1.1 Background

The Directorate-General of Public Works and Water Management of the Netherlands (Rijkswaterstaat, RWS) is required by law to periodically review the design conditions and the safety of the dikes and dunes along the Dutch coast. Therefore, the National Institute for Coastal and Marine Management of Rijkswaterstaat (RIKZ) has set-up the HYDRA-project to provide the hydraulic input parameters for this safety analysis along the coast and the estuaries of the Netherlands. The present study is aimed at the assessment of maximum wave conditions along the Dutch coast.

These wave conditions are usually estimated by extrapolating historic data, either observed or hindcasted. Such extrapolations provide fair estimates of extreme conditions as long as the physical regime of the waves does not change dramatically from the observed (or hindcasted) conditions to the extrapolated conditions. In shelf seas this may be a serious problem. It certainly is in the southern North Sea where the water depth is typically between 20 m and 40 m. In extreme conditions this implies that the waves will always be affected by the limited water depth. In fact, at many locations in the shallower parts one may expect the maximum significant wave height to be determined mostly by the local water depth, while the wind speed as a limiting factor becomes less important. The southern North Sea is well provided with measured data, but the amount of data is too small to draw any firm conclusions on this matter. The present study attempts to establish, with a numerical wave model, whether there is a well-defined upper limit of the significant wave height due to the water depth in the southern North Sea and if so, at what level.

## 1.2 General approach

The significant wave height is generally limited by the physics in extreme conditions of the atmosphere and the sea. In the present study both are approached.

Discussions with meteorologists of the Royal Netherlands Meteorological Institute indicated that the maximum possible wind speed over the North Sea is not well established. From rather general arguments based on the energy balance of the atmospheric boundary layer one may be able to find such a maximum wind speed. The opinion of the meteorologists is that this maximum is between 40 and 50 m/s (10 m elevation sustained wind speed). In this study the value was then taken to be 50 m/s. The spatial extent of a wind field with 50 m/s wind speed was not discussed but in the present study an unrealistic storm has been taken (a uniform wind over the entire North Sea, which is physically not realizable) and a realistic storm (taken from an analysis of historic storms).

The physics of the waves are also not well established in such extreme conditions of 50 m/s wind speed. The only approach that can be taken is to use the state-of-the-art of wave modelling (third-generation wave model) and apply it in these conditions. Sensitivity studies

in the sense of exploring the freedom of the state-of-the-art provides the uncertainty of the wave conditions within this state-of-the-art. This may seem a weak basis for estimating extreme wave conditions but it should be pointed out that third-generation models have been successfully applied in hurricanes where the wind speed is of the same magnitude as in the present study. However, this does not cover shallow water conditions and these remain uncertain. This study does not contribute to the state-of-the-art of wave modelling but one shallow water effect (depth induced wave breaking) was added to the third-generation wave model that was used in this study (a commonly used formulation taken from surf zone wave models).

### 1.3 Methodology

The method employed is essentially to estimate the maximum possible significant wave height within the freedom of third-generation wave modelling and within the constraint of a maximum wind speed of 50 m/s.

The wave model that is used is the third-generation model WAVEWATCH-II (Tolman, 1991; a version of the WAM model (Hasselmann et al., 1988), with second-order accurate wave propagation and wave-current interactions). It is a discrete spectral model that explicitly accounts for refractive propagation, generation by wind, resonant four-wave interaction, whitecapping and bottom friction. Several options representing the physical processes of generation and dissipation are available, including the representations of the WAM model (as published, Hasselmann et al., 1988 and as presently operational at ECMWF, Reading, England). In the present study depth induced breaking was found to be important, even at depths of about 20 m. It was therefore added to the WAVEWATCH-II model (two options).

The methodology that was used in the present study is illustrated below in *Fig. 1*. The two basic questions (the existence and the level of an upper limit of $H_s$) are addressed as follows:

"Does a well defined upper limit exist?"
The significant wave height is generally limited by the atmospheric input and the dissipation of the waves. Maximizing the first and minimizing the second within realistic limits will produce the maximum significant wave height for a given wind field and bathymetry.

In addition to the wind speed itself, the atmospheric input is controlled essentially by the scale of the generating wind field (space and time, indicated as fetch and duration) and the wind speed. The spatial scale is obviously determined by the horizontal dimension of the North Sea. For the southern North Sea maximum generation condition are provided by a uniform wind field with northerly wind directions. This effect of the wind direction will be investigated explicitly in Chapter 4 (section 4.1.1). The time scale of the wind is typically of the order of a few days in the North Sea. But initially wave conditions will be estimated (to investigate the existence of an upper limit of $H_s$) for uniform wind fields and stationary conditions (infinite wind duration).

A uniform wind field with different wind speeds (20 to 60 m/s) and from different directions (Northerly) was therefore imposed over the entire North Sea. This showed the tendency of the significant wave height to approach a maximum and the insensitivity of the significant wave height for the wind speed around 50 m/s.

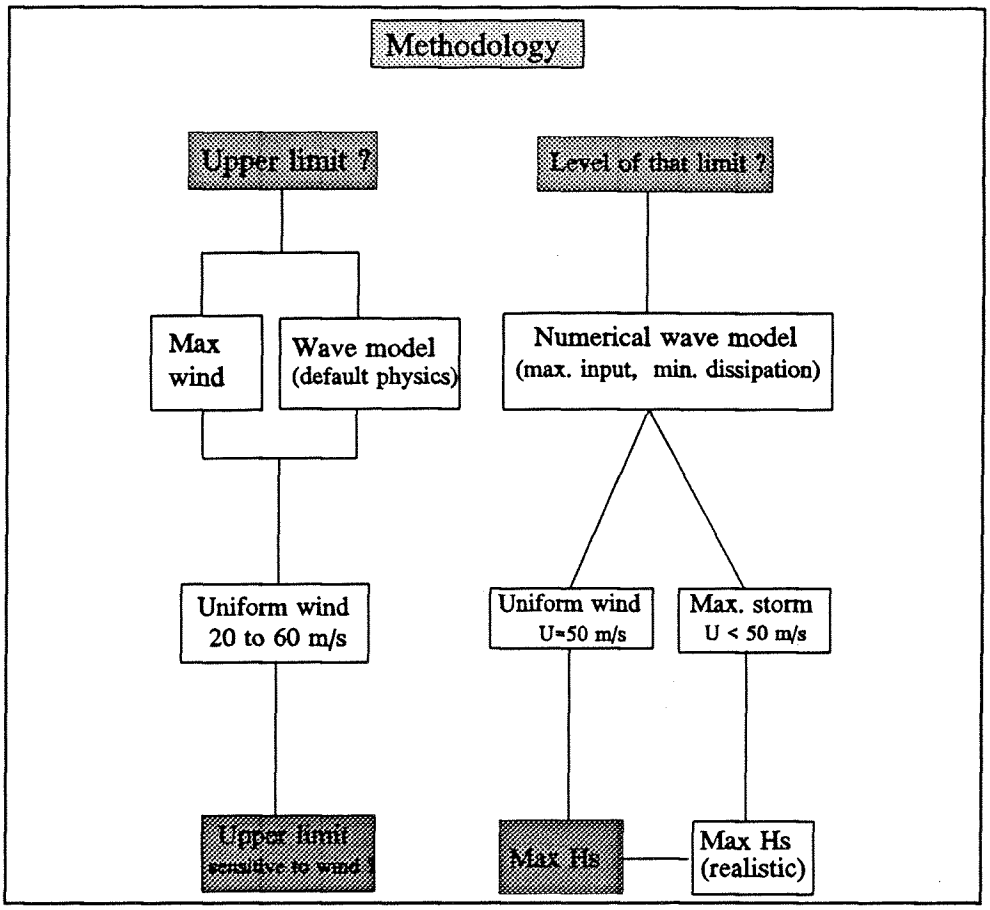


*Fig. I. The Methodology*

The conclusion of this first part of the study is that along the Dutch coast (water depth 25 m or less) the significant wave height practically levels off at wind speed of about 50 m/s.

"What is the level of the upper limit (if any)?"
The values of the significant wave height which were determined to answer the first question were computed with the WAVEWATCH-II wave model using default choices of the formulations to represent wave generation and dissipation (supplemented with a formulation for depth induced breaking). To further maximize the significant wave height, the generation was maximized and the dissipation was minimized within reasonable limits of the state-of the-art. This was done by individually and independently replacing each formulation by an alternative state-of-the-art formulation in the uniform wind field (50 m/s wind speed from 330° nautical direction) for wind sea generation and dissipation. A separate calibration was used to further minimize the dissipation. It turned out to result in dissipation that is normally applicable for swell conditions. The WAVEWATCH-II model was subsequently used with those formulations that each produced the maximum significant wave height (with the uniform wind speed of 50 m/s from 330° nautical with wind sea bottom friction and swell bottom friction separately).

A uniform wind field over the entire North Sea is not physically realizable. To investigate to what extent the results in the uniform wind field are realistic, an extreme storm that is consistent with historic storms was generated and used to obtain another estimate of the maximum significant wave height in the southern North Sea. The results of the maximum significant wave height thus obtained were almost identical to those in the uniform wind field.

The uncertainty of the computed significant wave heights within the chosen formulations of the wave model was estimated by using an error propagation technique based on realistic error ranges of the coefficients in the formulations of the physics in the model.

The credibility of the model results in extreme conditions has been investigated through verification of the WAVEWATCH-II model using two historic storms.

This report is arranged in the following way:

* The numerical wave model WAVEWATCH-II, is described in Chapter 2.
* The set-up of WAVEWATCH-II to perform computations in the North Sea is described in Chapter 3 (including bathymetry and computational grids).
* The numerical computations and the analysis to determine the maximum significant wave height is presented in Chapter 4.
* Chapter 5 describes the sensitivity and the uncertainty analysis, including the most important parameters in the formulations of wave physics in extreme wave conditions in the southern North Sea.
* Chapter 6 describes the validation and verification of the model through comparison with observations.
* Chapter 7 describes the model calibration.
* Finally the conclusions are given in Chapter 8.

It should be noted that this report summarizes the work done during the different phases of the project. Three progress reports describing these phases have been submitted to RIKZ. These are,

First phase : "The maximum significant wave height in the southern North Sea"
Expected values, Nov. 1993, Delft University Report, No. 7-93.
Second phase : "The maximum significant wave height in the southern North Sea"
Uncertainty analysis, May 1994, Delft University Report, No. 7-94.
Third phase : "The maximum significant wave height in the southern North Sea"
Validation study, Nov. 1994, Delft University Report, No. 13-94.

An additional report describing the parameterization of extreme storms is published. This is "Extreme parametric storms for waves in the southern North Sea", May 1994, Delft University Report, No. 8-93. Preliminary results have been presented at two international conferences. These are:
- Waves-Physical and Numerical Modelling, Vancouver, Aug. 1994.
- Coastal Engineering, Kobe, Oct. 1994.

# 2. Model Description

## 2.1 Introduction

This section describes the ocean wind wave model WAVEWATCH-II, Tolman (1991). The model features a third-generation approach to wave growth and decay, explicitly accounting for wind input, quadruplet wave-wave interactions and dissipation due to whitecapping and bottom friction. It furthermore incorporates effects of unsteady and inhomogeneous currents on ocean waves but this was not used in the present study. Depth induced breaking is not included in the model but as it seemed to be important in this study, it was added.

The following description is taken from the manual of WAVEWATCH-II (Tolman, 1992)

## 2.2 Governing equations

Wind waves propagating on a mean current **U** are generally described using energy or action density spectra. The wave components of such spectra in turn are defined by direction $\theta$, wave number $k$, absolute frequency $\omega$ (as observed in a fixed frame of reference) and relative frequency $\sigma$ (as observed in a frame of reference moving with the current **U**). If the current varies sufficiently slowly in time and space, the latter parameters are interrelated in the combined dispersion-Doppler relation

$$\sigma = (gk \tanh kd)^{1/2} = \omega - \mathbf{k}\cdot\mathbf{U} , \qquad (1)$$

where **k** is the wave-number vector with magnitude $k$ and direction $\theta$. The basic spectrum considered in WAVEWATCH-II is the action density spectrum $N(\omega,\theta,\phi,\lambda,t)$, which is directly related to the energy or variance density spectrum $F(\omega,\theta,\phi,\lambda,t)$ through, $N = F/\sigma$. This leads to the following basic equation to be solved (e.g., WAMDI group 1988, Tolman 1991):

$$\frac{\partial N}{\partial t} + (\cos\phi)^{-1}\frac{\partial}{\partial\phi}[c_\phi \cos\phi\ N] + \frac{\partial}{\partial\lambda}[c_\lambda N] + \frac{\partial}{\partial\omega}[c_\omega N] + \frac{\partial}{\partial\theta}[c_\theta N] = S \qquad (2)$$

in which $\phi$ is the latitude, $\lambda$ is the longitude and $t$ is the time and $S$ represents the net effect of all source terms for wave energy generation and dissipation. The first term at the left side of equation (2) represents the local rate of change of the energy density. The second and third terms describe propagation in latitude and longitude, respectively, the fourth term describes frequency shifts due to the unsteadiness of depth and current and the fifth term describes the change of wave direction, both due to great circle propagation and due to depth and current induced refraction.

It should be mentioned that in the WAVEWATCH-II model, a Cartesian definition of direction is used: $\theta$ is the direction in which the waves propagate, where $\theta=0°$ identifies wave propagating from west to east, and $\theta=90°$ identifies waves propagating from south to north. The output results, however, are given based on the oceanographic convention; $\theta$ is the direction from which the waves come, where $\theta=0°$ identifies waves propagating from north to south and $\theta=90°$ identifies waves propagating east to west.

$$c_\phi = \frac{d\phi}{dt} = \frac{c_g \cos\theta + U_\phi}{R}, \tag{3}$$

$$c_\lambda = \frac{d\lambda}{dt} = \frac{c_g \sin\theta + U_\lambda}{R\cos\phi}, \tag{4}$$

$$c_\omega = \frac{d\omega}{dt} = \frac{\partial\sigma}{\partial d}\frac{\partial d}{\partial t} + \mathbf{k}\cdot\frac{\partial \mathbf{U}}{\partial t}, \tag{5}$$

$$c_\theta = \frac{d\theta}{dt} = \frac{c_g \tan\phi \sin\theta}{R} - \frac{1}{k}\left[\frac{\partial\sigma}{\partial d}\frac{\partial d}{\partial m} + \mathbf{k}\cdot\frac{\partial \mathbf{U}}{\partial m}\right], \tag{6}$$

$$c_g = n\frac{\sigma}{k}, \quad n = \frac{1}{2} + \frac{kd}{\sinh 2kd}, \tag{7}$$

in which $m$ is a coordinate perpendicular to $\theta$. $R$ is the radius of the earth, $d$ is the local water depth, $c_g$ is the group velocity (direction $\theta$), and $c_\phi$, $c_\lambda$ and $c_\theta$ are the propagation velocities in the corresponding spaces. For brevity of notation, the dependence of $N$ and $S$ on $\omega$, $\theta$, $\phi$, $\lambda$ and $t$ has been omitted. Note that the action and energy density is given here as functions of longitude and latitude, and that they are defined as densities per unit ocean surface area.

The source term $S$ consists of a wind input $S_{in,l}$ (linear growth in time), a wind input $S_{in,e}$ (exponential growth in time), quadruplet nonlinear wave-wave interactions $S_{nl}$, energy dissipation due to whitecapping $S_{ds}$, energy dissipation due to bottom friction $S_{bot}$ and (added in this study) depth-induced wave breaking. For most of these source terms several optional formulations can be chosen by the user of the model and new formulations can easily be added. The available source term formulations will be discussed type-by-type below.

*Wind input (linear growth)*

The growth formulation of Cavaleri and Malanotte Rizzoli (1981) is available in the model, with or without a filter function $X$ to reduce the growth for frequencies lower than $f_{PM}$ (i.e., the equilibrium frequency for fully developed sea state according to Pierson and Moskowitz, 1964).

$$S_{in,l}(f_r,\theta) = 80\frac{2\pi}{ng^2}\left[\frac{\rho_a}{\rho_w}\right]^2\left\{U_* \max\left[0,\cos(\theta-\theta_w)\right]\right\}^4 X, \tag{8}$$

$$U_* = U_{10}\sqrt{(0.8+0.065U_{10})10^{-3}}, \tag{9}$$

$$X = \exp\left[-\left(\frac{f_r}{f_{PM}}\right)^{-4}\right] \quad , \quad f_{PM} = \frac{g}{28U_*} \quad , \tag{10}$$

where $\rho_a$ ($\rho_w$) is the density of air (water), $U_*$ is the wind friction velocity (Charnock 1955), $U_{10}$ is the wind speed at 10 m above the mean sea level and $\theta_w$ is the mean wind direction.

*Wind input (exponential growth)*

The first optional growth term for exponential growth is the slightly modified expression of Snyder et al. (1981), as used in the WAM model cycles 1 through 3 (WAMDI group 1988, Komen et al. 1984).

$$S_{in,e}(f_r,\theta) = 0.25\frac{\rho_a}{\rho_w}\max\left[0.,\left(\frac{28U_*}{c}\cos(\theta-\theta_w)-1\right)\right]\sigma\, F(f_r,\theta) \ , \tag{11}$$

The friction velocity $U_*$ in Eq. (11) is calculated using Eq. (9) and $c$ is the phase velocity $\sigma/k$.

The second option is the expression of Janssen (1991), cf. WAM cycle 4, which explicitly accounts for interactions between wind and waves. The source term is given as

$$S_{in,e}(f_r,\theta) = \beta\frac{\rho_a}{\rho_w}\left(\frac{U_*}{c}\right)^2\max[0,\cos(\theta-\theta_w)]^2\ \sigma\, F(f_r,\theta) \ , \tag{12}$$

where $\beta$ is the Miles constant, which is estimated from the nondimensional critical height $\lambda$.

$$\beta = \frac{1.2}{\kappa^2}\lambda\ln^4\lambda \ , \tag{13}$$

$$\lambda = \frac{gz_e}{c^2}e^{\kappa c/|U_*\cos(\theta-\theta_w)|} \ , \tag{14}$$

where $\kappa$ (= 0.4) is the Von Karman constant and $z_e$ is the effective surface roughness due to both wave stress $\tau_w$ and the turbulent stress $\tau_t$ ($\tau = \tau_w+\tau_t$ and, by definition, $U_*^2 = \tau/\rho_a$). The effective roughness length $z_e$, the turbulent roughness length $z_0$ and the corresponding wind profile $U(z)$ are given as

$$z_e = \frac{z_0}{\sqrt{1-\tau_w/\tau}} \ , \tag{15}$$

$$z_0 = 0.01 \frac{U_*^2}{g}, \tag{16}$$

$$U(z) = \frac{U_*}{\kappa} \ln\left(\frac{z+z_e-z_0}{z_e}\right), \tag{17}$$

Eq. (16) is a Charnock type relation, tuned to give correct stresses for old wind seas. Finally, the wave stress $\tau_w$ is calculated from the source term as

$$\tau_w = \rho_w \int_0^{\infty} \int_0^{2\pi} \sigma S(f_r,\theta)\, d\theta\, df_r . \tag{18}$$

In the wave model, the wind speed at $z$ = 10 m ($U_{10}$) and an approximately steady sea state $F(f_r,\theta)$ are given. Using this data, Eqs. (12) through (18) can be solved iteratively, using $U_*$ and $z_e$ from the previous time step or iteration. As in WAM cycle 4, the actual iteration is omitted here. This is allowed because wind and wave conditions are assumed to vary slowly compared to the model time steps.

*Quadruplet wave-wave interactions*

The quadruplet wave-wave interactions are modeled using the discrete interaction approximation of Hasselmann and Hasselmann (1985). In this approximation interactions are calculated only for the following type of quadruplets (i.e., sets of four spectral components which satisfy the resonance conditions):

$$\begin{aligned} \sigma_2 &= \sigma_1 \\ \sigma_3 &= (1+\lambda_{nl})\sigma_1 \\ \sigma_4 &= (1-\lambda_{nl})\sigma_1 \\ \boldsymbol{k}_4 &= \boldsymbol{k}_1 + \boldsymbol{k}_2 - \boldsymbol{k}_3 \end{aligned} \tag{19}$$

where $\lambda_{nl}$ is a constant equal to 0.25. For these quadruplets, the contribution $\delta S_{nl}$ to the interaction for each discrete frequency-direction combination of the spectrum corresponding to the central component of the quadruplet (i.e., component with suffix 1) is calculated as:

$$\begin{pmatrix} \delta S_{nl,1} \\ \delta S_{nl,3} \\ \delta S_{nl,4} \end{pmatrix} = D \begin{pmatrix} 2 \\ -1 \\ -1 \end{pmatrix} C\, g^{-4} f_{r,1}^{11} \left[ F_1^2 \left( \frac{F_3}{(1+\lambda_{nl})^4} + \frac{F_4}{(1-\lambda_{nl})^4} \right) - \frac{F_1 F_3 F_4}{(1-\lambda_{nl}^2)^4} \right], \tag{20}$$

where $F_1 = F(f_{r,1},\theta_1)$ etc. and $\delta S_{nl,1} = \delta S_{nl}(f_{r,1},\theta_1)$ etc. $C$ is a constant, where $Cg^{-4} = 3\times10^3$ ($s^{-8}m^4$) and $D$ is a scaling factor to account for shallow water effects:

$$D = 1 + \frac{5.5}{\bar{k}d}\left[1 - \frac{5\bar{k}d}{6}\right] e^{-1.25\bar{k}d} . \tag{21}$$

The overbar notation denotes straightforward averaging over the spectrum. For an arbitrary parameter $z$ the spectral average is given as:

$$\bar{z} = E^{-1} \int_0^{2\pi}\int_0^{\infty} z\, F(f_r,\theta)\, df_r\, d\theta \quad , \quad E = \int_0^{2\pi}\int_0^{\infty} F(f_r,\theta)\, df_r\, d\theta . \tag{22}$$

For numerical reasons, however, the mean normalized depth is estimated as

$$\bar{k}d = 0.75\hat{k}d , \tag{23}$$

where $\hat{k}$ is defined as in Eq. (26). The shallow water correction of Eq. (22) is valid for intermediate depths only. For this reason the mean relative depth $\bar{k}d$ is not allowed to become smaller than 0.5 (i.e., when the computed $\bar{k}d$ is smaller than 0.5 it is set to 0.5).

*Whitecapping*

Two options for the whitecapping formulation are available. The first is the expression of Komen et al. (1974), as used in the WAM model cycles 1 through 3 (WAMDI Group, 1988).

$$S_{ds}(f_r,\theta) = -2.33\cdot 10^{-5}\, \hat{\sigma}\, \frac{k}{\hat{k}} \left(\frac{\hat{\alpha}}{\hat{\alpha}_{PM}}\right)^2 F(f_r,\theta) , \tag{24}$$

$$\hat{\sigma} = \overline{\sigma^{-1}}^{-1} , \tag{25}$$

$$\hat{k} = \overline{1/\sqrt{k}}^{-2} , \tag{26}$$

$$\hat{\alpha} = E\, \hat{k}^2 g^{-2} , \tag{27}$$

The second formulation of the whitecapping source term is a modified version of Eq. (24), developed by Janssen (1991) for the use in combination with $S_{in}$ of Eq. (12) (WAM cycle 4).

$$S_{ds}(f_r,\theta) = -2.25\, \hat{\sigma}\, \hat{k}^4\, E^2 \left[\frac{k}{\hat{k}} + \left(\frac{k}{\hat{k}}\right)^2\right] F(f_r,\theta) . \tag{28}$$

*Bottom friction*

Three formulations for energy loss due to bottom friction are available. The first two are based on the JONSWAP parameterization (Hasselmann et al. 1973), as used in the WAM model (WAMDI group 1988).

$$S_{bot}(f_r,\theta) = 2\Gamma \frac{n-0.5}{gd} F(f_r,\theta) , \tag{29}$$

where $\Gamma$ is an empirical constant, which in the WAM model is taken to be as $\Gamma$ = -0.038 $m^2s^{-3}$ (Hasselmann et al. 1973, based on swell data). Also implemented is a version (second formulation) of Eq. (29) with $\Gamma$ = -0.067 $m^2s^{-3}$ as suggested by Bouws and Komen (1983) for wind seas.

The third formulation for bottom friction is that of Madsen et al. (1988).

$$S_{bot}(f_r,\theta) = -\frac{8}{3\pi} f_w u_{b,r} \frac{n-0.5}{d} F(f_r,\theta) , \tag{30}$$

where $f_w$ is a non-dimensional friction factor and $u_{b,r}$ is a representative near-bottom orbital velocity defined as

$$u_{b,r}^2 = 2 \int_0^{2\pi} \int_0^{\infty} \frac{\sigma^2}{\sinh^2 kd} F(f_r,\theta)\, df_r\, d\theta , \tag{31}$$

The friction factor $f_w$ is estimated as follows ($k_N$ is the bottom roughness length scale, which in the present study is set to 0.04 m and which seems to be a reasonable choice for the southern North Sea).

$$\frac{1}{4\sqrt{f_w}} + \log_{10}\left[\frac{1}{4\sqrt{f_w}}\right] = -0.08 + \log_{10}\left[\frac{a_{b,r}}{k_N}\right] , \tag{32}$$

$$a_{b,r}^2 = 2 \int_0^{2\pi} \int_0^{\infty} \frac{1}{\sinh^2 kd} F(f_r,\theta)\, df_r\, d\theta . \tag{33}$$

*Depth-induced breaking*

Two formulations have been added to WAVEWATCH-II to account for depth-induced breaking. These are Battjes and Janssen (1978) and Roelvink (1993). Both are formulated in terms of total rate of energy dissipation. They have been implemented in spectral form based on Eldeberky and Battjes (1995), where the energy dissipation due to wave breaking is distributed over the spectrum in proportion to the spectral energy density:

$$S_{db} = -\frac{\alpha}{4} f_m Q_b H_m^2 \frac{F(f_r,\theta)}{F(\theta)} \tag{34}$$

where $f_m$ is the mean frequency, $Q_b$ is the fraction of breaking waves, $H_m$ is the maximum wave height taken as the depth-limited maximum (the steepness-limited maximum of the Battjes and Janssen model is already accounted for in the whitecapping source term).

$$H_m = \gamma h \tag{35}$$

in which the values for $\gamma$ and $\alpha$ are 0.8 and 1 respectively.

In the formulation given by Roelvink (1993), the wave height distribution in the surf zone is assumed to be Weibull distribution which degenerates into Rayleigh in deep water. In a spectral form it follows equation (34), however the definition of fraction of breaking wave $Q_b$ is different from that of Battjes and Janssen model (for details refer to Roelvink, 1993) reference).

*Combination of source terms*

Some of the available formulations for the different source terms have to be used in combination (they have been tuned as such). This relates to the three "basic" source terms $S_{in,e}$, $S_{nl}$ and $S_{ds}$. The other source terms are essentially additional processes which are important in specific conditions only, i.e., in truly initial growth ($S_{in,i}$) or in shallow water ($S_{bot}$, $S_{db}$).

Recommended combinations of the three basic source terms are:
(i) $S_{in,e}$ from Eq. (11), $S_{nl}$ from Eq. (20) and $S_{ds}$ from Eq. (24), which results in the parameterizations of the physics as used in WAM cycles 1 through 3.
(ii) $S_{in,e}$ from Eqs. (12) through (18), $S_{nl}$ from Eq. (20) and $S_{ds}$ from Eq. (28), which results in the parameterizations of the physics as used in WAM cycle 4.

## 2.3 Numerics

The action balance equation implemented in WAVEWATCH-II is a slightly modified version of Eq. (2):

$$\frac{\partial N(\omega,\theta)}{\partial t} + \frac{\partial}{\partial x}[c_x N] + \Delta x^{-1}\frac{\partial}{\partial y}[c_y N \Delta x] + \frac{\partial}{\partial \omega}[c_\omega N] + \frac{\partial}{\partial \theta}[c_\theta N] = S\,, \tag{36}$$

where $x$ and $y$ are physical space coordinates in the east-west and south-north directions, $\Delta x$ is a grid increment and $(c_x,c_y) = \mathbf{c_g}+\mathbf{U}$. The grid increments $\Delta x$ and $\Delta y$ follow directly from the longitude and latitude increments $\Delta\lambda$ and $\Delta\phi$:

$$\Delta x = 2\pi R \, \Delta\lambda \, \cos\phi \, , \tag{37}$$

$$\Delta y = 2\pi R \, \Delta\phi \, . \tag{38}$$

Equation (36) is identical to Eq. (2), but has the advantage that it is applicable for propagation over a sphere *and* for propagation over a plane grid (provided that the first term in the right side of Eq. (6), that accounts for great circle propagation, is incorporated or ignored respectively). Both options are available in WAVEWATCH-II. Note that Eqs. (2) and (36) both consider energy and action densities per unit ocean surface area. Equation (36) is discretized using constant increments in the $x$, $y$ (or $\lambda$, $\phi$) and $\theta$ spaces. In the frequency space, however, an exponential grid is used to allow for economical integration of Eq. (20).

$$f_{r,i+1} = \gamma f_{r,i} \, . \tag{39}$$

The constant $\gamma$ is presently set to 1.1 in a parameter statement, and may be changed without further modifications of the code.

Following WAM, input source terms are calculated as the average source term for wind at the beginning and the end of the time step. Wind data is spatially interpolated by components (in the wind preprocessing program) and interpolated by absolute value and direction in time (cf. WAM). Wave boundary data are taken at the end of the time step considered and are interpolated bin-by-bin in each time step. Note that all input data are interpolated within the model, so that input fields may have any (irregular) time interval.

In the model propagation and source terms are treated separately using a fractional step method, although some propagation schemes require source term information. Propagation schemes, source term integration methods and source term parameterizations can be combined at will (though not necessarily with successful results, see previous section). Propagation and source term integration are listed below for details refer to Tolman (1992).

Propagation

Several propagation schemes are available.

1- First-order upstream scheme, before source term integration
2- First-order upstream scheme, after source term integration
3- Second-order accurate scheme.

Source term integration

Four methods are available for the numerical integration of the source terms.
1- Static explicit integration, with fixed time step equal that of the propagation.
2- Static semi-implicit integration.
3- Dynamic explicit integration, with variable time step method.
4- Dynamic semi-implicit integration.

# 3. Model Setup

## 3.1 Bathymetry

The Directorate-General of Public Works and Water Management of the Netherlands (Rijkswaterstaat) delivered the bathymetry of the North Sea at a grid with about 8km resolution (in fact 0.1250° W-E and 0.0833° N-S resolution; referred to as the 8km grid or CSM-grid). The grid consists of 200 x 173 grid points in the N-S direction and E-W direction respectively. The grid extends from longitude 11.9375° W to 12.9375° E and from latitude 48.0416° N to 62.3750° N (see below *Fig. II.*)

The bathymetry of the southern North Sea was delivered by the Directorate-General of Public Works and Water Management at a grid with about 3 km resolution (in fact 0.0416° W-E and 0.0277° N-S resolution; referred to as the 3 km grid or ZUNOBOL-grid). The grid consisted of 226 x 120 grid points in the N-S direction and E-W direction respectively. The grid extended from longitude 0.6042° W to 8.7708° E and from 51.0417° N to 54.3472° N.

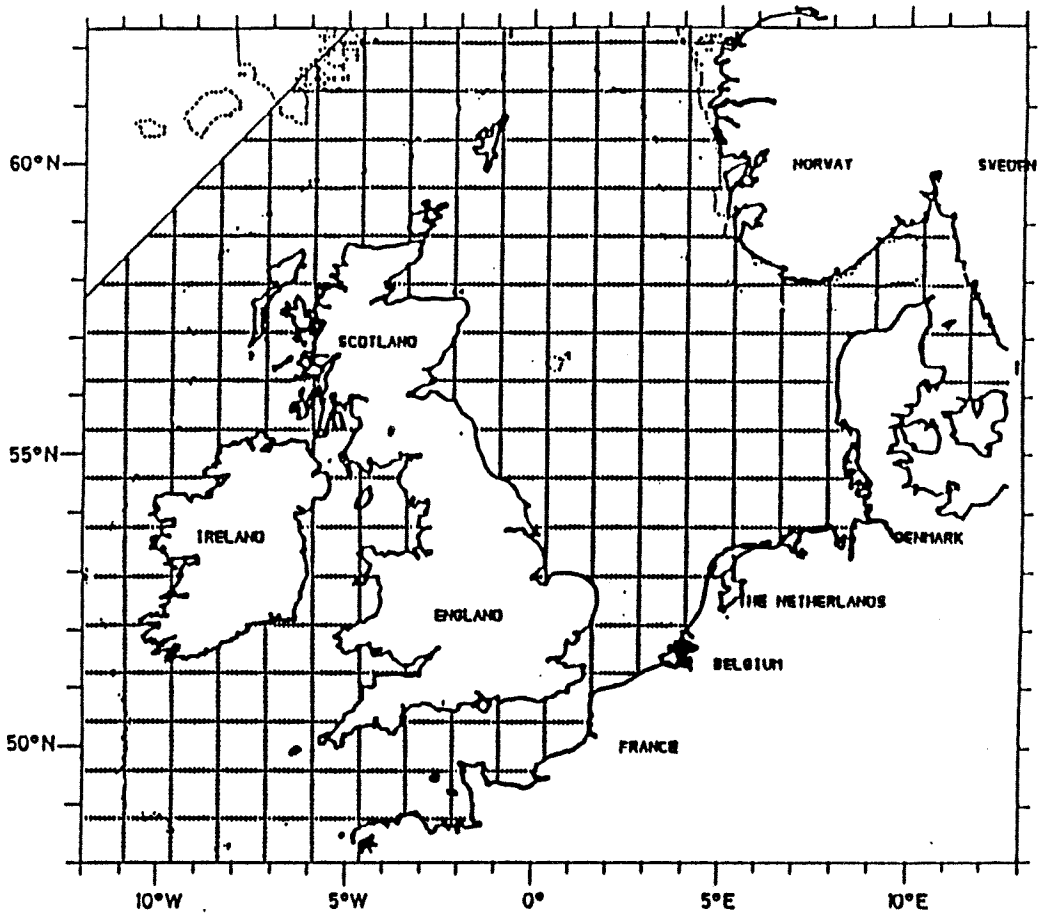


*Fig. II* *Geography of the North Sea.*

A large scale computational grid (8 km resolution, North Sea with surroundings) was used to set-up the model. It is based on the CSM grid. Some consideration have been taken into account in defining the computational grid. Since waves do not enter the southern North Sea through the Dover Straits for NW wind condition (the expected wind directional sector for the maximum waves), this computational grid does not incorporate the Dover Straits. Also waves in the Irish Sea are not of importance for the North Sea, so the Irish Sea is filled as land. At the northern boundary of the North Sea (at the latitude of northern Scotland) significant wave energy will enter the model for NW and N storm cases, therefore the grid for WAVEWATCH-II includes the northern part of the North Sea up to 62.3750° N. The northern North Atlantic does not affect the waves in the southern North Sea and we therefore moved the western boundary of the grid to 5.0625° W.

The bathymetry of the CSM grid is given in Fig. 1. The geographic locations and water depths at various locations are given in Table 1. For the entire study the model was operated with longitude-latitude coordinates to account for great circle propagation.

The smaller scale computational grid (3 km resolution, southern North Sea) taken from the ZUNOBOL bathymetry appeared to contain depth information that did not correspond to the local depth at the some stations. In consultation with the Directorate-General of Public Works and Water Management of the Netherlands (Rijkswaterstaat) it was therefore decided to modify the ZUNOBOL depth around stations K13 and EUR. The corrections were roughly between 0 m and 5 m in an area of 1000 km$^2$ around EUR and in an area of about 100 km$^2$ around K13 (smoothing of an apparent mega-ripple).

### 3.2 Model set-up

To perform numerical calculation with the WAVEWATCH-II model, a bathymetry, wind field, water level and wave boundary conditions are required. It is therefore essential to properly set-up the WAVEWATCH-II model to the North Sea including the computational spatial and spectral grid and the boundary conditions. The aim of this section is to analyze the sensitivity of the computational results in the North Sea to a number of factors in order to decide on the final set-up of the model. The sensitivity is examined for: geographic location of the boundaries, spatial resolution, boundary conditions, frequency range, frequency and directional resolution, initial conditions and the inclusion of depth-induced breaking.

First the options are described, then the results are given and analyzed.

#### 3.2.1 Model settings

*Physics and numerics*

Different integration methods can be used in WAVEWATCH-II. Because we are searching for a steady-state solution in simple conditions, the impact of numerical methods on the final results is expected to be small. We have therefore selected the most economical numerical method (see below). An added benefit of using the first-order scheme is that its inherent numerical diffusion avoids spurious oscillation as present in many higher-order schemes, and hence helps reaching a steady state quickly.

The standard set of physics (referred to as WAM$^+$-settings) and numerics which is used in

this study is summarized as follows:

Physics:

| | | |
|---|---|---|
| Wind input | : | Snyder et al. (1981) |
| Quadruplet wave interactions | : | Hasselmann and Hasselmann (1985) |
| Whitecapping | : | Komen et al. (1974) |
| Bottom friction | : | Madsen et al. (1988) |
| Depth-induced breaking | : | Battjes and Janssen (1978) |

Numerics:

First order upstream (before source term integration)
Explicit and static source term integration

*Computational grid resolution*

The spatial resolution of the computational grid is an important factor in determining the accuracy of the estimated wave condition. Two spatial resolutions have been used for the large-scale computational grid in the North Sea. The computational grid for the entire North Sea has either an 8 km resolution or a 16 km resolution (generated by diluting the CSM 8 km grid). Small scale computational, taken from the ZUNOBOL grid, has 3 km resolution.

*Boundary condition and initial condition*

During severe storms from NW and N, practically no waves enter the North Sea from the southern or the eastern boundary, therefore those boundaries are closed during the computation i.e. considered as land points. The northern and western (62.3750° N and -5.0625° W respectively) boundary are kept open; they retain the initial wave conditions throughout the computations.

The initial condition of the entire North Sea is characterized by a fetch-limited JONSWAP spectrum based on the local wind speed and direction. Two fetches have been used during the sensitivity study: 2000 km to account for waves travelling from the North Cape to the northern boundary of the model (the waves will decay to a final level), and 16 km (equal to the grid resolution of the 16 km grid; the waves will grow to a final level). In cases with 2000 km fetch initial condition, the open boundary points retain the very high initial spectrum, i.e. these boundary points radiate energy into the model continuously during the computational time. Comparing computations with the 2000 km fetch and the 16 km fetch gives insight in the effect of this boundary condition.

All other boundaries (land) are fully absorbing.

*Wind field*

In setting up the model, a uniform wind field over the entire grid has been used. The wind speed has been chosen to be 30 m/s which represents an average value for the wind speed in medium storm. The wind direction is North-Western, i.e., 345° (nautical convention is used throughout this report).

*Water level and current condition*

Extreme wind conditions lead to high storm surge levels. Therefore a uniform storm surge level of 5.0 m (over the entire North Sea) has been used during the model set-up. This will also be the case for any further computations (except those, which will be indicated). No currents are present during the entire study.

*Spectral grid*

The quality of the numerical wave propagation is affected by the spectral resolution. Two exponential frequency distributions have been examined with resolution 8% and 10% in frequency and two resolutions for the direction: 10° and 15°.

Some care has to be paid in choosing the lower limit ($f_l$) and the upper limit ($f_h$) of the frequency range in order to account for different sea states. In other words, it is essential to make sure that the spectrum at different locations at different times fits well within the frequency range. Two frequency ranges have been used, the first one is $f_l$=0.031 Hz to $f_h$=0.792 Hz and the second one is $f_l$=0.034 Hz to $f_h$=0.718 Hz.

*Time step during the computation*

The time step during the computation has to be determined in such a way that the Courant criteria for the numerical stability of the computation has been fulfilled. Therefore for the runs with 16 km grid, a time step of 360 s has been used. For the 8 km grid a 180 s time step is chosen for the time step. Computations at 3 km resolution have not been carried out for the model set-up.

*Depth-induced breaking*

The original version of the WAVEWATCH-II model, as an intermediate depth wave model, does not include a formulation for depth-induced breaking. In applying the model to the North Sea, it was found that depth induced wave breaking has considerable effect on the waves especially in the southern part of the North Sea which is the main concern of this study. In this set-up analysis one run is carried out without depth-induced breaking.

### 3.2.2 Description of test cases

The test cases are designed in such way as to start with a reference case (referred to as RREF) and then to vary only one of the above mentioned factors in each subsequent test case (always returning to the reference case for the next variation). In that way we can study the effect of each factor independently from the others. A summary for these test cases is given in Table 2.

It has to be mentioned here that for each run the computation is continued until the wave fields become stationary and then the computational results are considered at some stations along the Dutch coast. These stations are SON, ELD, K13, YM6, EUR, LEG, and AUK (see Table 1 and Fig. 3). Since the initial condition is one with 2000 km fetch, the convergence to the stationary condition is from the very high initial values of the significant wave height to the lower stationary values. The computations were stopped when the rate of change in significant wave height was less than 0.01 m per hour.

### 3.2.3 Results

*Sensitivity to the computational grid resolution*

Two spatial grid resolutions have been examined: 16 km (reference run, RREF) and 8 km (test run RGR8). First of all we have to mention that both grids feature the main topography of the North Sea very well (e.g. Dogger Bank and the Devils' Hole).

Comparing the wave fields of the above mentioned two runs (RREF and RGR8; Tables 3 and 4) shows a difference less than 20 cm for approximately 10 m significant wave height which represents about 2%. With respect to the mean wave period a difference less than 0.15 s for approximately 11 s which represents less than 2%. However, with respect to the computation time there is a difference of a factor 8 (smaller for the 16 km grid) which really does not compensate for an accuracy of 2% in the computational results. Therefore the 16 km grid has been chosen to be used for all further large-scale (CSM) computations to establish the model set-up.

Two directional resolutions have been used, 15° for the reference run (RREF) and 10° for the testing run (RT10). Comparing the results of the two runs (Tables 3 and 6) shows a difference of less than 10 cm for approximately 10 m significant wave height which represents about 1%. With respect to the mean wave period a difference less than 0.15 s for approximately 11 s which represents less than 2%. However with respect to the computation time there is a difference of factor 1.5 (smaller for the 15° direction grid). Therefore the 15° resolution has been chosen to be used for any further large-scale (CSM) and small-scale (ZUNOBOL) computations reported in this report. Notice that the WAM model too works with 15° directional resolution.

Examining the frequency resolution is done in run R108. The run is executed with an exponential frequency distribution with factor 1.08 (8% resolution) and the number of frequency bands is 42 in order to cover the same frequency range (0.031 to 0.792 Hz) used in the reference run RREF (that has 10% resolution and 34 frequency bands from 0.031 to 0.792 Hz). Comparing the results (Tables 3 and 7) shows hardly any difference: less than 0.3% in both significant wave height and mean wave period. The computational time for the reference run (RREF) a factor 1.33 less compared with that of the testing run (R108). Therefore a 10% resolution has been used for both the large-scale (CSM) and small-scale (ZUNOBOL) computations.

Testing the lower and upper limits of the frequency grid is done in run RF32, where a grid of 32 frequency bands (from 0.034 to 0.718 Hz) is compared with the reference 34 frequency bands (from 0.031 to 0.792 Hz). Comparing the results (Tables 3 and 5) shows hardly any difference. However we have preferred to use the larger range considering that we might run into storm cases with higher wind speeds which generate more low frequency energy. In fact, in the extreme uniform wind field with 50 m/s wind speed, we use $f_l$=0.022 Hz (large-scale (CSM) and small-scale (ZUNOBOL) computations). Notice that the WAM model uses a frequency grid of 24 bands from 0.04 Hz to 0.4 Hz.

*Sensitivity to the boundary and initial conditions*

The sensitivity to the boundary condition is investigated by doing the run RNFT with a 16

km fetch initial condition (that is retained at the open boundaries during the computations). The effects in deep water are different from those in shallow water. Comparing the results with the reference run in which the boundary condition has a 2000 km fetch (RREF and RNFT, Tables 3 and 8) at a deep-water station, i.e. AUK, shows a difference of a few meters for 17 m significant wave height. However for the rest of the stations (shallower stations) the difference is less than 20 cm which represents about 2% of the computed significant wave height and less than 4% in the mean wave period.

*Sensitivity to depth-induced breaking*

Run RBJO tests the sensitivity of the computational results for disabling the formulation of Battjes and Janssen for depth induced-breaking. Comparison with the reference run in which the depth induced breaking is switched on (RREF and RBJO; Tables 3 and 9) one can see that the differences appear at the shallower station where the effect of depth-induced breaking becomes pronounced (differences of about 0.1 m to 1.0 m for a significant wave height of about 8 to 9 m). Preliminary computations with very high wind speeds (60 m/s) showed larger effects (significant wave height reduced from 12 m to 8 m in 20 m water depth; not reported here).

### 3.3 Computational grids

The computations have been performed, throughout this study, with three computational grids. The primary computational grid (henceforth denoted as G1; see Fig.1) covers the North Sea with a grid resolution of 16 km (obtained by diluting the CSM bathymetry). In a later phase of the study two spatial grid have been used for nested runs, G2; with 8 km grid resolution (obtained from the CSM bathymetry) and G3; with 3km grid resolution (obtained from the ZUNOBOL bathymetry). The bathymetry for these two grids are given in Figs. 2 and 3. The lateral boundaries of the computational grids G2 and G3 are chosen to cover only the area near the Dutch coast where refined results are needed.

The Boundaries of the computational grids are given below.

| Grid | $\Delta\lambda$ | $\Delta\phi$ | Western. boundary | Eastern. boundary | Southern. boundary | Northern. boundary |
|---|---|---|---|---|---|---|
| G1 | 0.2500° | 0.1666° | -5.0625° E | 9.9375° E | 50.8750° N | 62.3750° N |
| G2 | 0.1250° | 0.0833° | 1.9375° E | 7.6875° E | 50.9583° N | 54.8750° N |
| G3 | 0.0416° | 0.0277° | 2.4791° E | 7.0208° E | 51.3194° N | 54.3472° N |

It should be noted that in all figures for computations with grid G1, the illustration is only given up to 57° latitude and not to the northern boundary of the grid (62° latitude). This is done to magnify the southern North Sea.

# 4. The maximum significant wave height

As mentioned in the introduction, the present study attempts to establish whether there is a well defined upper limit of the significant wave height due to the water depth in the southern North Sea and if so, at what level. This chapter deals with the answer to those questions. Uniform wind fields are used in section 4.1 to investigate the existence of an upper limit and to determine the formulations of wave physics that produce the highest waves. Section 4.2 deals with both historic and synthetic storms.

## 4.1 Uniform wind field

### 4.1.1 The Standard wave model (standard physics)

*Computations*

In search for the existence of a physical upper-limit of the significant wave height in the southern North Sea, it seems obvious to consider a high wind speed from northerly directions, constant over the entire North Sea (even if this is not physically realizable). For investigating this existence of an upper-limit, we have used the standard setting of WAVEWATCH-II (see section 3.2.1). The level of the maximum significant wave height computed with other formulations of physics will presented next.

First the wind direction which produces the highest waves is searched. The searching covers the northern and the north-westerly directions since they seem be to the most relevant directions for maximum wave conditions in the southern North Sea. Therefore, the following directions are used in the search: 240°, 270°, 300°, 330°, 360°, and 30° nautical. A wind speed of 50 m/s has been chosen as this was deemed the maximum possible wind speed in the North Sea. This choice is based on discussions with meteorologists.

Having established the direction of maximum waves, we vary the wind speed from 20 up to 60 m/s: 20, 30, 40, 50, 60 m/s wind speed to show the (possibly: lack of) convergence to an upper limit and to obtain the sensitivity of the significant wave height to variations in the wind speed around 50 m/s.

The computations are performed with grid G1 (16 km grid resolution) and directional resolution of 15°. In high wind speed (> 40 m/s), the frequency grid is extended to lower frequencies (.022 Hz) to include the expected generation of low frequency energy.

*Results*

Wind direction dependency

Figure 4 show the variation of significant wave height at different locations for varying wind direction with 50 m/s wind speed. The slight maximum in the results show that the highest waves come from 330° nautical direction. The results are listed in Table 10.

Wind speed dependency

Figure 5 shows the dependency of the significant wave height at different locations for the wind speed from direction 330°. Clearly the wave height increases by increasing the wind speed up to some level (near 50 m/s wind speed) where it seems to be nearly insensitive to the wind speed, but some continued increase can be seen for the deeper stations. The results are listed in Table 11.

### 4.1.2 The maximum wave model (maximum input, minimum dissipation)

*Variations of source term formulations*

Having thus established that a physical limitation is nearly reached in the model at 50 m/s wind speed, those formulations were selected of the wave physics in the model that would generate the highest significant wave height. To that end the formulations of the physics in the model were varied to each of the available options in WAVEWATCH-II which is considered to be the uncertainty in the state-of-the-art. It may be noted that the option of Janssen (1991) is operational in the present version of the WAM model e.g., at the European Center of Medium-Range Weather Forecasting, Reading, England. For each variation independently the significant wave height was hindcasted at all indicated stations for the extreme uniform wind field, i.e., 50 m/s wind speed from 330° nautical direction.

The standard source term formulations (WAM$^+$-setting) are as follows:

| | | |
|---|---|---|
| Wind input | : | Snyder et al. (1981) |
| Quadruplet wave interactions | : | Hasselmann and Hasselmann (1985) |
| Whitecapping | : | Komen et al. (1974) |
| Bottom friction | : | Madsen et al. (1988) |
| Depth-induced breaking | : | Battjes and Janssen (1978) |

Three variations from the standard settings have been used:

| | | |
|---|---|---|
| Bottom friction | : | JONSWAP (Bouws and Komen, 1983) |
| Wind input and whitecapping | : | Janssen (1991) |
| Depth-induced breaking | : | Roelvink (1993) |

The computation were done in a sequence such as to start with a reference run using the standard setting of WAVEWATCH-II and then to vary one of the above mentioned source terms. Each time the model was set to its standard setting before the next variation. In this way the effect of each variation separately was examined. Comparison between the results of $H_s$ at various stations for different variations are given in Table 12.

It was found that the formulation of bottom friction (JONSWAP) produces a significant wave height about 0.7 m higher than the standard set of formulations. The formulations of wind input and whitecapping by Janssen give a significant wave height which is about 0.5 m higher than the standard formulations. Using the depth induced breaking of Roelvink reduces the wave height typically by about 3 m.

Thus the maximum source term formulations (the maximum wave model) are:

| | | |
|---|---|---|
| Wind input and whitecapping | : | Janssen (1991) |
| Quadruplet wave interaction | : | Hasselmann and Hasselmann (1985) |
| Bottom friction | : | JONSWAP (Bouws and Komen, 1983) |
| Depth-induced breaking | : | Battjes and Janssen (1978) |

*Results*

Having established the maximum formulation for wave physics, we hindcast the significant wave height in the southern North Sea with the selected formulations of the physics combined. The hindcasting is done using the extreme uniform wind field over the entire North Sea with 50 m/s wind speed coming from north west direction, i.e., 330° nautical direction.

Computation has been carried out using the maximum wave model on the large-scale grid G1. The results are given in Table 12 (last column), show the largest significant wave height within the freedom of the state-of-the-art at 16 km resolution.

To obtain high resolution results along the Dutch coast, we refined the computations in the southern North Sea with nested computations from the above results at G1 (16 km grid) via G2 (8 km grid) to G3 (3 km grid).

The propagation time step is determined for each computational grid based on Courant criteria. The time steps for each computational grid is therefore as follows:

G1 (16 km grid): time step = 360 s
G2 (8 km grid): time step = 240 s
G3 (3 km grid): time step = 120 s

The waves are hindcasted until a stationary situation is achieved (rate of change less than 0.01 m per hour).

The geographic distribution of the significant wave height and mean period (based on second moment) obtained from computation with G1 (16 km grid resolution) are given in Figs. 6 and 7 respectively. The pattern of significant wave height is very similar to the pattern of the bathymetry, suggesting that the maximum significant wave height in the southern part of the North Sea is depth controlled. However in the northern deeper part, depth effects are less noticeable.

The computations are refined closer to the Dutch coast with nested computation to G3 (3 km grid resolution) via G2 (8 km grid resolution). The geographic distribution of significant wave height and mean period obtained from the computation with G2 are given in Figs. 8 and 9 respectively. The geographic distribution of significant wave height and mean period obtained from the computation with G3 are given in Figs. 10 and 11 respectively. The significant wave height pattern matches that of the bathymetry implying the dominant effect of the bottom in determining the wave conditions. It is interesting to notice that the 12 m wave height contour line corresponds to 30 m water depth contour line suggesting the value 0.4 for wave height-water depth ratio. Table 13 gives the significant wave height, and wave direction at various locations along the Dutch coast.

## 4.2 Realistic extreme storm (the maximum wave model)

To investigate whether the maximum wave conditions found in the above uniform wind fields are physically realizable (even if the uniform wind fields are not), the waves were hindcasted in an extreme storm that was synthesized from historic storms. This storm was selected with search procedures involving wave hindcasts in a large number of synthetic storms (about 800). The details of this work are described in Ferier et al. (1993). Here only a summarized description for the procedure is mentioned.

An extra attempt to find a realistic extreme storm based on the Feb. 1953 storm is reported in the Appendix.

### 4.2.1 Storm synthesis

*Storm parameterization*

To represent the atmospheric pressure in the synthetic storms a spatial Gaussian distribution was used with the radius to maximum wind different along the four (orthogonal) major axes of the storm. This created an elliptical, asymmetrical pressure field. From this pressure field the geostrophic wind was computed and reduced to 65% and turned counter-clockwise by 15° to estimate the surface wind at 10 m elevation. Storms with surface wind speeds exceeding 50 m/s were removed from the search (due to the incremental nature of the search, small overshoots of about 2 m/s were permitted). The parameters of these synthetic storms were all assumed to vary linearly in time, characterized by a one value at the moment when the center of the storm is located at 10° W and one value 72 hours later.

These time histories were varied in the following search procedures within limits obtained from historic storms. To that end five storms were analyzed that are considered by meteorologists to be the severest storms in the southern North Sea over the last decades. These are all storms from westerly or north-westerly directions: 1st Feb '53, 21st Dec '54, 3rd Jan '76, 19th-25th Nov '81 and 26th Feb - 2nd March '90. (It was verified with extra hindcasts that storms with tracks from more northerly directions were irrelevant.) These storms were followed on standard weather maps after they passed 10° W longitude and the following parameters were visually estimated as a function of time: the forward speed, the central pressure, the orientation of the major axes and the radii along these axes. For each of these parameters five time histories were thus obtained. By roughly approximating the upper and lower envelope of these time histories with straight lines, the limits of values at the start of the storm and 72 hours later were estimated. For the start and end positions of the storms the results of an earlier and more extensive analysis of historic storms by Zwart (1993) were used.

For economic reasons the wave hindcasts in the search procedure were carried out at station K13 with the second-generation wave model DOLPHIN-B described by Holthuijsen and de Boer (1988). This wave model has been adapted for shallow water and tuned to resemble the behavior of the WAVEWATCH-II model (initial setting) in the storm of Feb. 1953. Computations showed that the storms that generated the largest significant wave heights at station K13 also generated the largest values at the other locations along the Dutch coast.

*The search procedure*

To determine which synthetic storm would lead to the largest significant wave height in the southern North Sea, a sequential binary search was used with the storm parameters varying within the limits obtained from the above analysis of historic storms. First a reference hindcast is carried out with the value of all storm parameters (start and end values considered separately) set at their mid-range value. In sequence each storm parameter is then investigated: it is set at two values, one at the center of the upper half-range and one at the center of the lower half-range. All other parameters retain their reference value. Two hindcasts then decide which of these two values produces the largest significant wave height. The reference value of this parameter is then replaced by this selected value (it retains this value during the continuation of the search). Then the next storm parameter is modified similarly. After all storm parameters are thus investigated and selected the procedure is repeated twice, each time cutting the range of the storm parameter in half and centering it at the last selected reference value (three iterations in all).

To increase the probability that the proper storm has been selected, a synoptic binary search (replacing the reference values only after each of the three iterations has been completed) and a random search (shifting the mean to the selected value and reducing the widths of the assumed distributions by 50% after each of three iterations) were also carried out. A total of about 800 hindcasts was thus carried out. As all three searches were carried out with three iterations each, the resolution of the results is 1/8 of the original parameter range. For a two-parameter case, the three corresponding search paths through the parameter space are indicated in *Fig. III.*

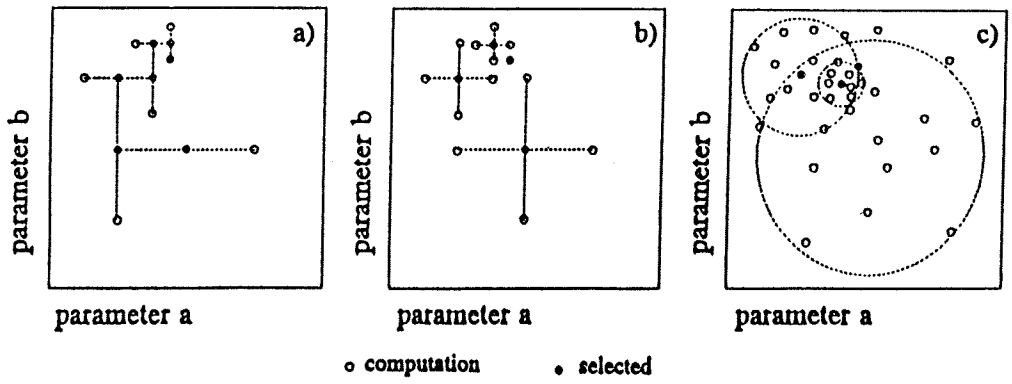


*Fig. III Search paths for two parameter case (three techniques).*

The storm with the maximum significant wave height was selected by the sequential binary search. It is a fairly small but intense storm (300 to 400 km radius) tracking across the southern North Sea from a westerly direction. With a maximum wind speed of 51.8 m/s, it generated (with the DOLPHIN-B model) a maximum significant wave height (at station K13) of 15.25 m. An inspection of the results suggests that to achieve this extreme value, the wave field in the southern North Sea requires a locally high wind speed to compensate for locally, bottom-induced dissipation (particularly breaking). Within the permitted range of atmospheric pressure, this locally high wind speed can be achieved only with a fairly small radius of the storm. The results of the other searches (synoptic binary and random) were storms that were similar in pattern to the one found with the sequential binary search but with somewhat lower significant wave heights.

### 4.2.2 Computations and results

*Computations*

To obtain the results with third-generation formulations, we carried out the hindcast for the selected synthetic storm with the WAVEWATCH-II model with the formulations selected for maximum effect of the physics.

The computations are carried out with grids identical to those mentioned in the case of the uniform wind field. Therefore, to obtain high resolutions results along the Dutch coast, the computations have been refined in the southern North Sea with nested computations from G1 grid (16 km) via G2 grid (8 km) to G3 grid (3 km).

Since the wind field in this extreme storm varies strongly in time, the parametric wind field is renewed every 1/2 hour.

The idealized storm considered here varies strongly in time. For the wave model to be able to cope with the large temporal variations in the wind and wave field, the dynamic implicit integration scheme has been used. This scheme dynamically adjusts the time step of integration, depending on the local variability of wind and waves. The time steps of propagation and source term integrations are given below for all computational grids.

G1 grid: time step = 360 s (propagation) and 30 s (source term integration)
G2 grid: time step = 240 s (propagation) and 30 s (source term integration)
G3 grid: time step = 120 s (propagation) and 30 s (source term integration)

*Results*

The geographic distribution of significant wave height and mean period obtained from computations with the G1 grid (16 km grid resolution) are given in figures 12 and 13 respectively at the peak of the storm (the time where the maxima is obtained at station K13). The geographic distribution of the significant wave height and mean period obtained from computation with the G2 grid are given in figures 14 and 15 respectively at the peak of the storm. Figures 16 and 17 show the geographic distribution of the significant wave height and mean period respectively obtained from computation with G3 grid (3 km grid resolution) at the peak of the storm. The similarity of the geographic distribution of the significant wave height with the bathymetry shows that in the southern part of the North Sea, the significant wave height is depth controlled (similar to the case of extreme uniform wind).
The significant wave height pattern is almost identical to that obtained from the computation with the extreme uniform wind indicating that the maximum wave conditions in the uniform wind field are realistic, even when the uniform wind field itself is not.

The maximum at every grid point during the storm period is presented in figures 18 and 19 for significant wave height and mean period respectively at 3 km resolution. Table 14 gives the significant wave height, mean period and wave direction at various locations along the Dutch coast at the local peak of the storm. Finally the spectra at those locations and times are presented in figures 20 to 27.

Bedoeling Rijkswaterstaat ?

# 5. Uncertainty Analysis

## 5.1 Introduction

An essential part of the present study is to analyze the sensitivity of the computational results to changes in the coefficients of the WAVEWATCH-II model. A sensitivity analysis has therefore been carried out for each source term of the maximum wave model. This analysis indicates which source term strongly influences the final results. The uncertainty in the coefficients of these source terms is used to estimate the uncertainty in the computed value of the maximum significant wave height.

The sensitivity computations are carried out with grid G1 (16 km resolution) using the maximum uniform wind field (i.e., 50 m/s wind speed and 330° nautical direction).

The maximum wave model (see section 4.1.2) is defined as follows

| | | |
|---|---|---|
| Quadruplet wave interactions | : | Hasselmann and Hasselmann (1985) |
| Bottom friction | : | JONSWAP (Bouws and Komen, 1983) |
| Wind input and whitecapping | : | Janssen (1991) |
| Depth-induced breaking | : | Battjes and Janssen (1978) |

## 5.2 Sensitivity to source terms coefficients

*Quadruplet wave-wave interactions*

Quadruplet wave-wave interactions are modeled using the discrete interaction approximation of Hasselmann and Hasselmann (1985). In this approximation interactions are calculated only for the following type of quadruplets (i.e., sets of four spectral components which satisfy the resonance conditions):

$$\begin{aligned} \sigma_2 &= \sigma_1 \\ \sigma_3 &= (1+\lambda_{nl})\sigma_1 \\ \sigma_4 &= (1-\lambda_{nl})\sigma_1 \\ k_4 &= k_1 + k_2 - k_3 \end{aligned} \qquad (40)$$

where $\lambda_{nl}$ is a constant equal to 0.25. In the sensitivity study $\lambda_{nl}$ is varied to 0.26 to examine the sensitivity of the results for this variation (large variations produce unrealistic growth curves in the ideal fetch-limited conditions; unpublished study of L. Luping, Delft University of Technology, 1987).

The computed significant wave height at each location is given in Table 15. Column 1 represents the reference run (REF16), which is done with the standard setting of the maximum wave model. The result of the computation using $\lambda_{nl} = 0.26$ are given in column 2. The results show that the computed maximum significant wave height is not sensitive (compared with the other source terms, see below) to the small variation in $\lambda_{nl}$. The difference in $H_s$ is less than 0.14 m.

*Bottom friction*

The JONSWAP parameterization (Hasselmann et al. 1973), as used in the WAM model (WAMDI group 1988).

$$S_{bot}(f_r,\theta) = 2\Gamma \frac{n-0.5}{gd} F(f_r,\theta) , \tag{41}$$

where $\Gamma$ is an empirical constant, and equal -0.067 $m^2s^{-3}$ as suggested by Bouws and Komen (1983) for wind seas.

The range of variability of $\Gamma$ was determined using the movable bed model (Tolman, 1993). This model indicates that for extreme shallow water waves the bottom roughness is generated by a combination of wash-out ripples and sheet-flow of sediment in the wave boundary layer. The roughnesses predicted by this model can be translated to effective values of $\Gamma$ (Tolman, 1993). Assuming that the bottom of the North Sea consists of relatively fine clean sand (effective grain diameter 0.2 mm, critical Shields number for initial sediment motion 0.05) effective values of $\Gamma$ have been calculated for all stations using wave conditions as predicted for the February 1, 1953 storm with the WAVEWATCH-II model. Around the peak of the storm, effective values of $\Gamma$ varied between -0.097 and -0.047

The above mentioned limits have been used for the sensitivity computations in the North Sea. The results are given in Table 15 columns 3 and 4 for $\Gamma$ is -0.097 and -0.047 respectively. The results show that the variation in the maximum significant wave height is limited to 0.14 m for $\Gamma$ equal -0.097 and to 0.16 m for $\Gamma$ equal -0.047.

*Wind input*

The wind input and whitecapping source terms of Janssen (1991) are coupled. The wind input source term is the expression of Janssen (1991), cf. WAM cycle 4, which explicitly accounts for interactions between wind and waves. The source term is given as

$$S_{in,e}(f_r,\theta) = \beta \frac{\rho_a}{\rho_w}\left(\frac{U_*}{c}\right)^2 \max\left[0,\cos(\theta-\theta_w)\right]^2 \sigma F(f_r,\theta) , \tag{42}$$

where $\beta$ is the Miles constant, which is estimated from the nondimensional critical height $\lambda$.

$$\beta = \frac{\beta_{max}}{\kappa^2} \lambda \ln^4\lambda , \tag{43}$$

Here $\beta_{max}=1.2$. To determine the sensitivity of the results for the uncertainty in $\beta_{max}$, realistic variations in its value are required. To obtain these, growth curves of Kahma (1992) was used. The lower limit of $\beta_{max}$ (the lower limit of the growth curves) was found to be 0.65 and 1.35 for the upper limit (the upper limit of the growth curves).

The above mentioned values were used to perform sensitivity computations. The results are

given in Table 15, columns 5 and 6. They show that the computed significant wave height is sensitive to variation in the wind input coefficient.

*Whitecapping*

The parameterization of the whitecapping source term developed by Janssen (1991) for the use in combination with $S_{in}$(WAM cycle 4).

$$S_{ds}(f_r,\theta) = \alpha\ \hat{\sigma}\ \hat{k}^4\ E^2 \left[\frac{k}{\hat{k}} + \left(\frac{k}{\hat{k}}\right)^2\right] F(f_r,\theta)\ . \tag{44}$$

where $\alpha$=-2.25. Discussions with P. Janssen (the author of the above formulations) for the present study, indicated that the uncertainty in the factor $\alpha$ is equal to the uncertainty in the wave energy in the fully developed wave case. For this, the difference between the Shore Protection Manual (SPM; CERC, 1973) and Pierson Moskowitz (1964) was taken. It is found to be about 15%, hence $\alpha$ is varied between -1.9 and -2.6.

The sensitivity of the computed significant wave height to variation in $\alpha$ is examined. The results are given in Table 15, columns 7. They show that the model results are not sensitive to the variation in the whitecapping coefficient.

*Depth-induced breaking*

The formulation of Battjes and Janssen (1978) has been used. It has been implemented in a spectral form based on Eldeberky and Battjes (1995) as follows

$$S_{sf} = -\frac{\alpha}{4} f_m Q_b H_m^2 \frac{F(f_r,\theta)}{F(\theta)} \tag{45}$$

where $H_m$ is the maximum significant wave height, reformulated to account only for depth induced breaking as follows

$$H_m = \gamma h \tag{46}$$

The breaking coefficient $\gamma$ has been chosen to be 0.8 in combination with factor $\alpha$ equal 1. In the sensitivity study the lower limit for $\gamma$ was 0.6 and the upper limit was 0.83 (refer to Battjes and Stive, 1985)

To examine the sensitivity of the computed significant wave height to the variation in $\gamma$, one computational run is performed for the North Sea with $\gamma$=0.83. The result is given in Table 15 column 8, it shows that the choice of $\gamma$ has a significant influence in the computed $H_s$.

Summarizing, it has been found that for estimating the uncertainty of the maximum significant wave height, the parameters of the wind input ($\beta_{max}$) and the depth induced wave breaking ($\gamma$) are dominant among all other source term parameters. Therefore the uncertainty analysis has

been performed for those two parameters. The wind field that has been used is the extreme uniform wind field (i.e. 50 m/s wind speed and 330° nautical direction). The computations were done with the G1 grid (16 km resolution) and refined with G3 grid (3 km resolution).

### 5.3 Uncertainty computations

The uncertainty in $H_s$ is computed as follows

$$\sigma^2_{H_s} = (\Delta H_s)^2_\beta + (\Delta H_s)^2_\gamma \qquad (47)$$

Where $\Delta H_s$ is the difference in $H_s$ due to the variation in either $\beta$ or $\gamma$, and $\sigma_{Hs}$ is the total uncertainty in $H_s$.

The reference value, upper and lower limits of both $\gamma$ and $\beta$ are summarized here.

| | depth-induced breaking $\gamma$ | wind input $\beta$ |
|---|---|---|
| upper limit (high) | 0.83 | 1.35 |
| reference value (stand.) | 0.80 | 1.20 |
| lower limit (low) | 0.60 | 0.65 |

Due to the fact that the variation in both parameters is not symmetric around its standard values, the uncertainty in $H_s$ will also not be symmetric. Therefore, the uncertainty in $H_s$ will be computed two times, first to estimate the upper limit and second to estimate the lower limit.

The sequence of the computational runs for the uncertainty is given in sketch below in *Fig. IV*. The computation has been done in two stages. First with the G1 grid (16 km resolution) to provide the boundary conditions for the second stage with the G3 grid (3 km resolution). As illustrated in the figure, the variation in the depth-induced breaking parameter $\gamma$ is considered after considering the variation in the wind input parameter $\beta$.

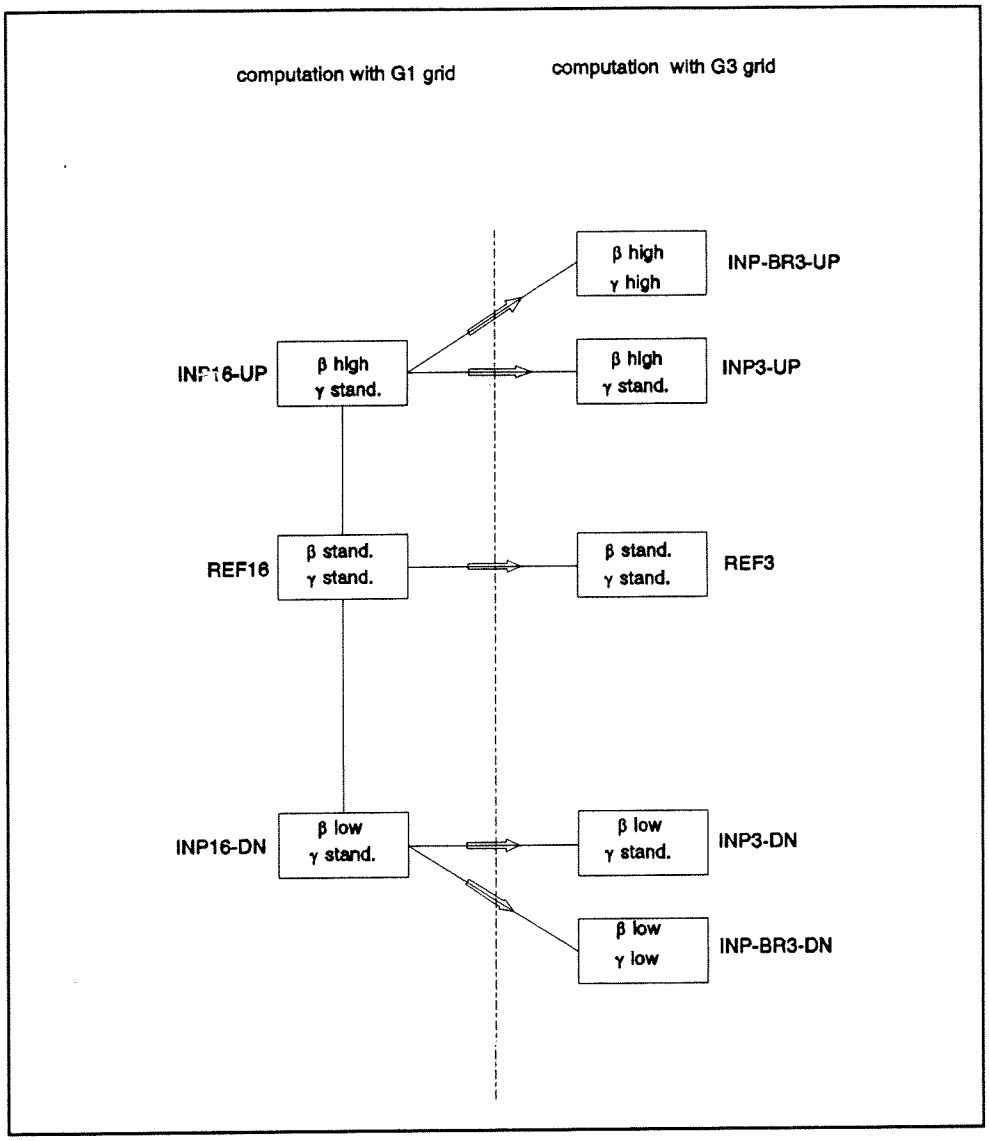


*Fig. IV The Scheme for the computational procedure of the uncertainty analysis.*

The results of the computations with the G3 grid (3 km resolution) are summarized in Table 16.

The computational run INP3-UP (see sketch) has produced $H_s$ values which are not much different than those of REF3 (although one would expect higher results, in fact it is slightly lower at some location). At the moment, the only possible explanation can be given is that the REF3 run was performed via nesting from computation via the G2 grid (8 km resolution), however INP3-UP is performed via nesting from computation with the G1 grid (16 km resolution) directly.

The uncertainty calculations have been performed using Eq. 47. The first term in the right hand side is computed at the G1 grid (Table 15) for the variation in $\beta$ (upward or downward)

by taking the difference between the reference run REF16 and INP3-DN for the lower limit, and the difference between REF16 and INP3-UP for the upper limit. The second term in the right hand side is computed at the G3 grid (Table 16) for the variation in $\gamma$ (upward or downward) by taking the difference between the INP3-UP and INP-BR3-UP for the upper limit and the difference between INP3-DN and INP-BR3-DN for the lower limit (Table 16).

The range of uncertainty in the values of significant wave height is given in Table 17. The results show that this range is 5% upward and 25% downward in the maximum significant wave height. Finally the limits of maximum significant wave height are given in Table 18.

### 5.4 Effect of storm surge level

Severe wind conditions are not only accompanied by extreme waves but also by extreme storm surges. These extreme storm surges have not been investigated in the present study. They were simulated with 5 m extra water depth. To show the sensitivity of the results of this study for this assumption, the storm surge level was varied from 5 to 6 m in the case of the extreme synthetic storm of section 4.2. The computation is carried out with the maximum formulation of the wave physics with the G1 grid over the entire North sea.

Results

Table 19 shows a comparison between the computed significant wave height for both a 5 and a 6 m storm surge level. The results show that 1 meter increase in the water level results in an increase of about 0.25-0.45 meter in $H_s$. The increase in $H_s$ is such that the ratio $H_s/h$ did not change. This suggests that in extreme condition, the increase in $H_s$ is linear with the increase in the water level and that, independent of the water level, the ratio $H_s/h$ is constant and equal to about 0.4.

# 6. Validation and verification

In this chapter a validation and verification for the WAVEWATCH-II model is presented. The chapter is divided into 3 sections. First the WAVEWATCH-II model is compared with another numerical wave model HISWA over the North Sea in the extreme uniform wind. Second the WAVEWATCH-II is verified in academic test with standard growth curves. Finally the WAVEWATCH-II model is validated in a historic storm.

## 6.1 Comparison between WAVEWATCH-II and HISWA results over the North Sea

Computations have been performed with WAVEWATCH-II and HISWA (Holthuijsen et al., 1989) using computational grid G1 over the North Sea. The extreme uniform wind field is used, i.e., 50 m/s and 330° nautical direction. Both WAVEWATCH-II and HISWA are used with their standard settings. For the standard settings of WAVEWATCH-II refer to section 3.2.1.

*Results*

The comparison between the results computed by WAVEWATCH-II and HISWA is given in Table 20. The results show significant differences between the model results (25% higher in WAVEWATCH-II). In this extreme condition, the results of WAVEWATCH-II model are more credible than HISWA results. Because the formulations of the physical processes are better founded in theory in WAVEWATCH-II than in HISWA. For example, the wind input formulation in WAVEWATCH-II model is scaled with the friction velocity ($U_*$), whereas in HISWA, it is scaled with $U_{10}$ (wind speed at 10 m elevation). In fact, scaling with $U_{10}$ underestimates the wave growth considerably in extreme cases. This matter is investigated in the next section.

## 6.2 Comparison between a standard growth curve and WAVEWATCH-II

The growth rate of the waves in the WAVEWATCH-II model has been investigated for various water depths. The investigation is done for the standard and the maximum model. The computation has been done for an ideal situation of constant water depth, infinite fetch, and uniform wind. Two wind speed have been used, 20 m/s and 50 m/s.

Fig. 28 shows the comparison between the growth curves of the standard and maximum models with the SPM (Shore Protection Manual) growth curve for 20 m/s wind speed. Clearly the results of the standard WAVEWATCH-II model are in fair agreement with SPM.

Fig. 29 shows the comparison between the growth curves of the standard and maximum models with the SPM growth curve re-scaled with $U_*$ (friction velocity) for 50 m/s wind speed. The scaling method is given below. Without this scaling the agreement is extremely poor (errors of order factor 5 or more). The same effect does not appear in case of $U_{10}$=20 m/s because the SPM growth curve is scaled for 15 m/s.

*Scaling with $U_*$:*

The wind input source term in WAVEWATCH-II model is formulated in terms of the friction velocity $U_*$. Where $U_*$ is related to $U_{10}$ by the drag coefficient C as follows.

$$U_{10} = U_*/C^{0.5} \tag{48}$$

the relation for the drag coefficient at 10 m height :

$$C = (0.8 + 0.065\ U_{10})\ /1000 \tag{49}$$

with an average value $\bar{C}$ equal to $1.775 \times 10^{-3}$ for $U_{10}$= 15 m/s.

The dimensionless significant wave height according to SPM and scaled with $U_*$ is as follows (Holthuijsen ,1980)

$$\tilde{H} = \frac{C}{\bar{C}}\, 0.283 \tanh[0.57(\tilde{d}\frac{\bar{C}}{C})^{0.75}] \tag{50}$$

Here $\tilde{H}$ is the dimensionless wave height, and $\tilde{d}$ is the dimensionless water depth.

## 6.3 Validation of WAVEWATCH-II in a historic storm

*Observations*

Rijkswaterstaat provided observations (with WAVEC buoys) in the storm of Dec 19th, 1990 at several locations near the Dutch coast. The wind fields are available every 3 hours. The measurements are provided as time histories of significant wave height and one-dimensional energy density spectra and mean direction and direction spread as function of frequency.

*Numerical simulations*

The wind fields are used to perform computations over the entire North sea using the G1 grid with nesting to the Dutch coast to the G3 grid via the G2 grid. In all computations a storm surge level of 2.5 m is used. This value is based on actual measurements. In the computations, we used the maximum wave model except $\gamma$=0.73 instead of 0.80. This value of the breaking coefficient is chosen because it represents an average value for the coefficients obtained from the laboratory and field data presented by Battjes and Stive (1985). The source term formulations are therefore (referred to as 'credible model'):

| | | |
|---|---|---|
| Wind input and whitecapping | : | Janssen (1991) |
| Quadruplet wave interactions | : | Hasselmann and Hasselmann (1985) |
| Bottom friction | : | JONSWAP (Bouws and Komen, 1983) |
| Depth-induced breaking | : | Battjes and Janssen (1978) with $\gamma$=0.73 |

For the source term integration the implicit and dynamic scheme is used. The propagation time steps are equal to those used in the extreme synthetic storm.

*Results*

The computed time histories of significant wave height are compared with the observed ones at various locations near the Dutch coast. The results are presented in Figs. 30 to 36. The computed significant wave height is almost always too low compared with the observations (0.5 to 1 m), in particular during the decay of the storm. The discrepancies at the peak are within 10% except at station SON which has an error of 26% (Table 21). The discrepancy in the model behavior at location SON might be due to excessive dissipation induced by bottom effects. Further investigation are needed for the region around location SON.

Tables 22, 23 and 24 give comparisons of wave parameters between the model results and observations at stations AUK, EUR, and K13 respectively at the peak of the storm, 3 hours before and after. The energy spectra, directions, and directional spreading at these locations and times are compared in Figs. 37 to 45.

# 7. Calibration

The purpose of this part of the study is to calibrate the WAVEWATCH-II model. The motivation for the calibration is that the numerical simulation with the wind fields of the historic storm of Dec 1990 (section 6.3) showed that generally the model underestimates the significant wave height compared with observations. This is apparently due to excessive dissipation induced by the bottom. Here we have chosen to calibrate the coefficients of the source terms which represent the bottom effects. These are the source terms of depth-induced breaking and bottom friction which are formulated using Battjes and Janssen (1978) and JONSWAP (Bouws and Komen, 1983) respectively.

The model calibration is done using wave observations for two historic storms. These are the storm of Dec 1990 and the storm of Feb 1993. The observations are provided at six locations near the Dutch coast. These are SON, ELD, K13, YM6, EUR, and LEG. Three numerical simulations are performed for each historic storm; reference run with the standard coefficients, second run with variation in the breaking coefficient, and third run with variation in the friction coefficient. Each of these runs is performed by nesting from grid G1 (16 km resolution) to grid G3 (3 km resolution) via grid G2 (8 km resolution).

The source term coefficients were varied in order to reduce the bottom dissipation. Therefore the breaking coefficient $\gamma$ was varied from 0.73 (reference value) to 1.2, and the friction coefficient from -0.067 (reference value for wind sea given by Bouws and Komen, 1983) to -0.038 (the value for swell as proposed by Hasselmann et al., 1973).

The calibration is performed assuming linear dependency between the coefficient to be calibrated and the computed wave parameters such as $H_s$. The calibrated coefficients can then be obtained by either interpolating or extrapolating the coefficients to obtain best agreement in least-squares sense between the computed wave parameters and the measured ones.

It should be mentioned that due to the large discrepancy between the model prediction of the wave parameters and the measurements at SON, the calibration is done both including and excluding SON.

The calibration procedures are repeated several times according to the following :
1- calibration including and excluding SON
2- calibration based on $H_s$ only and both $H_s$ and $T_m$.

Each calibration run is characterized by a run-id consists of two characters according to the following abbreviations:

| | | |
|---|---|---|
| 1st character | A = all locations | S = all except SON |
| 2nd | H = only $H_s$ | T = both $H_s$ and $T_m$ are used |

It is found that in the numerical simulations for both historic storms that the wave parameters (i.e., $H_s$, and $T_m$) are not sensitive to the variation in the breaking coefficient $\gamma$. This is ascribed to the fact that the wave conditions in these historic storms are not affected by depth-induced breaking. It becomes a very important factor only in extreme conditions.

The results of the calibration analysis are listed below.

| run-id | breaking coefficient | friction coefficient |
|---|---|---|
| AH | no effect | -0.029 |
| SH | no effect | -0.032 |
| AT | no effect | -0.037 |
| ST | no effect | -0.038 |

Comparisons between the observations and the model results (both credible and calibrated) in the two historic storms at various locations are given in Figs. 46-51.

It may be noticed that the values of the friction coefficient obtained from the different calibration are close to the value of swell sea (-.038) as proposed by Hasselmann et al. (1973). Thus, the maximum calibrated model is similar to the maximum model, except for the bottom friction coefficient which is equal to that of swell sea instead of wind sea.

Finally, the maximum calibrated model is used to perform computations in the extreme uniform wind (50 m/s wind speed from 330° nautical direction).

The maximum calibrated model used is defined as:

| | | |
|---|---|---|
| Wind input and whitecapping | : | Janssen(1991) |
| Quadruplet wave interactions | : | Hasselmann and Hasselmann (1985) |
| Bottom friction | : | JONSWAP (Hasselmann et al., 1973), friction coefficient= -.038 |
| Depth-induced breaking | : | Battjes and Janssen (1978), breaking coefficient= 0.8 |

The extreme uniform wind is defined as:

wind speed = 50 m/s
wind direction = 330° nautical
storm surge level = 5.0 m

The wave parameters obtained from the numerical simulation are listed in Table 25. The variation of significant wave height and mean wave period are given in Figs. 52 and 53 respectively. The wave spectra at various locations are given in Figs. 54 and 55. It may be noticed that the spectra at some locations (SON, ELD and K13) have double peaks indicating swell at these stations. This is probably due to the long distance (some 2000 km from 62° latitude to the southern North Sea) over which the waves from the north are generated by the high wind speed (50m/s). This swell is generated in an unrealistic wind field. In fact, it is not present in the extreme synthetic but realistic storm of section 4.2. At the southern stations (YM6, EUR, LEG and BBR), the low frequency peak is not observed. This may be because the wind sea is overtaking the dissipating swell. Future work is probably needed to examine this matter.

# 8. Conclusions

The maximum possible wave conditions along the Dutch coast have been estimated with the third-generation numerical wave model WAVEWATCH-II in extreme wind conditions.

This type of numerical wave model represents the state-of-the-art in wave modelling which has been shown elsewhere to accurately compute wave conditions in deep water hurricane conditions. A version of the model that maximizes the generation and minimizes the dissipation of the waves produces an uncertainty of the computed maximum significant wave height in the southern North Sea of about 5% upwards and 25% downwards. The results of a calibrated version of the model (used only for the final run) in historic storms (Dec. 1990 and Feb. 1993) are generally good (errors less than 10% in the significant wave height at the peak of the storm) except at one location (SON) where the source of the error of 18% is not clear. This storm was not sufficiently severe to verify shallow water wave dissipation, in particular depth-induced wave breaking.

In consultation with meteorologists, the maximum sustained wind speed over the North Sea was chosen to be 50 m/s. The results of a sensitivity analysis show that the results of this study are not very sensitive for this choice of wind speed. This illustrates that the maximum possible wave conditions in the southern North Sea are controlled by bottom induced dissipation (friction and breaking).

The wave conditions in a uniform wind field (50 m/s wind speed, and 5 m uniform storm surge and model formulations chosen to maximize the wave heights) are at a maximum for a wind direction of 330° N (i.e., from NNW). The significant wave heights computed with WAVEWATCH-II in these conditions at the locations of this study vary between 9.7 m at station BBR (near the Belgian border) and 14.2 m at station EUR. These values are approximately 25% higher than obtained in these conditions with the second-generation wave model HISWA (using default settings). Computations with the WAVEWATCH-II model in an extreme synthetic storm that was selected after a search procedure involving some 800 hindcasts (with the second-generation wave model DOLPHIN-B) showed that the wave conditions in this relatively small, intense storm are almost identical to those in the uniform wind field of 50 m/s wind speed. The ratio of significant wave height over local water depth (for depth less than 40 m) is nearly constant and equal about 0.4. This ratio is maintained when a uniform 6 m storm surge is used in the computations. The insensitivity to variations in wind speed, wind field structure and storm surge level supports the notion that the maximum possible wave conditions in the southern North Sea are controlled by the local water depth.

The context of the present study is the extrapolation of observed or hindcasted wave conditions from fairly high probability condition to low probability condition. The essence of the difference between these two types of conditions is in the bottom effects. These effects are fairly limited in the high probability condition but they are dominant in the low probability condition. Accounting for these difference in the procedure of extrapolation is not trivial. The present study only indicates the maximum possible values of significant wave height from the physical point of view (and it is rather conservative estimate, i.e., an estimate that is likely to be high). An extrapolation should not exceed this value of significant wave height even at the lowest probability of exceedance. For slightly less extreme value of probability, the bottom also effects the wave conditions. This implies of course that at these

limits, the extrapolation is also effected. This has not been investigated but it is conceivable that the bottom effects increase rapidly when the significant wave height approaches the maximum level (much higher than in any historic records). The reason for this speculation is that depth-induced breaking increases rapidly at a certain wave height-depth ratio. At lower ratios and therefore in less extreme condition, bottom friction is probably the dominating factor. This implies that perhaps three regimes should be accounted for in the extrapolations; (a) relatively deep water condition, (b) shallow water condition with bottom dissipation dominant, (c) shallow water condition with depth-induced breaking dominant.

Finally, in this study we used the state-of-the-art formulations of wave physics that have been shown elsewhere to accurately compute wave conditions in deep water hurricane conditions. In extreme conditions, the southern North sea becomes a shallow water region. In these conditions, the applicability of the source term formulations is not well established. Future research is needed to examine this matter.

## ACKNOWLEDGMENTS

For the determination of the maximum possible wind speed over the North Sea, we are greatly indebted to B. Zwart of KNMI. We had some very interesting and crucial discussion with him. We also wish to thank KNMI for permitting E. Bouws to spend time and effort on this study. We extend the same thanks to Delft Hydraulics for the time and effort of G.Ph. van Vledder who contributed to the discussions of this study.

## REFERENCES

Battjes, J.A. and J.P.F.M. Janssen, 1978, Energy loss and set-up due to breaking of random waves, *Proc. 16th Int. Conf. Coastal Engineering*, Hamburg, 569 - 587

Battjes, J.A. and M.J.F. Stive, 1985, Calibration and verification of a dissipation for random wave breaking, *J. Geophy. Res.*, 90(C5):9159-9167.

Eldeberky, Y. and J.A. Battjes, 1995, Spectral modelling of wave breaking; application to Boussinesq equations, Submitted to *J. Geophy. Res.*

Bouws, E., and G.J. Komen, 1983, On the balance between growth and dissipation in an extreme depth-limited wind-sea in the southern North Sea. *J. Phys. Oceanogr.*, **13**, 1653-1658.

Bouws, E., 1986, Provisional results of a wind wave experiment in a shallow water (Lake Marken, The Netherlands), Memo 86-21, KNMI

Cavaleri, L. and P. Malanotte Rizzoli, 1981, Wind wave prediction in shallow water: theory and applications. *J. Geophys. Res.*, **86**, 10961-10973.

CERC, 1973, Shore Protection Manual, U.S. Army Coastal Engineering Research Center

Charnock, H., 1955, Wind stress on a water surface. *Quart. J. Roy. Meteor. Soc.*, **81**, 639-640.

Hasselmann, K., T.P. Barnett, E. Bouws, H. Carlson, D.E. Cartwright K. Enke, J.A.Ewing, H. Gienapp, D.E. Hasselmann, P. Kruseman, A. Meerburg, P. Müller, D.J. Olbers, K. Richter, W. Sell and H. Walden, 1973, Measurements of wind-wave growth and swell decay during the Joint North Sea Wave Project (JONSWAP). *Ergänzungsheft zur Deutschen Hydrographischen Zeitschrift*, Reihe A (8) Nr. 12, 95 pp.

Hasselmann, S. and K. Hasselmann, 1985, Computations and parameterizations of the nonlinear energy transfer in a gravity-wave spectrum, Part I: A new method for efficient computations of the exact nonlinear transfer integral, *J. Phys. Oceanogr.*,15, 1369-1377

Holthuijsen, L.H., 1980, Methoden voor golfvoorspelling, *Technische Adviescommissie voor de Waterkeringen.*

Holthuijsen, L.H., and S. de Boer, 1988, Wave forecasting for moving and stationary targets, In: *Computer Modelling in Ocean Engineering,* Eds. B.Y. Schrefler and O.C. Zienkiewicz, Balkema, Rotterdam, 231-234

Holthuijsen, L.H., N. Booij, T.H.C. Herbers, 1989, A prediction model for stationary, short-crested waves in shallow water with ambient currents. *Coastal Engineering*, Vol 13, pp 23-54.

Janssen, P.A.E.M., 1991, Quasi-linear theory of wind-wave generation applied to wave forecasting, *J. Phys. Oceanogr.*, 21, 1631 - 1642

Kahma K.K., Calkoen C.J., 1992, Reconciling discrepancies in the observed growth of wind-generated waves. *J. Phys. Oceanogr.*, 22, 1389 - 1405.

Komen, G.J., S. Hasselmann and K. Hasselmann, 1984, On the existence of a fully developed wind-sea spectrum. *J. Phys. Oceanogr.*, **14**, 1271-1285.

Kuik, A.J, G.Ph. van Vledder and L.H. Holthuijsen, 1988, A method for the routine analysis of pitch-and-roll buoy wave data, *J. Phys. Oceanogr.*, **18**, 1020-1034

Madsen, O.S., Y.-K. Poon and H.C. Graber, 1988b, Spectral wave attenuation by bottom friction: theory. *Proc. 21st Int. Conf. Coastal Eng.*, ASCE, Malaga, 492-504.

Pierson, W.J. and L. Moskowitz, 1964, A proposed spectral form for fully developed wind seas based on the similarity theory of S.A. Kitaigorodskii. *J. Geophys. Res.*, **69**, 5181-5190.

Roelvink, J.A., 1993, Dissipation in random wave groups incident on a beach, *Coastal Engineering,* 19, 127-153

Snyder, R.L., F.W. Dobson , J.A. Elliott and R.B. Long, 1981, Array measurements of atmospheric pressure fluctuations above surface gravity waves. *J. Fluid Mech.*, **102**, 1-59.

Tolman, H.L., 1991, A third-generation model for wind waves on slowly varying, unsteady, and inhomogeneous depths and currents, *J. Phys. Oceanogr.*, 21 (6), 782 -797

Tolman, H.L., 1992, User manual for WAVEWATCH-II, NASA/GSFC, Laboratory for Oceans

Tolman, H.L., 1993, Wind-waves and moveable-bed bottom friction, Accepted for publication in *J. Phys. Oceanogr.*

WAMDI group, 1988, The WAM model - a third generation ocean wave prediction model. *J. Phys. Oceanogr.*, **18**, 1775-1810.

Zwart, B., 1993, De stormvloed van 1 februari 1953, Memorandum KNMI, VEO 93 - 01, pp. 20, in Dutch

Yamartino., 1984, *J. Climate Appl. Meteor.*, 23, 1362-1366

## Appendix

### Historic storms

In this part of the study, the computations have been carried out using two historic storms that have also been used in a study to estimate extreme storm surges (Zwart, 1993). These are the storms of February 1, 1953 and the storm of February 21, 1993 (available and used every 3 hours).

The computations have been done with the standard wave model. The spatial resolution is 16 km (G1) and the spectral grid is the standard obtained from the model setup.

The results are given as time histories of the significant wave height in Figs. A1-A11. Because the '53 storm (legend: SV53), with maximum local wind speed of 37 m/s, produced a higher significant wave height than the '93 storm (maximum local wind speed 28 m/s), its wind field was subsequently manipulated in a manner similar to the one used in the storm surge study of Zwart (1993) (only characteristic extreme manipulations of that study were taken):

- enhancing the original wind speed with 25%, the maximum wind speed is then 45 m/s. (legend: S53E)
- enhancing the original wind speed with 25% and shifting the wind fields 160 km to the north and 80 km to the east. (legend ESNE)
- enhancing the original wind speed with 25% and shifting the wind fields 160 km to the south and 80 km to the east. (legend ESSE)

The comparison between different manipulation of '53 storm are shown in Figs. A1-A11. It was found that enhancing and shifting to the south-east produced the largest significant wave height compared with the other manipulations (significant wave height varied between 9 to 11 m in the southern North Sea).

# FIGURES

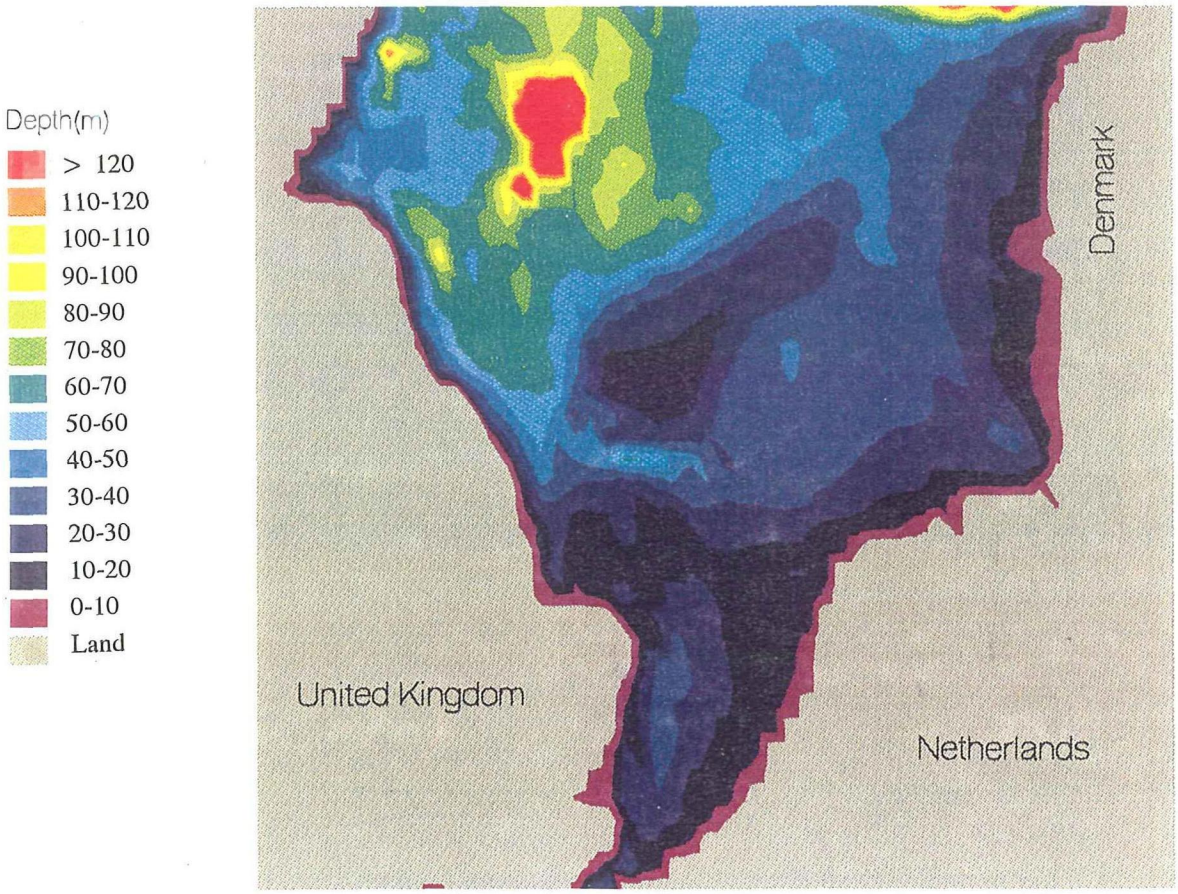


| Bathymetry of the North Sea with 16 km grid resolution (Grid G1) | HSMAX |
|---|---|
| | |
| Delft University of Technology | Fig. 1 |

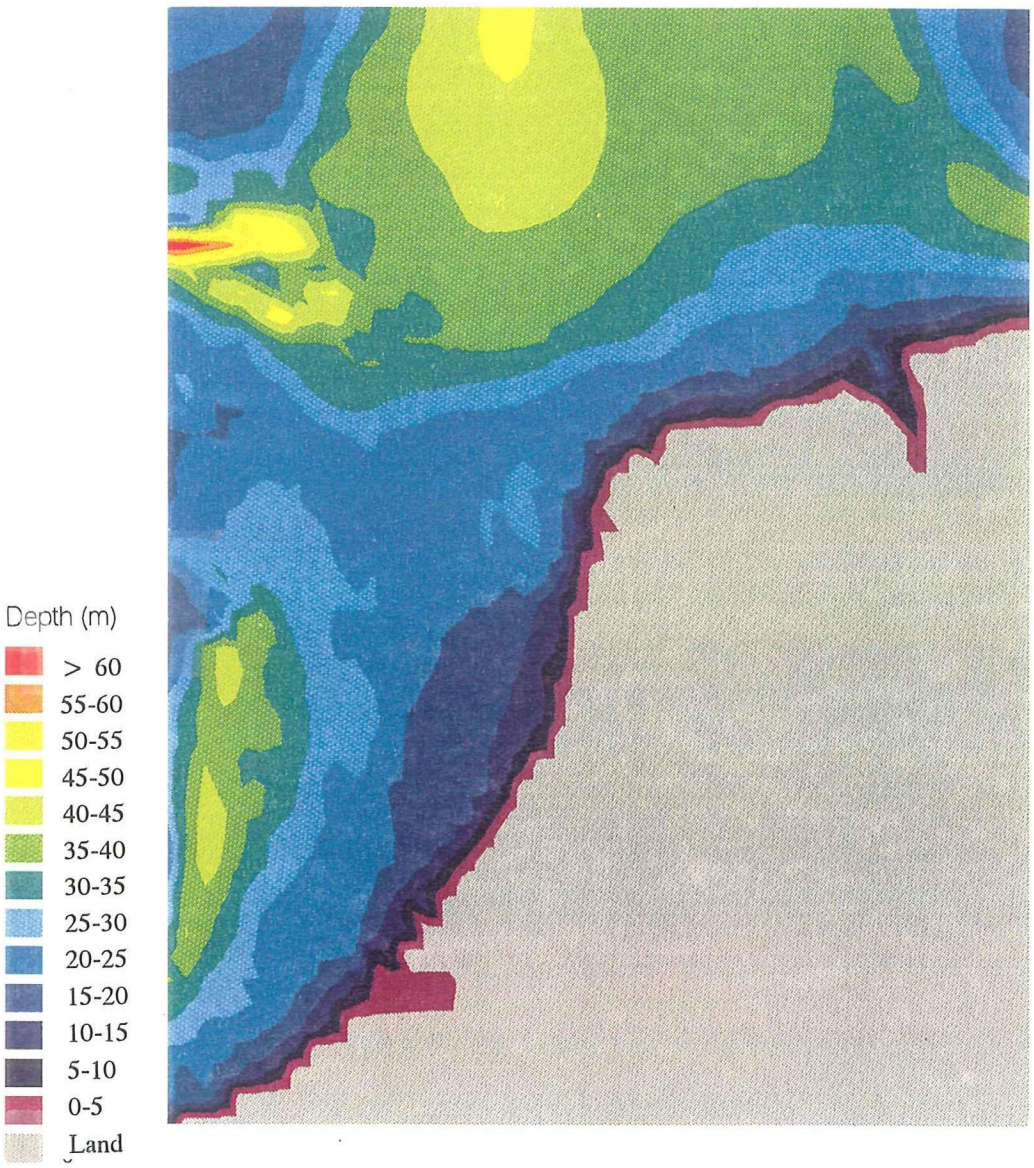


| | |
|---|---|
| Bathymetry of the southern North Sea with 8 km grid resolution (Grid G2) | HSMAX |
| Delft University of Technology | Fig. 2 |

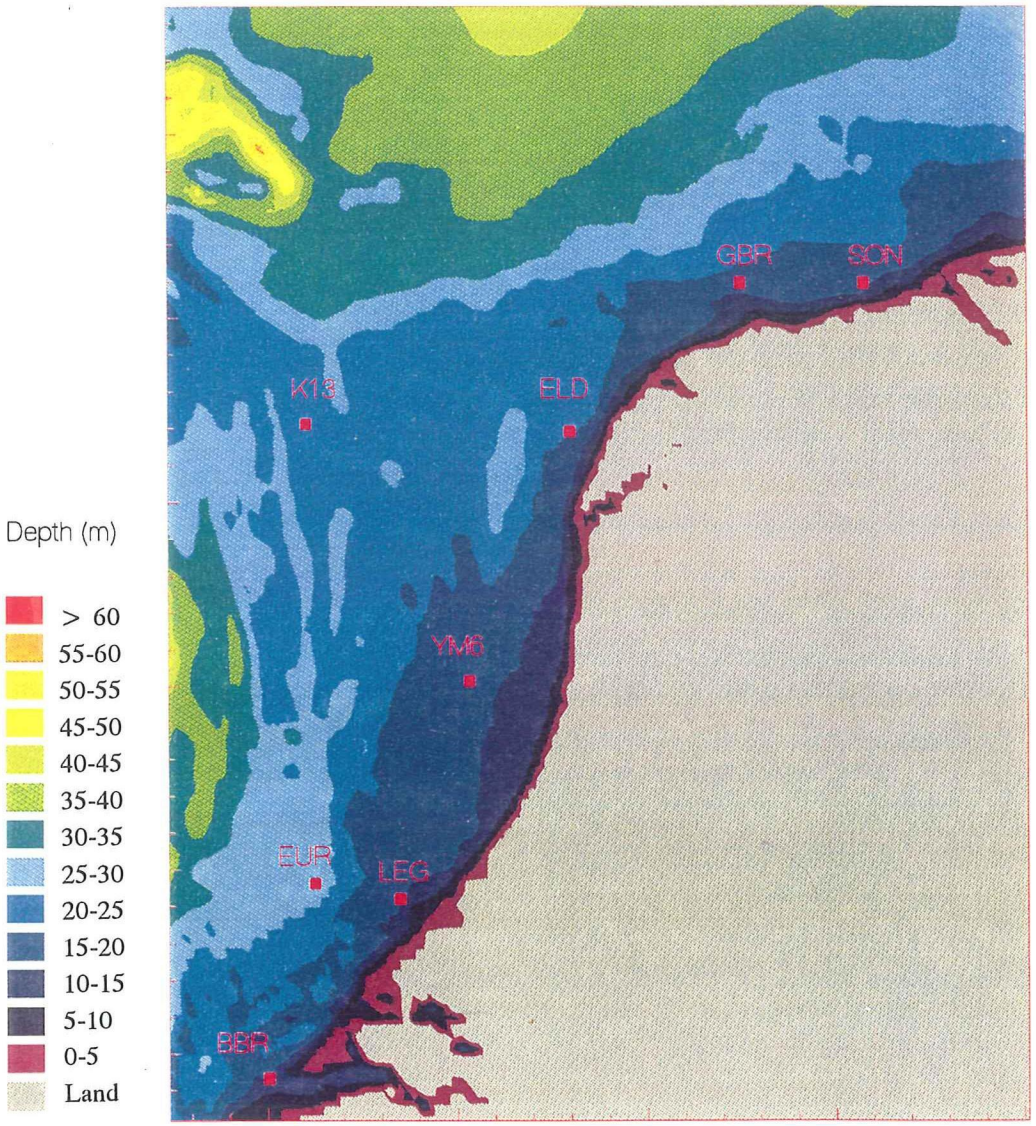


| | |
|---|---|
| Bathymetry of the southern North Sea with 3 km grid resolution (Grid G3) | HSMAX |
| Delft University of Technology | Fig. 3 |

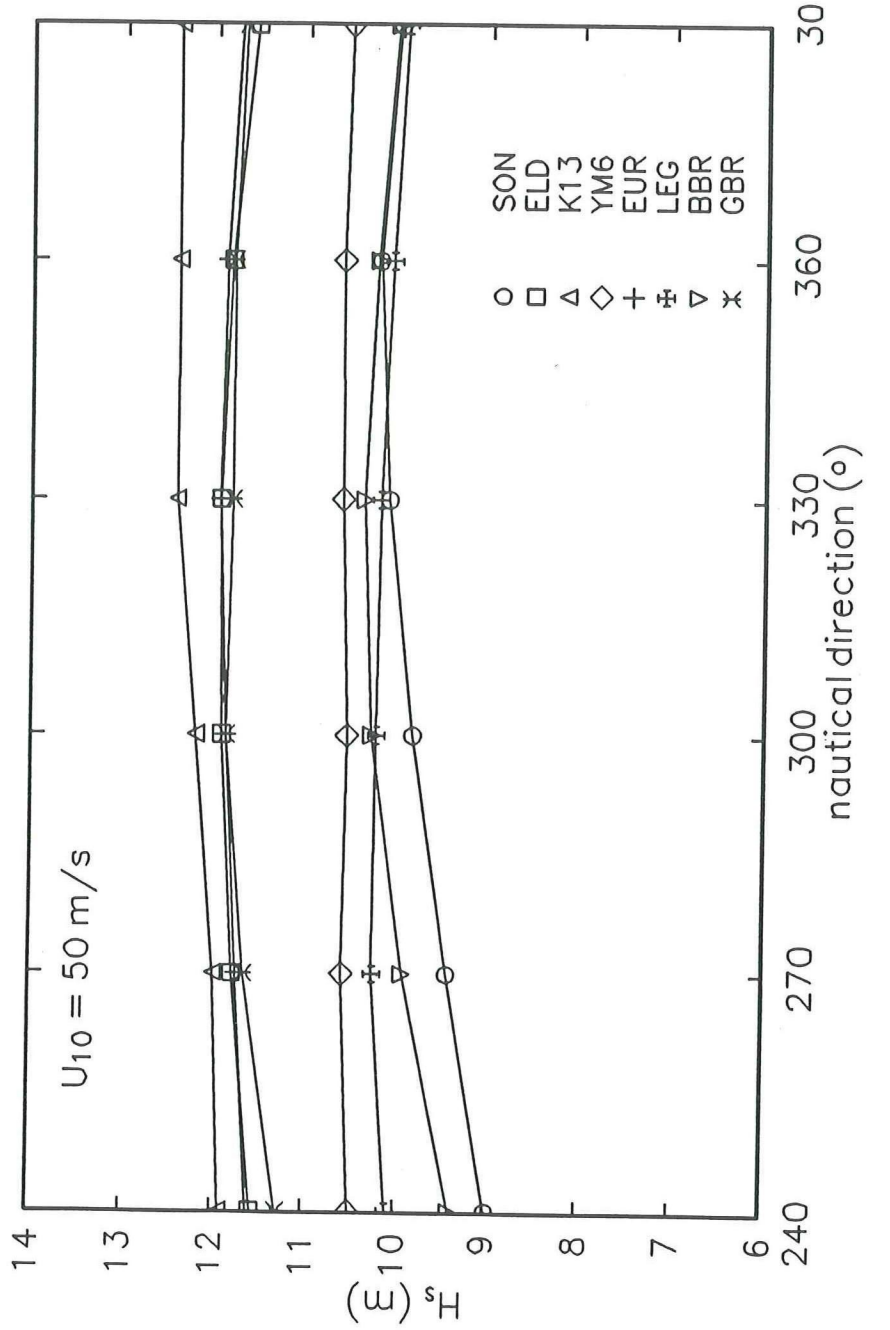


(Computations with the standard wave model and grid G1)

| | |
|---|---|
| Significant wave height as a function of wind direction (wind speed=50 m/s) | HSMAX |
| | |
| Delft University of Technology | Fig. 4 |

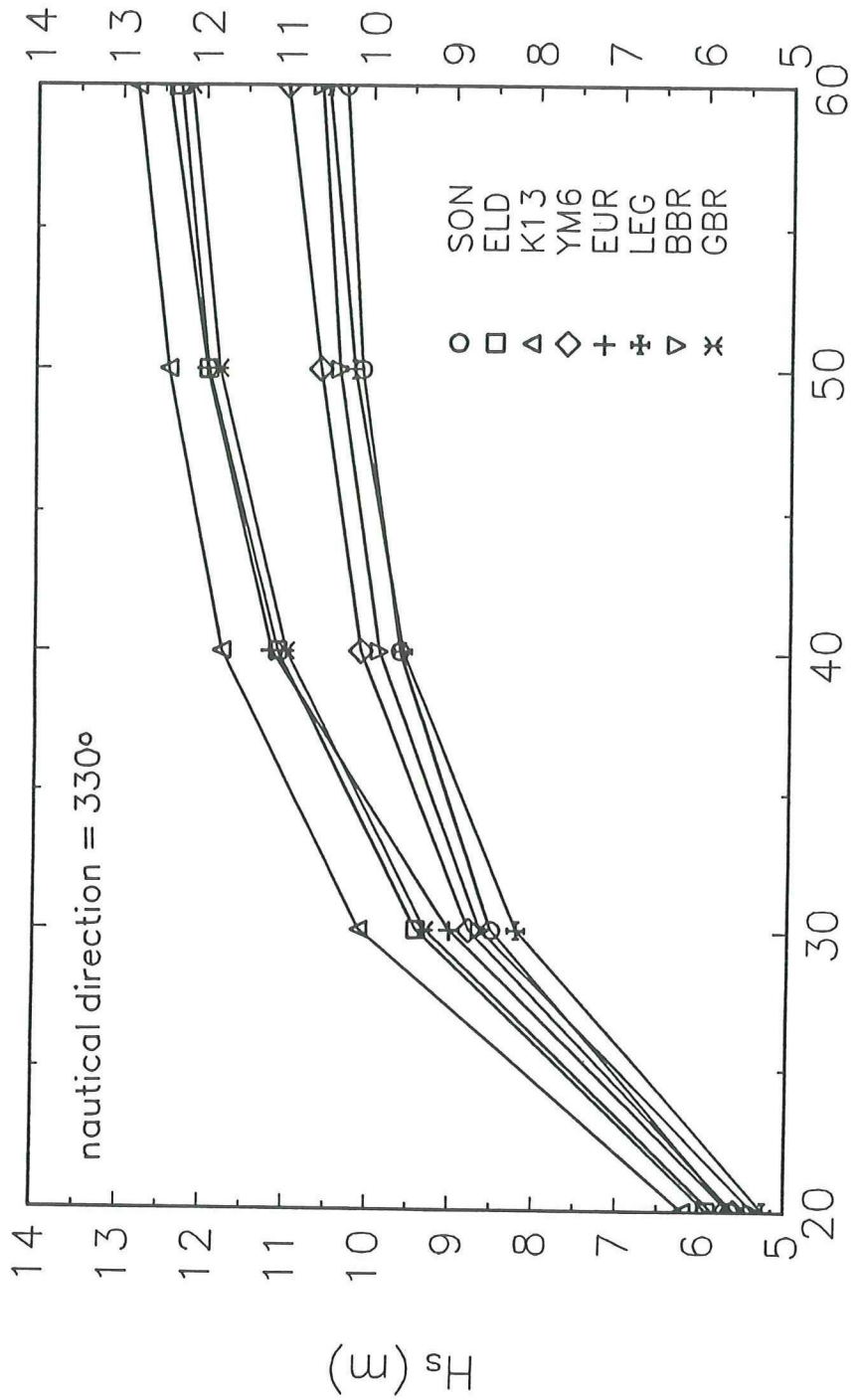


| | |
|---|---|
| Significant wave height as a function of wind speed (wind direction=330° n) | HSMAX |
| Delft University of Technology | Fig. 5 |

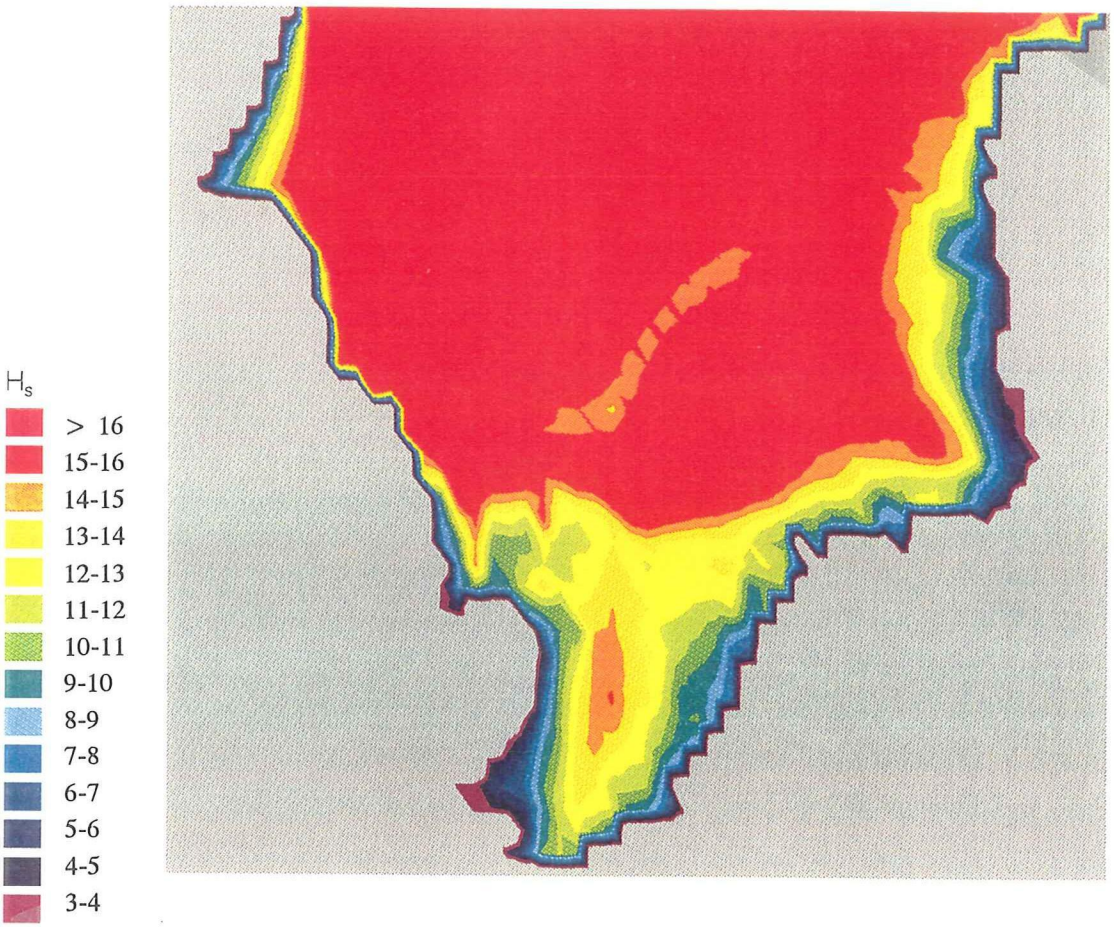


| | |
|---|---|
| Significant wave height in the extreme uniform wind (computation with the maximum wave model and grid G1) | HSMAX |
| Delft University of Technology | Fig. 6 |

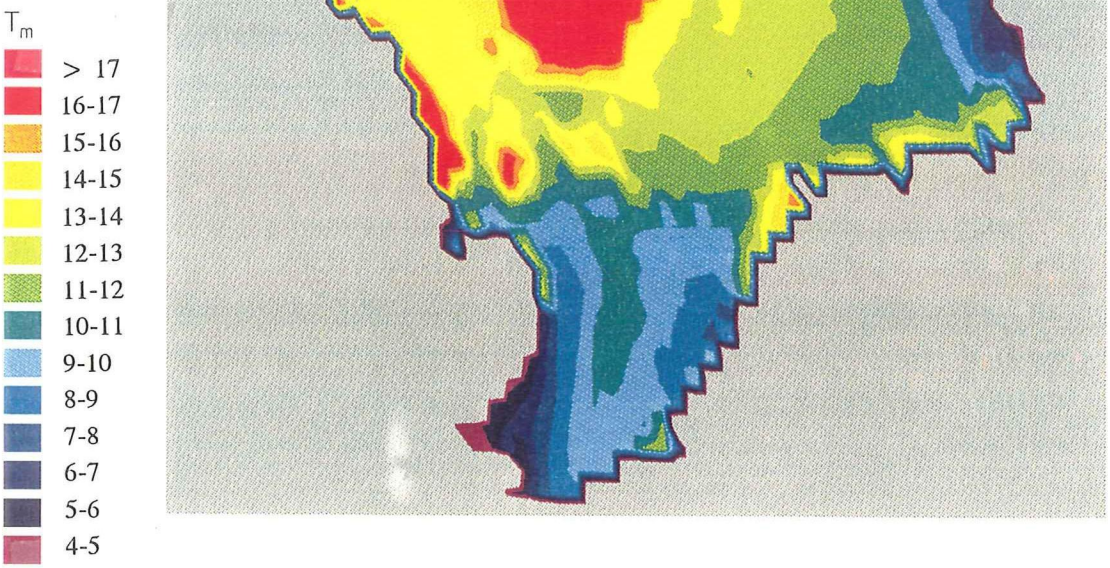


| Mean wave period in the extreme uniform wind (computation with the maximum wave model and grid G1) | HSMAX |
|---|---|
| Delft University of Technology | Fig. 7 |

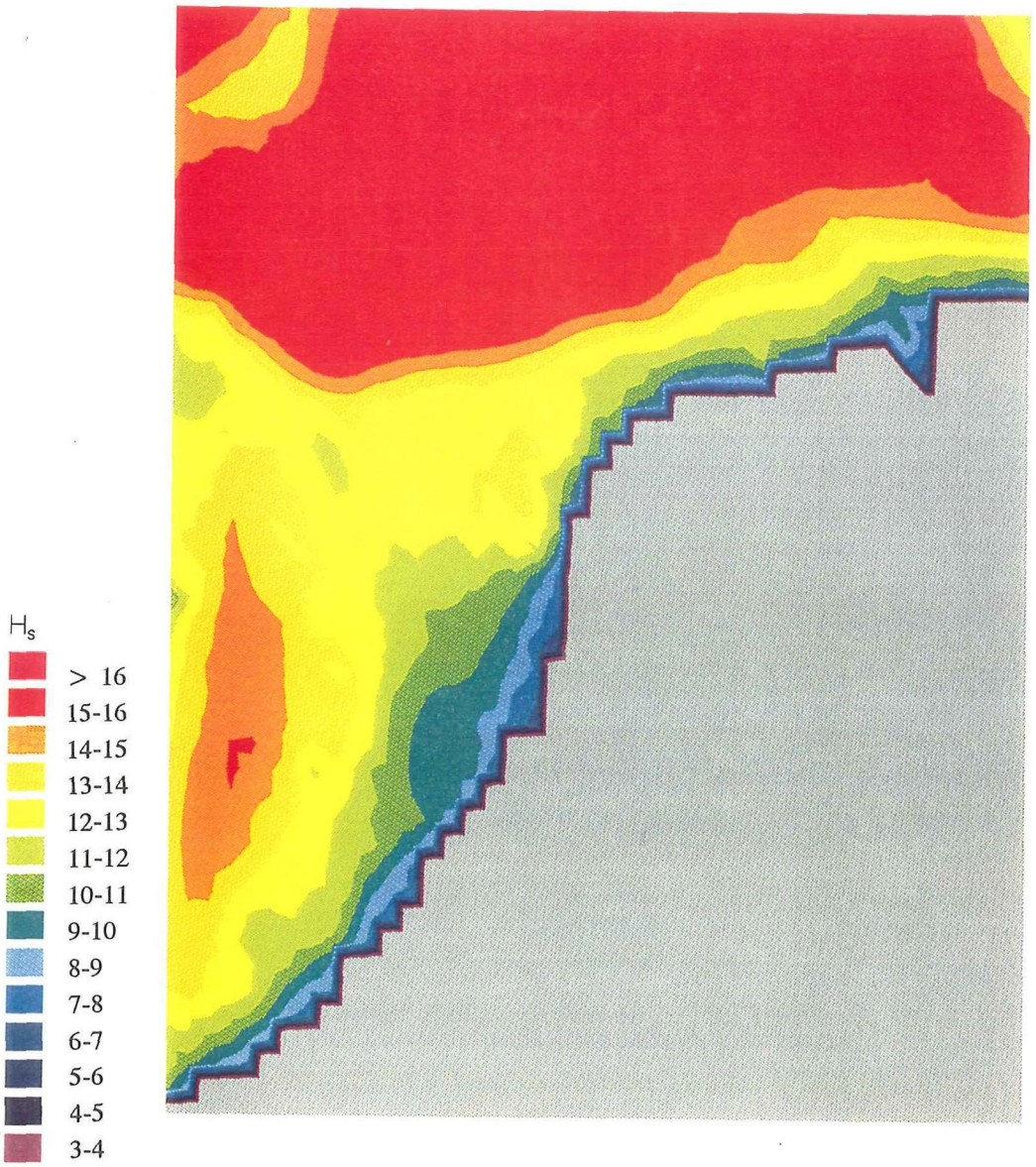


| | |
|---|---|
| Significant wave height in the extreme uniform wind (computation with the maximum wave model and grid G2) | HSMAX |
| Delft University of Technology | Fig. 8 |

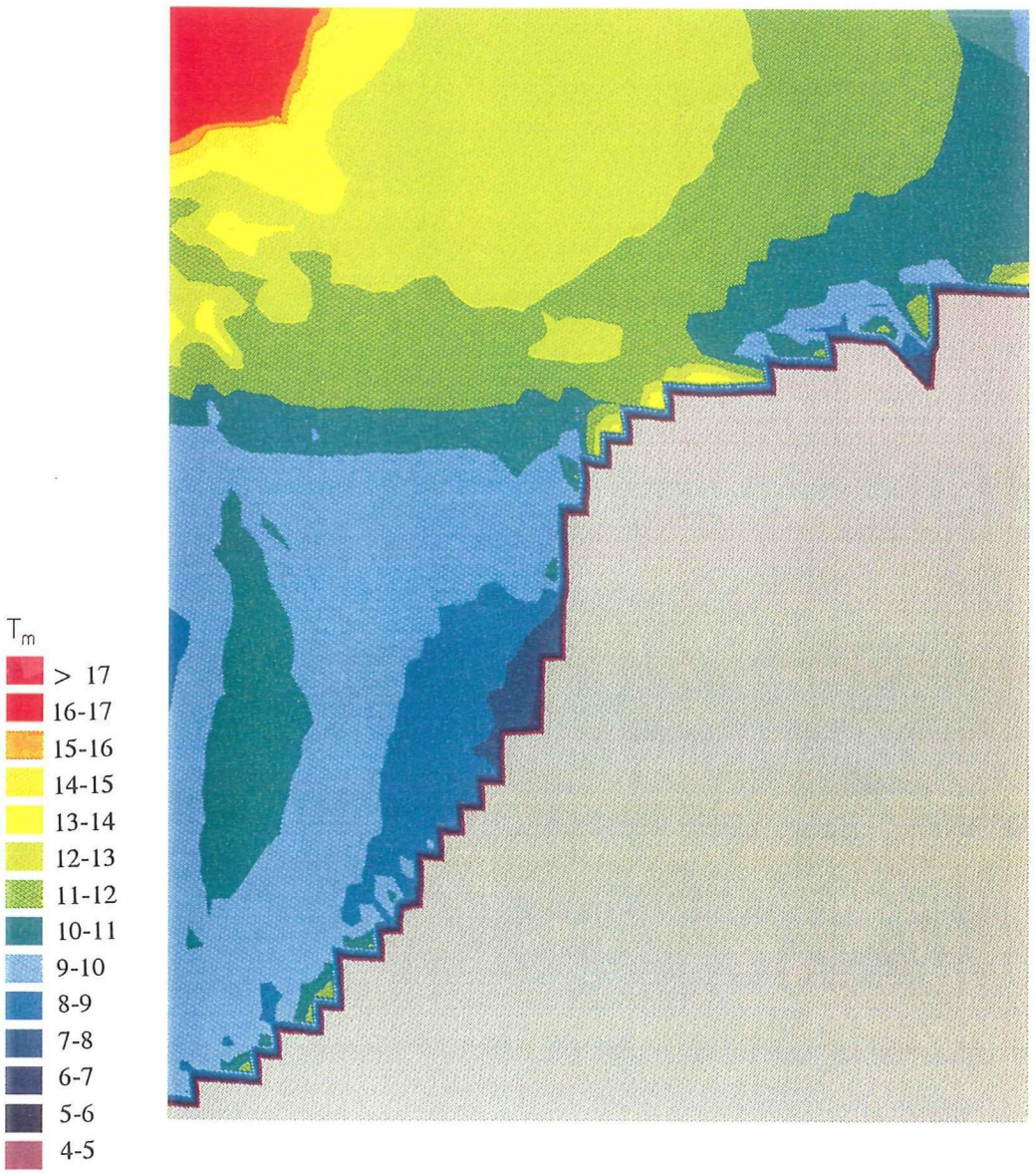


| | |
|---|---|
| Mean wave period in the extreme uniform wind<br>(computation with the maximum wave model and grid G2) | HSMAX |
| Delft University of Technology | Fig. 9 |

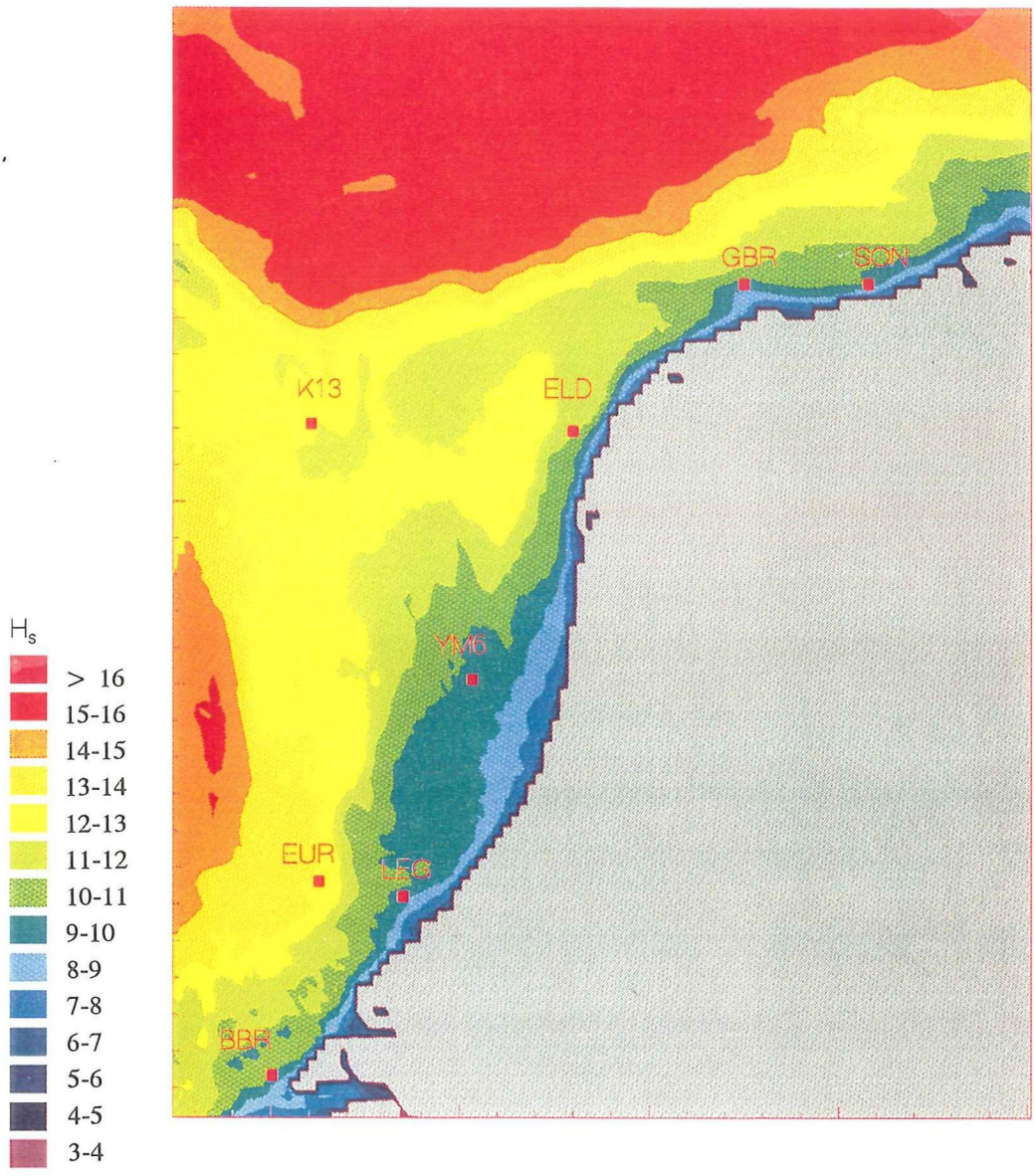


| | |
|---|---|
| Significant wave height in the extreme uniform wind (computation with the maximum wave model and grid G3) | HSMAX |
| Delft University of Technology | Fig. 10 |

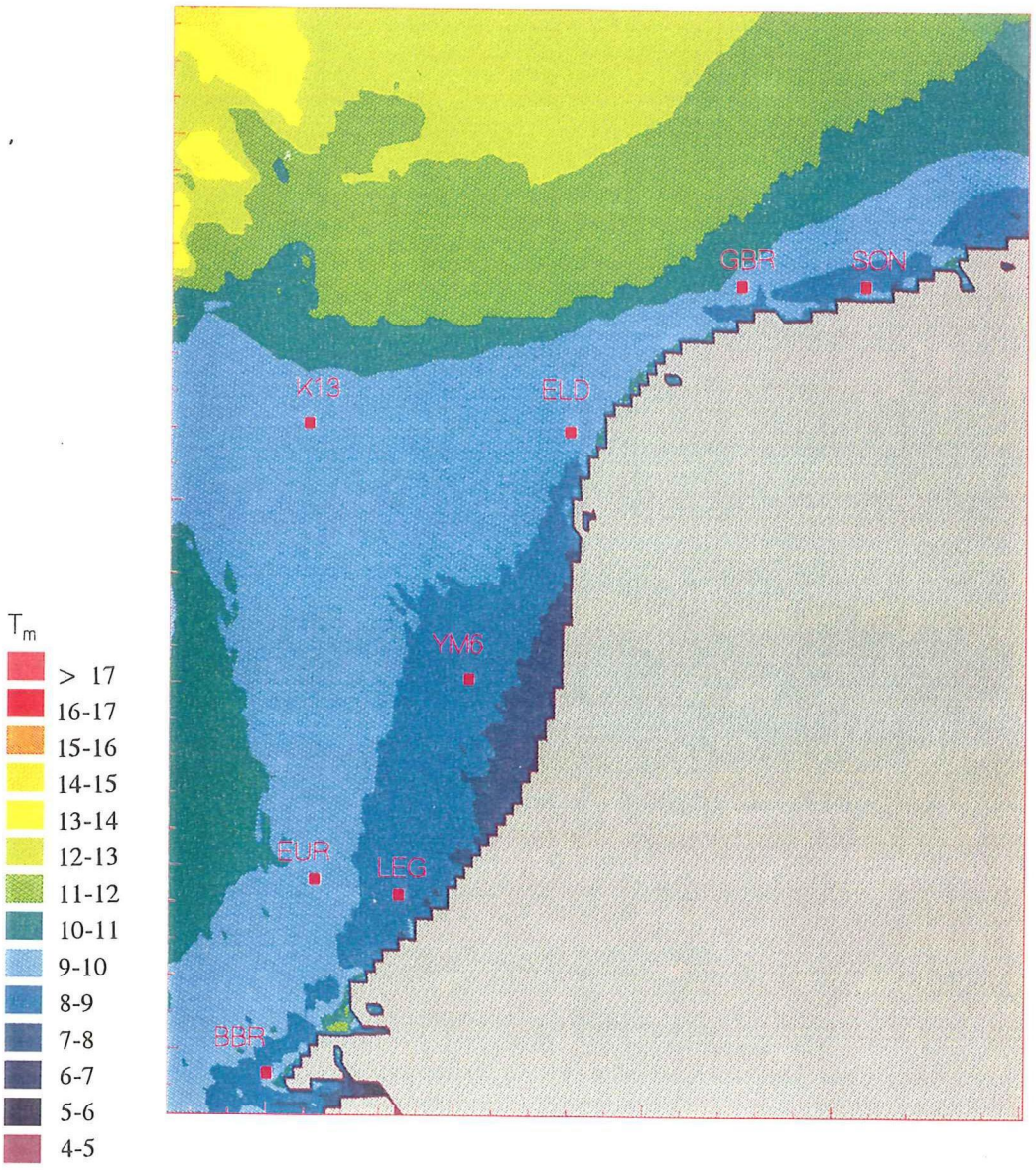


$T_m$

- > 17
- 16-17
- 15-16
- 14-15
- 13-14
- 12-13
- 11-12
- 10-11
- 9-10
- 8-9
- 7-8
- 6-7
- 5-6
- 4-5

| | |
|---|---|
| Mean wave period in the extreme uniform wind (computation with the maximum wave model and grid G3) | HSMAX |
| Delft University of Technology | Fig. 11 |

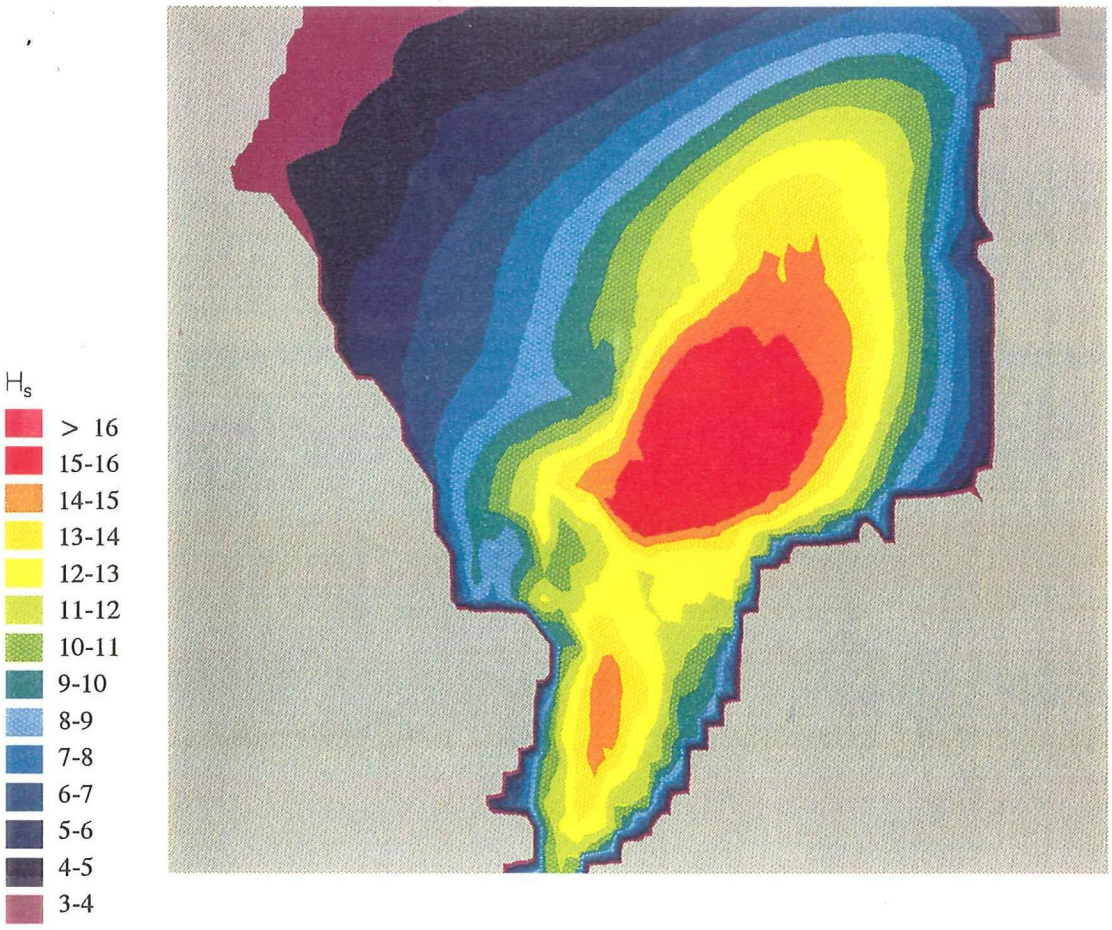


| | |
|---|---|
| Significant wave height in the extreme synthetic storm (computation with the maximum wave model and grid G1) | HSMAX |
| Delft University of Technology | Fig. 12 |

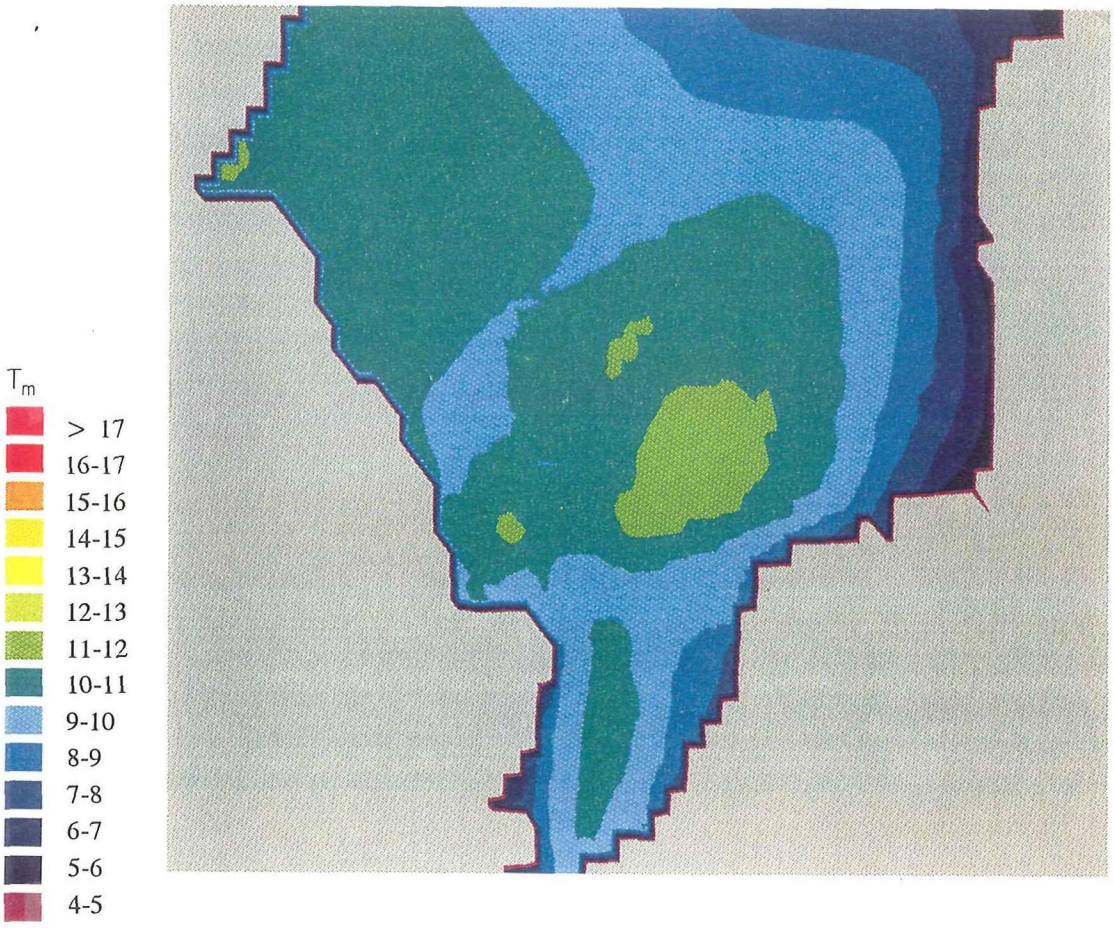


| | |
|---|---|
| Mean wave period in the extreme synthetic storm (computation with the maximum wave model and grid G1) | HSMAX |
| Delft University of Technology | Fig. 13 |

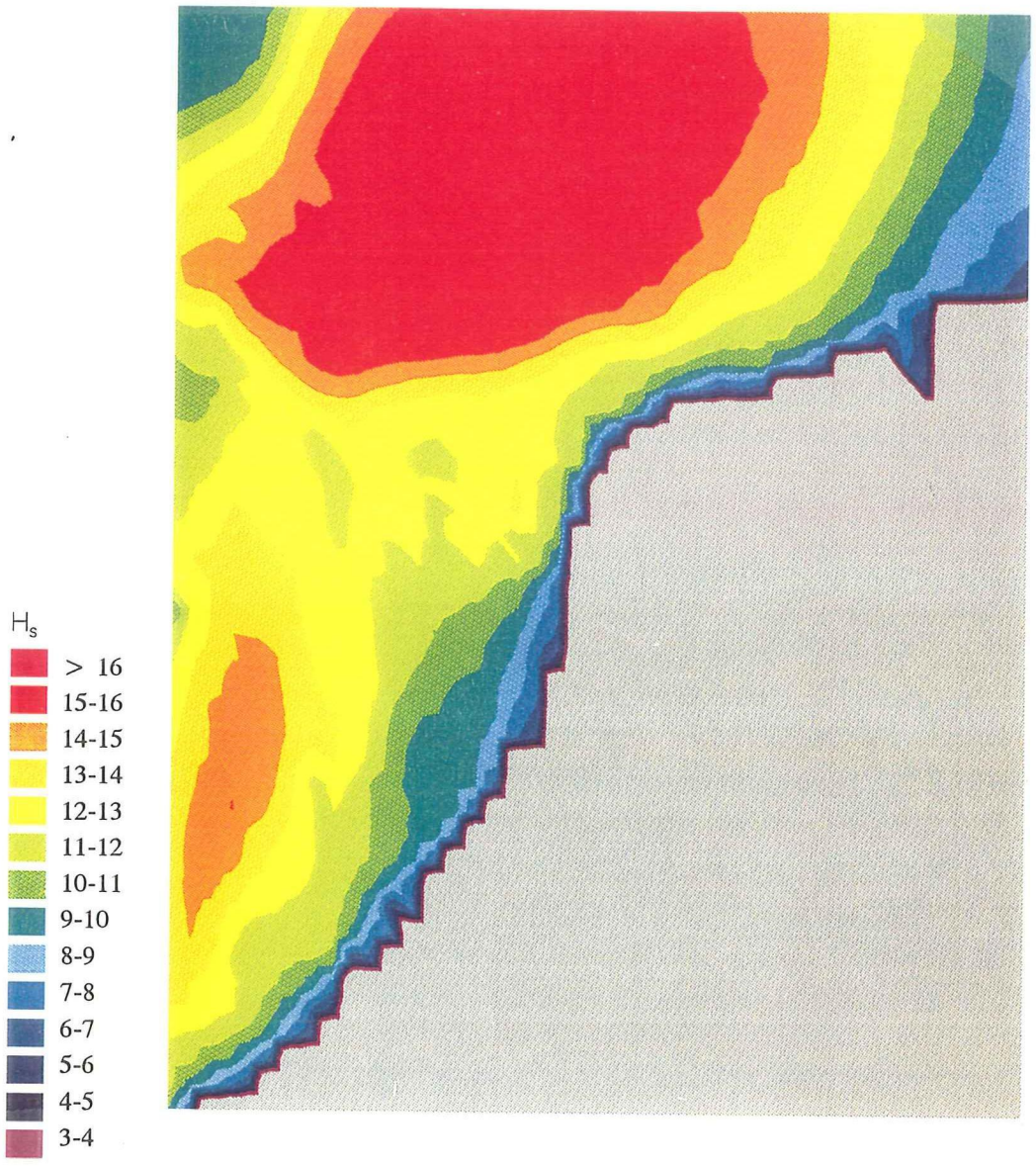


| Significant wave height in the extreme synthetic storm (computation with the maximum wave model and grid G2) | HSMAX |
|---|---|
| Delft University of Technology | Fig. 14 |

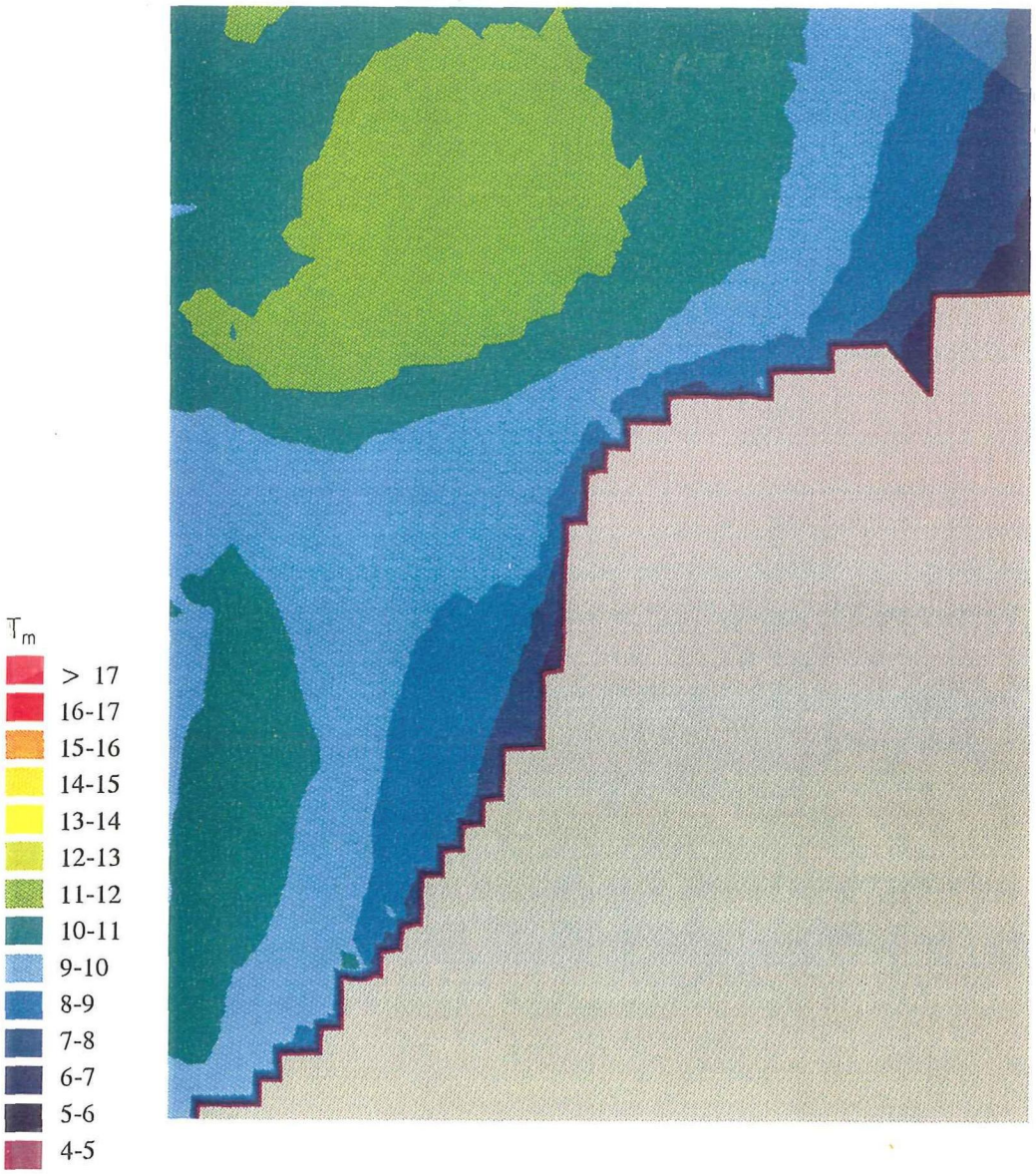


| | |
|---|---|
| Mean wave period in the extreme synthetic storm (computation with the maximum wave model and grid G2) | HSMAX |
| Delft University of Technology | Fig. 15 |

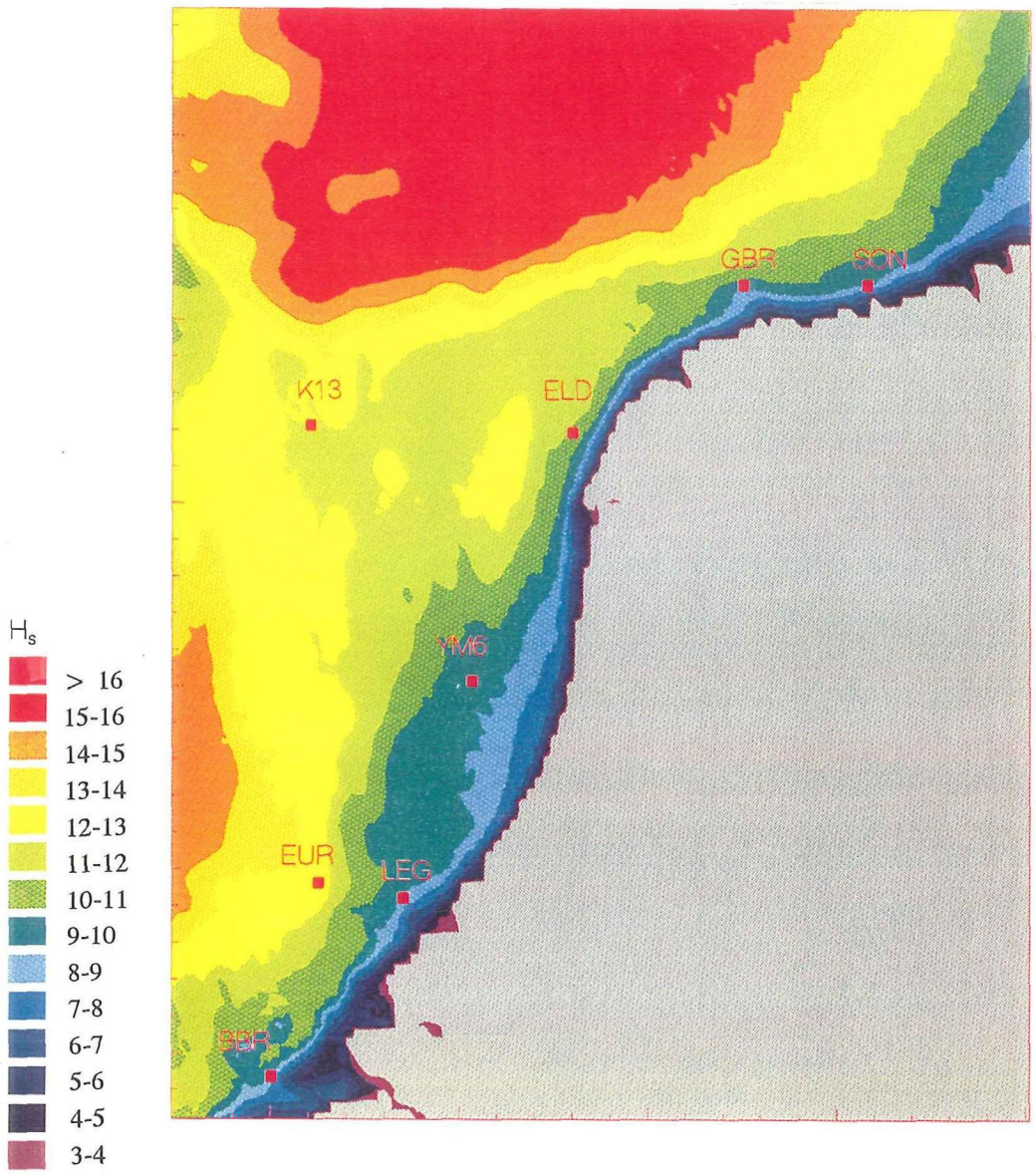


| | |
|---|---|
| Significant wave height in the extreme synthetic storm (computation with the maximum wave model and grid G3) | HSMAX |
| Delft University of Technology | Fig. 16 |

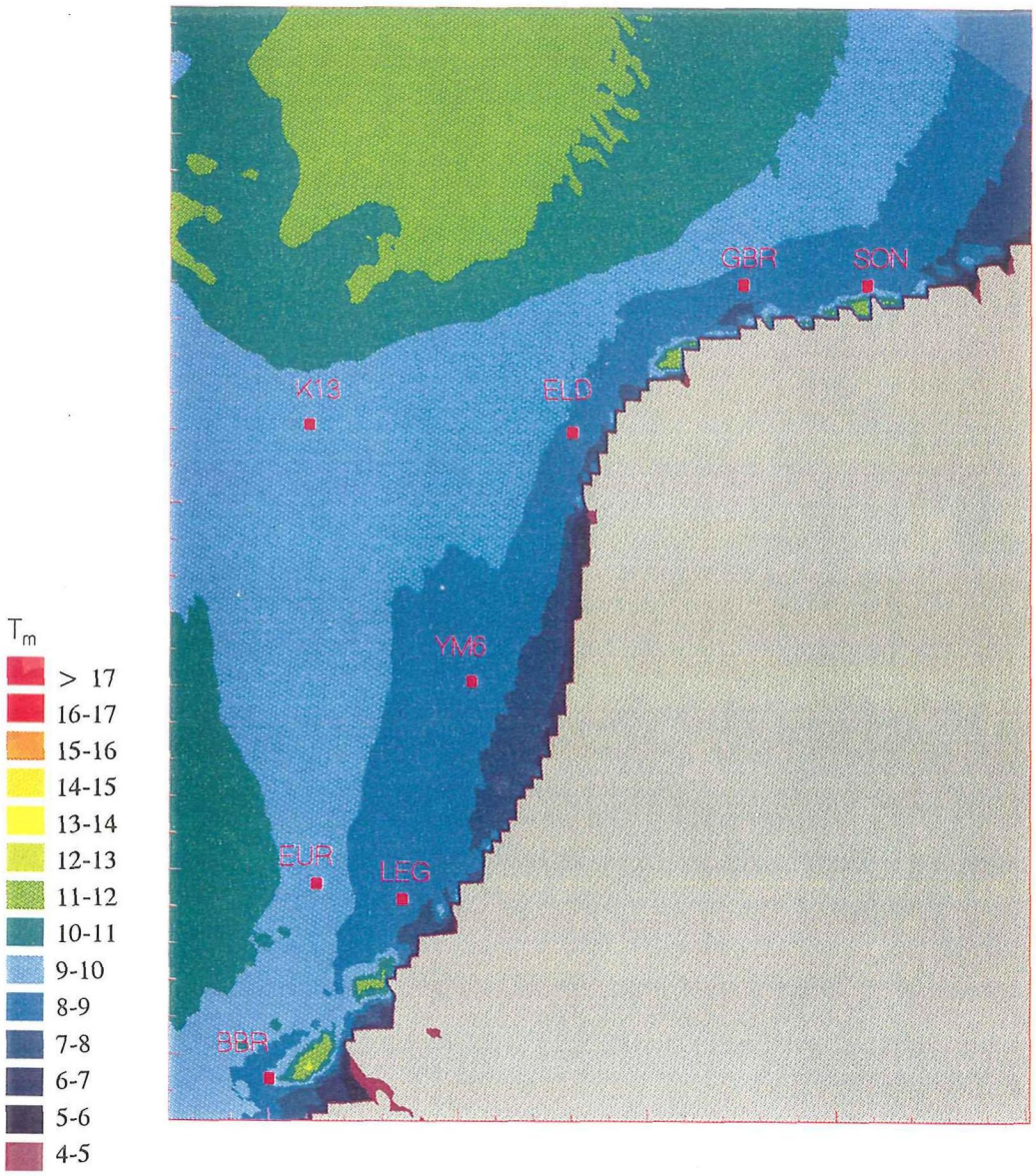


| | |
|---|---|
| Mean wave period in the extreme synthetic storm (computation with the maximum wave model and grid G3) | HSMAX |
| Delft University of Technology | Fig. 17 |

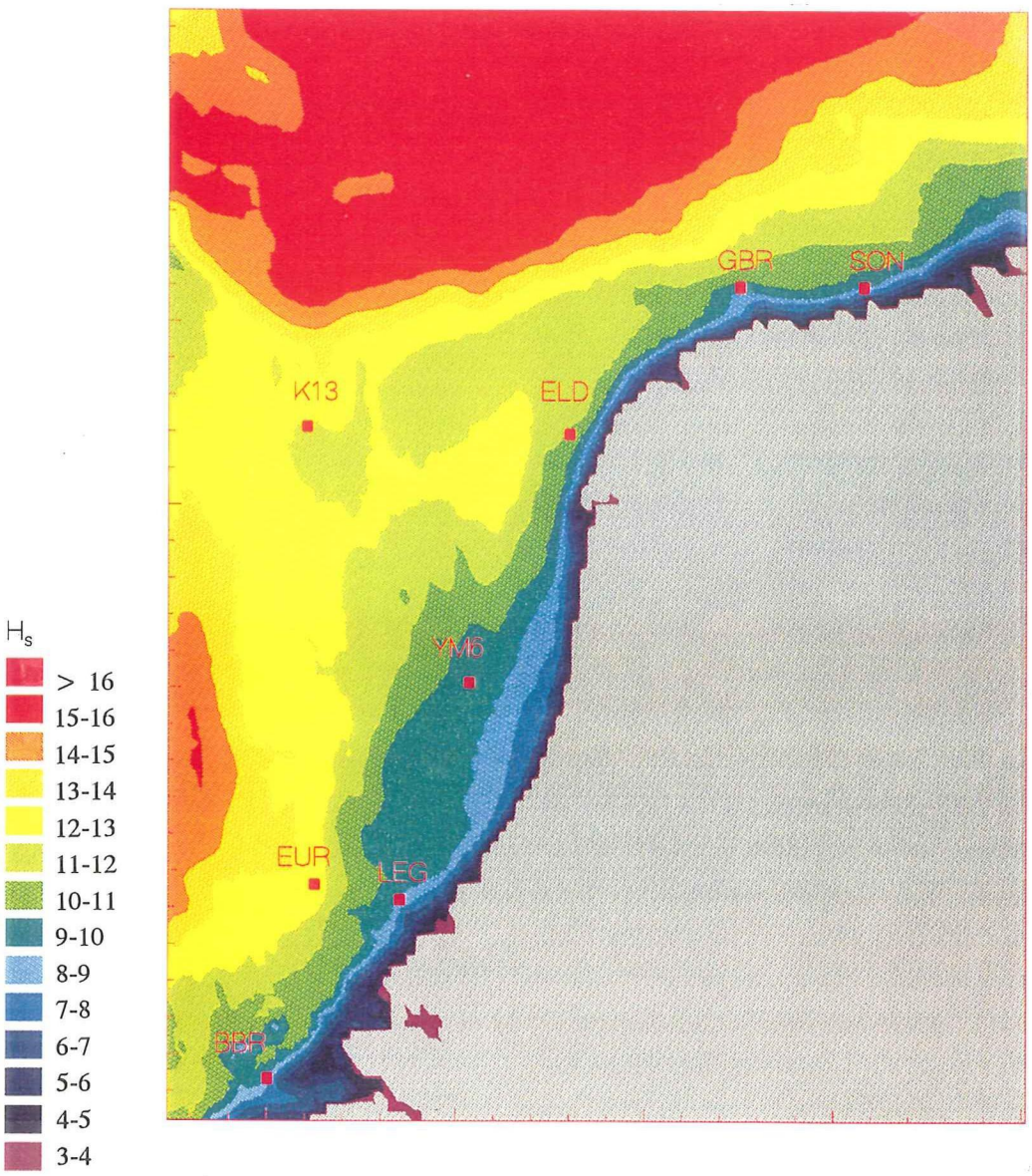


| | |
|---|---|
| Maximum significant wave height in the extreme synthetic storm (computation with the maximum wave model and grid G3) | HSMAX |
| Delft University of Technology | Fig. 18 |

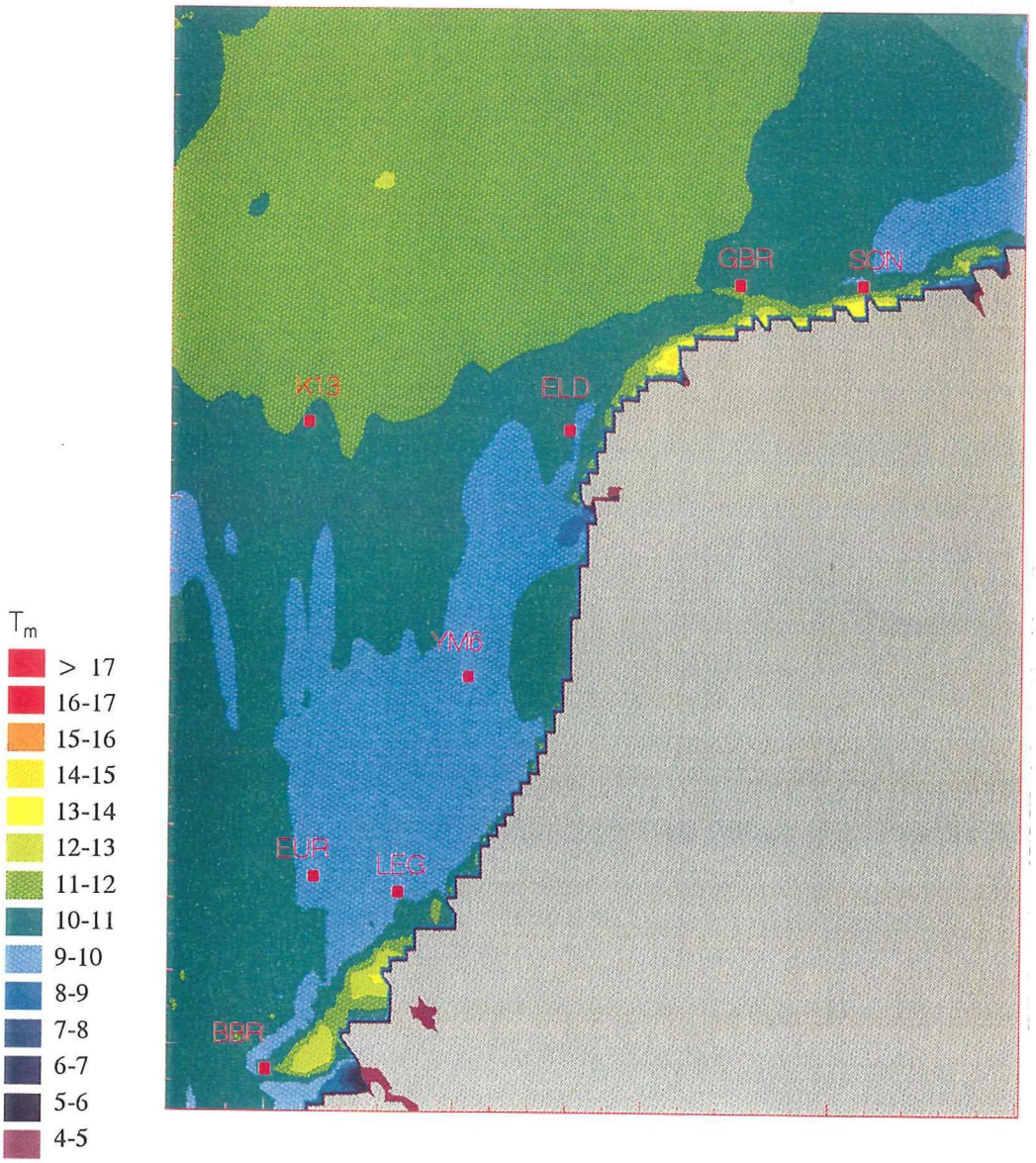


| | |
|---|---|
| Maximum mean wave period in the extreme synthetic storm (computation with the maximum wave model and grid G3) | HSMAX |
| | |
| Delft University of Technology | Fig. 19 |

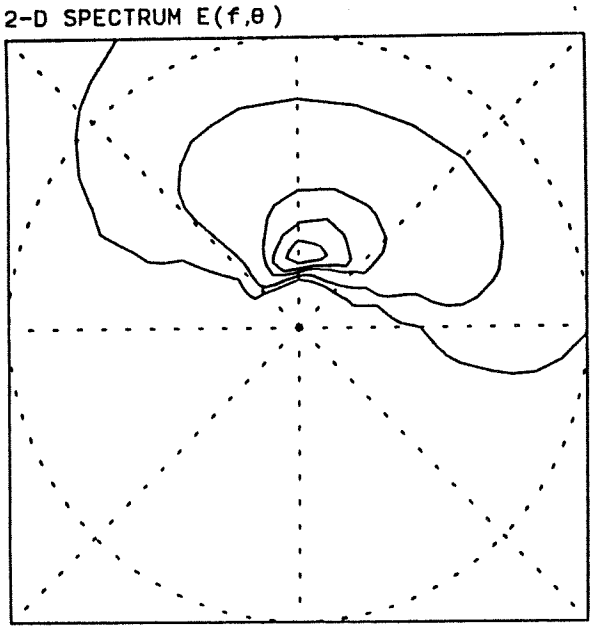


Contour levels :

.600 $E_{max}$
.250 $E_{max}$
.100 $E_{max}$
.010 $E_{max}$
.001 $E_{max}$

Freq. scales :

.250 Hz

North :

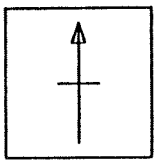

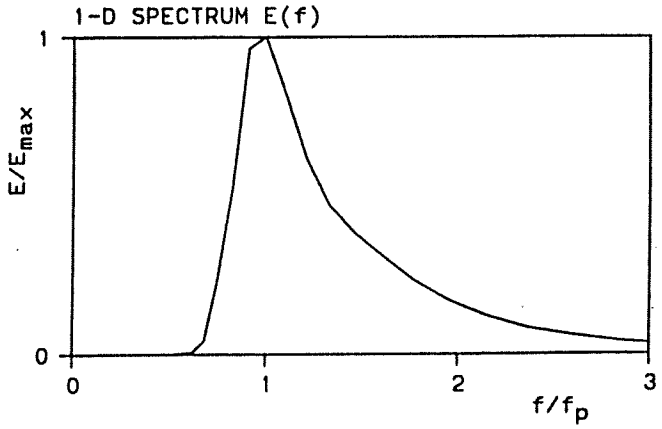


Integral parameters :

$H_s$ = 10.38 m
$f_p$ = .066 Hz
$\bar{f}$ = .102 Hz
$\bar{\theta}$ = 12.9 °
$\bar{\sigma}_\theta$ = 23.9 °

(Computations with the maximum wave model and grid G3)

| | |
|---|---|
| Polar plot of computed wave spectrum at the peak of the extreme synthetic storm at SON | HSMAX |
| Delft University of Technology | Fig. 20 |

2-D SPECTRUM E(f,θ)

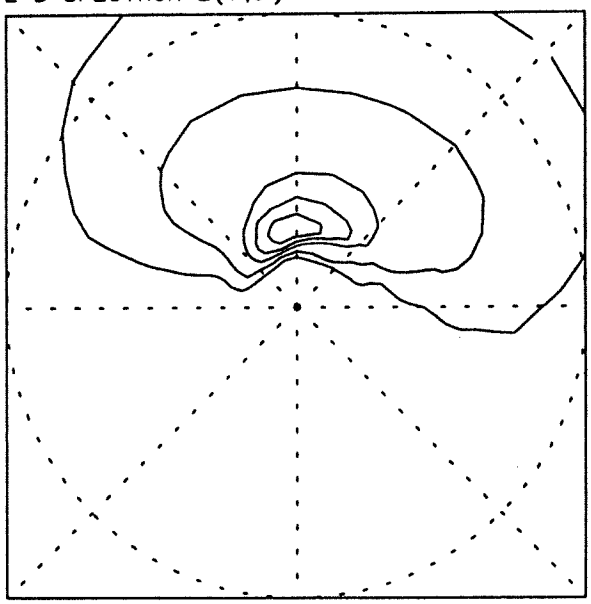

Contour levels :

.600 $E_{max}$
.250 $E_{max}$
.100 $E_{max}$
.010 $E_{max}$
.001 $E_{max}$

Freq. scales :

.250 Hz

North :

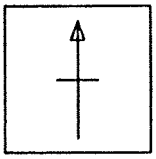

1-D SPECTRUM E(f)

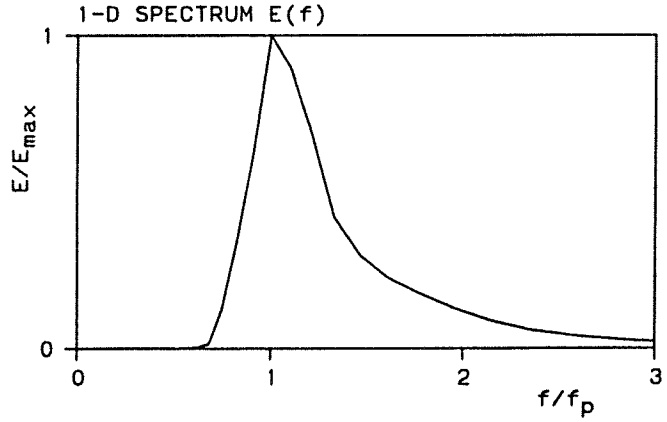


Integral parameters :

$H_s$ = 12.16 m
$f_p$ = .066 Hz
$\bar{f}$ = .098 Hz
$\bar{\theta}$ = 4.7 °
$\bar{\sigma}_\theta$ = 25.5 °

(Computations with the maximum wave model and grid G3)

| | |
|---|---|
| Polar plot of computed wave spectrum at the peak of the extreme synthetic storm at ELD | HSMAX |
| Delft University of Technology | Fig. 21 |

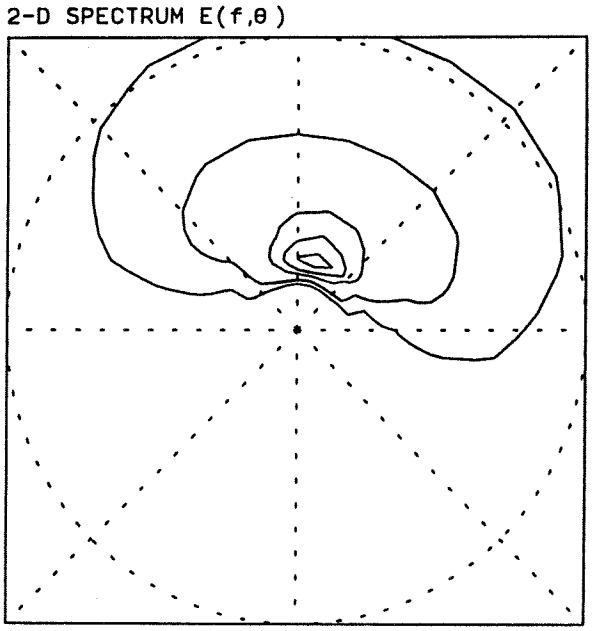


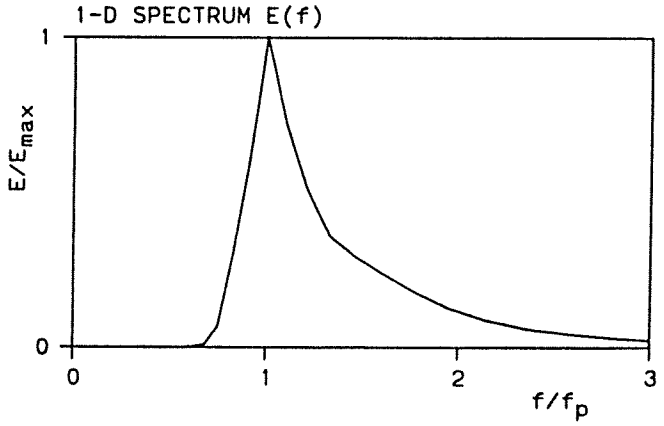


Integral parameters :

$H_s$ = 12.99 m
$f_p$ = .060 Hz
$\bar{f}$ = .092 Hz
$\bar{\theta}$ = 14.0 °
$\bar{\sigma}_\theta$ = 24.5 °

(Computations with the maximum wave model and grid G3)

| | |
|---|---|
| Polar plot of computed wave spectrum at the peak of the extreme synthetic storm at K13 | HSMAX |
| Delft University of Technology | Fig. 22 |

2-D SPECTRUM E(f,θ)

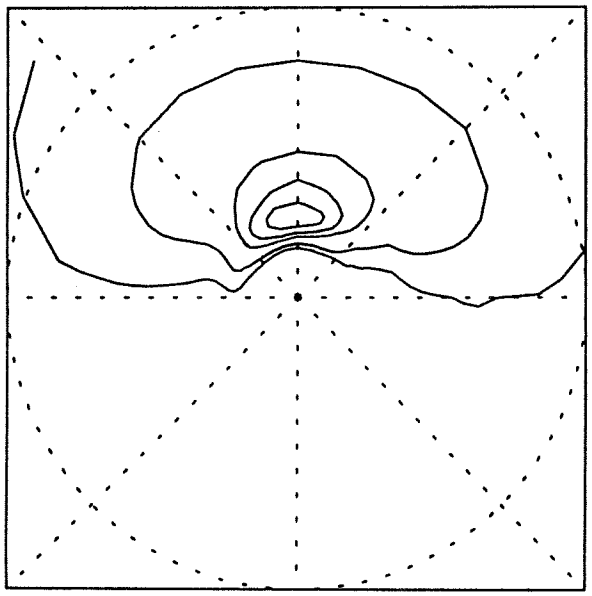

Contour levels :

.600 $E_{max}$
.250 $E_{max}$
.100 $E_{max}$
.010 $E_{max}$
.001 $E_{max}$

Freq. scales :

.250 Hz

North :

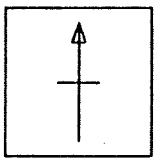

1-D SPECTRUM E(f)

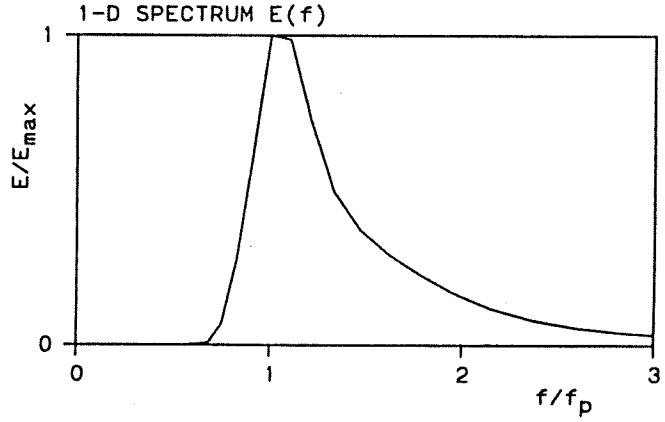


Integral parameters :

$H_s$ = 10.60 m
$f_p$ = .066 Hz
$\bar{f}$ = .103 Hz
$\bar{\theta}$ = .1 °
$\bar{\sigma}_\theta$ = 25.2 °

(Computations with the maximum wave model and grid G3)

| | |
|---|---|
| Polar plot of computed wave spectrum at the peak of the extreme synthetic storm at YM6 | HSMAX |
| Delft University of Technology | Fig. 23 |

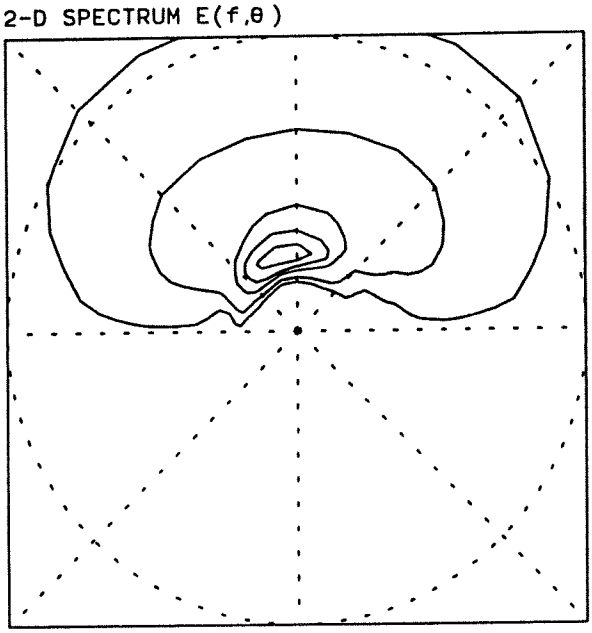


Contour levels :

.600 $E_{max}$
.250 $E_{max}$
.100 $E_{max}$
.010 $E_{max}$
.001 $E_{max}$

Freq. scales :

.250 Hz

North :

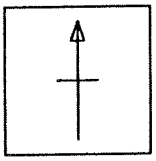

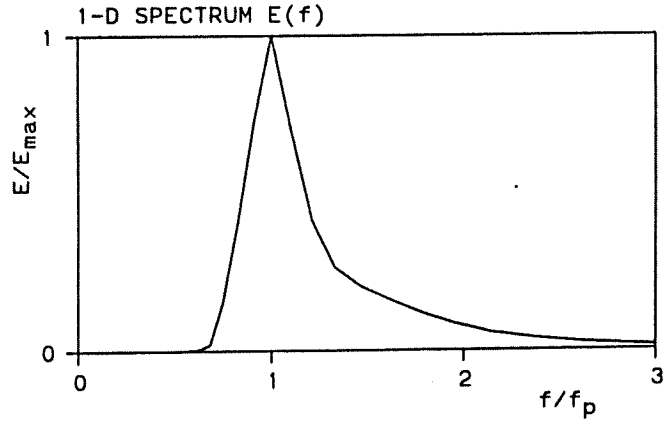


Integral parameters :

$H_s$ = 13.54 m
$f_p$ = .066 Hz
$\bar{f}$ = .092 Hz
$\bar{\theta}$ = 353.3 °
$\bar{\sigma}_\theta$ = 25.0 °

(Computations with the maximum wave model and grid G3)

| | |
|---|---|
| Polar plot of computed wave spectrum at the peak of the extreme synthetic storm at EUR | HSMAX |
| Delft University of Technology | Fig. 24 |

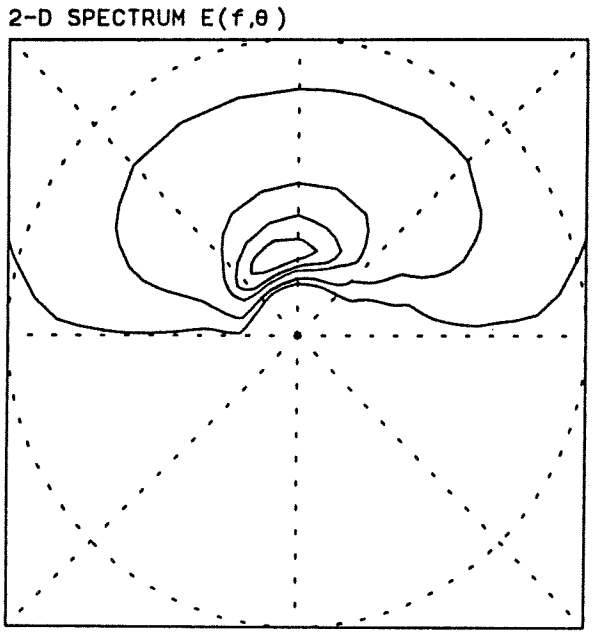


Contour levels :

.600 $E_{max}$
.250 $E_{max}$
.100 $E_{max}$
.010 $E_{max}$
.001 $E_{max}$

Freq. scales :

.250 Hz

North :

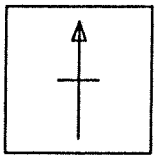

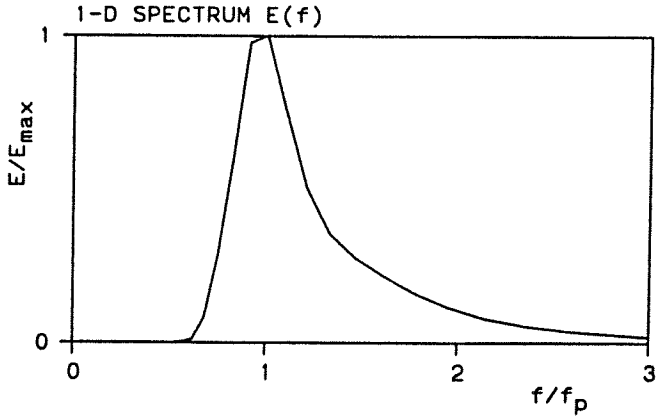


Integral parameters :

$H_s$ = 10.54 m
$f_p$ = .073 Hz
$\bar{f}$ = .102 Hz
$\bar{\theta}$ = 352.7 °
$\bar{\sigma}_\theta$ = 26.3 °

(Computations with the maximum wave model and grid G3)

| | |
|---|---|
| Polar plot of computed wave spectrum at the peak of the extreme synthetic storm at LEG | HSMAX |
| | |
| Delft University of Technology | Fig. 25 |

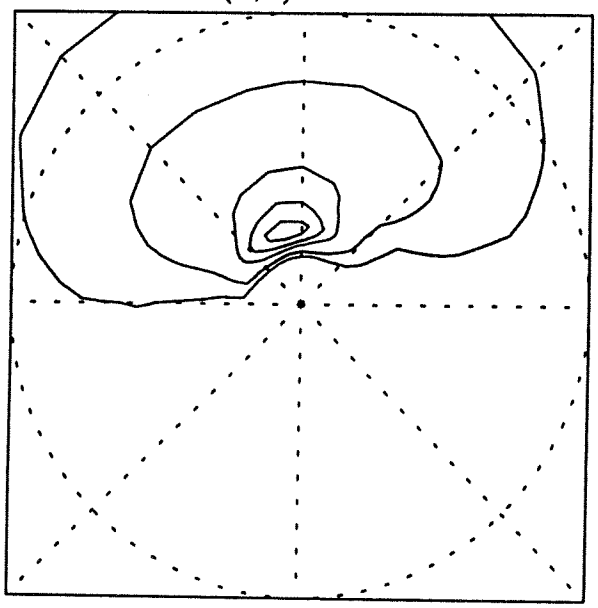


Contour levels :

.600 $E_{max}$
.250 $E_{max}$
.100 $E_{max}$
.010 $E_{max}$
.001 $E_{max}$

Freq. scales :

.250 Hz

North :

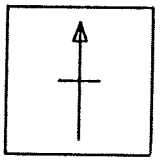

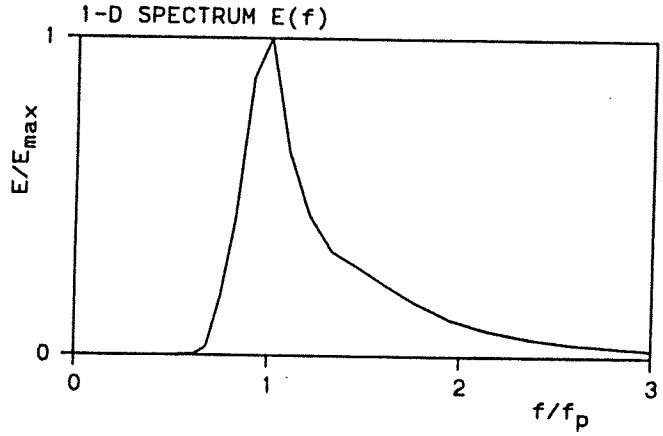


Integral parameters :

$H_s$ = 9.35 m
$f_p$ = .066 Hz
$\bar{f}$ = .098 Hz
$\bar{\theta}$ = 348.3 °
$\bar{\sigma}_\theta$ = 23.4 °

(Computations with the maximum wave model and grid G3)

| | |
|---|---|
| Polar plot of computed wave spectrum at the peak of the extreme synthetic storm at BBR | HSMAX |
| Delft University of Technology | Fig. 26 |

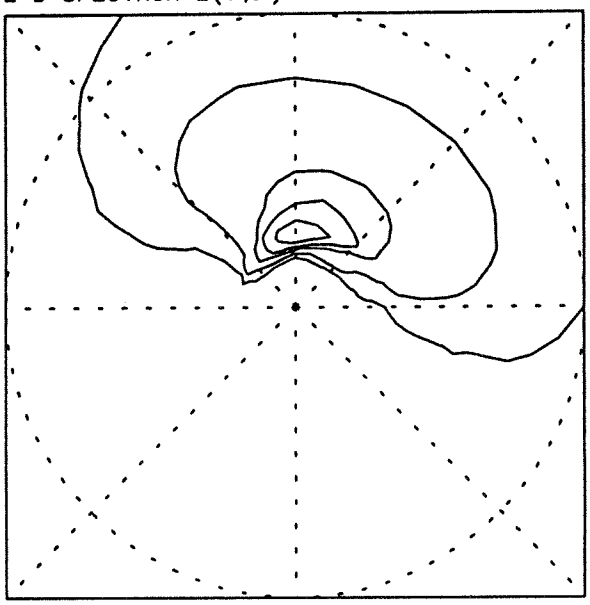


Contour levels :

.600 $E_{max}$
.250 $E_{max}$
.100 $E_{max}$
.010 $E_{max}$
.001 $E_{max}$

Freq. scales :

.250 Hz

North :

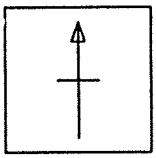

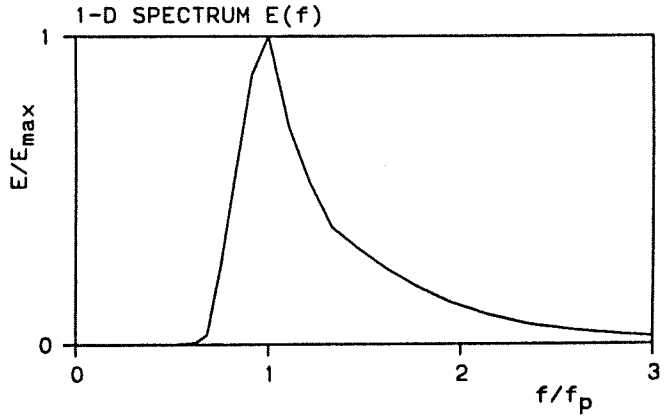


Integral parameters :

$H_s$ = 11.85 m
$f_p$ = .066 Hz
$\bar{f}$ = .098 Hz
$\bar{\theta}$ = 13.4 °
$\bar{\sigma}_\theta$ = 25.9 °

(Computations with the maximum wave model and grid G3)

| | |
|---|---|
| Polar plot of computed wave spectrum at the peak of the extreme synthetic storm at GBR | HSMAX |
| Delft University of Technology | Fig. 27 |

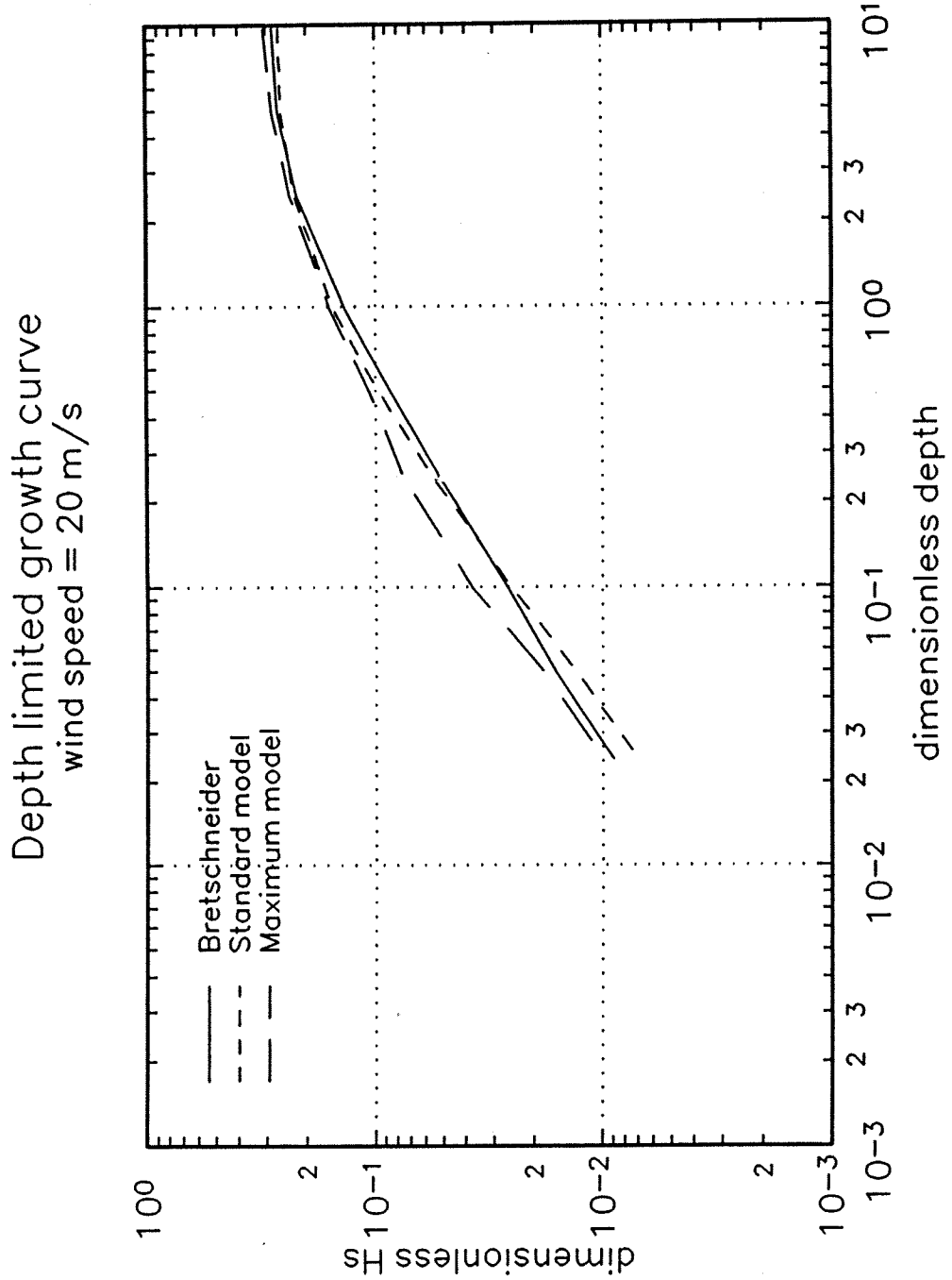


| | |
|---|---|
| Depth limited growth curves for 20 m/s wind speed | HSMAX |
| | |
| Delft University of Technology | Fig. 28 |

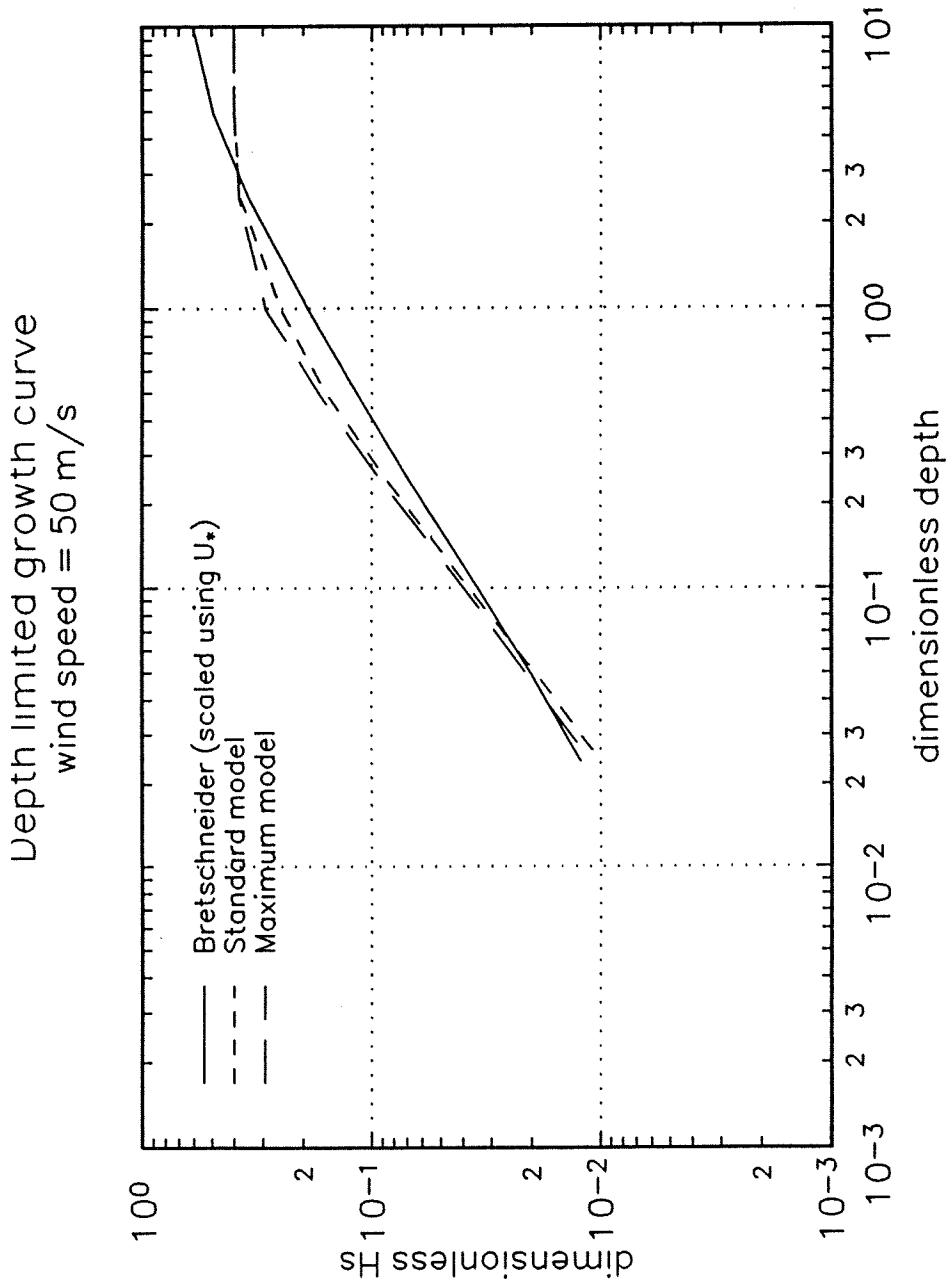


| | |
|---|---|
| Depth limited growth curves for 50 m/s wind speed | HSMAX |
| | |
| Delft University of Technology | Fig. 29 |

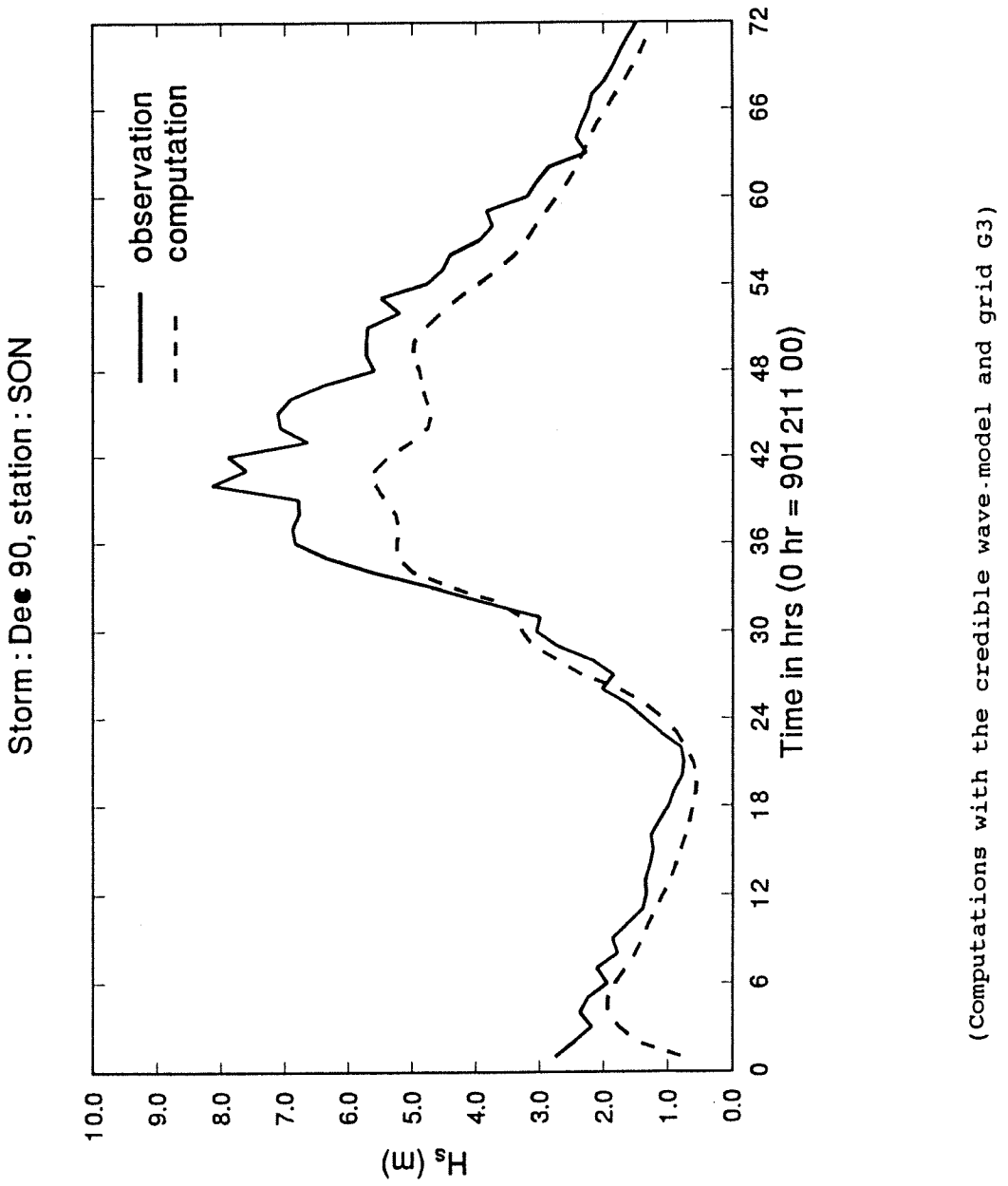


| | |
|---|---|
| Comparison between observed and computed significant wave height for Dec 90 storm at SON | HSMAX |
| Delft University of Technology | Fig. 30 |

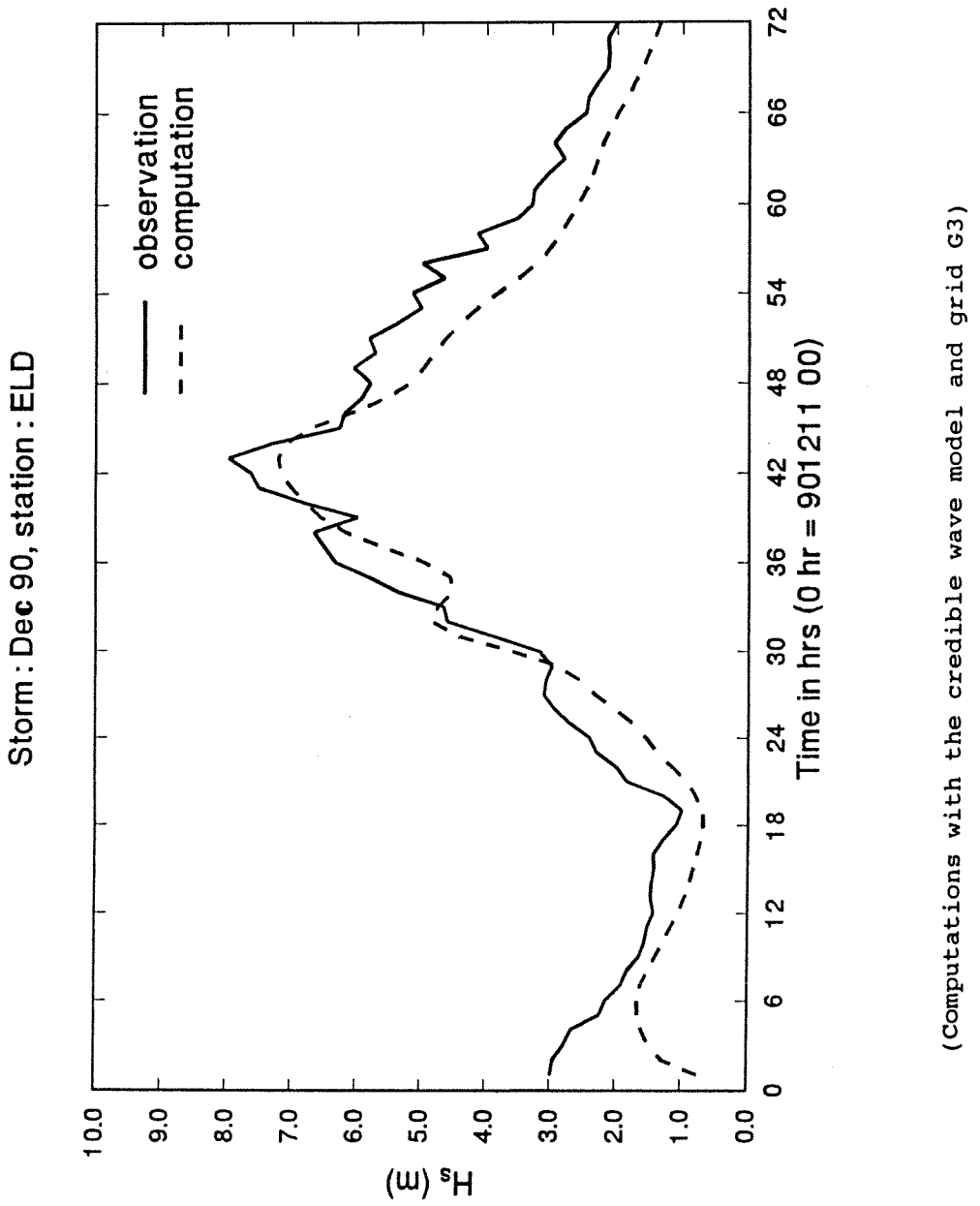


| | |
|---|---|
| Comparison between observed and computed significant wave height for Dec 90 storm at ELD | HSMAX |
| Delft University of Technology | Fig. 31 |

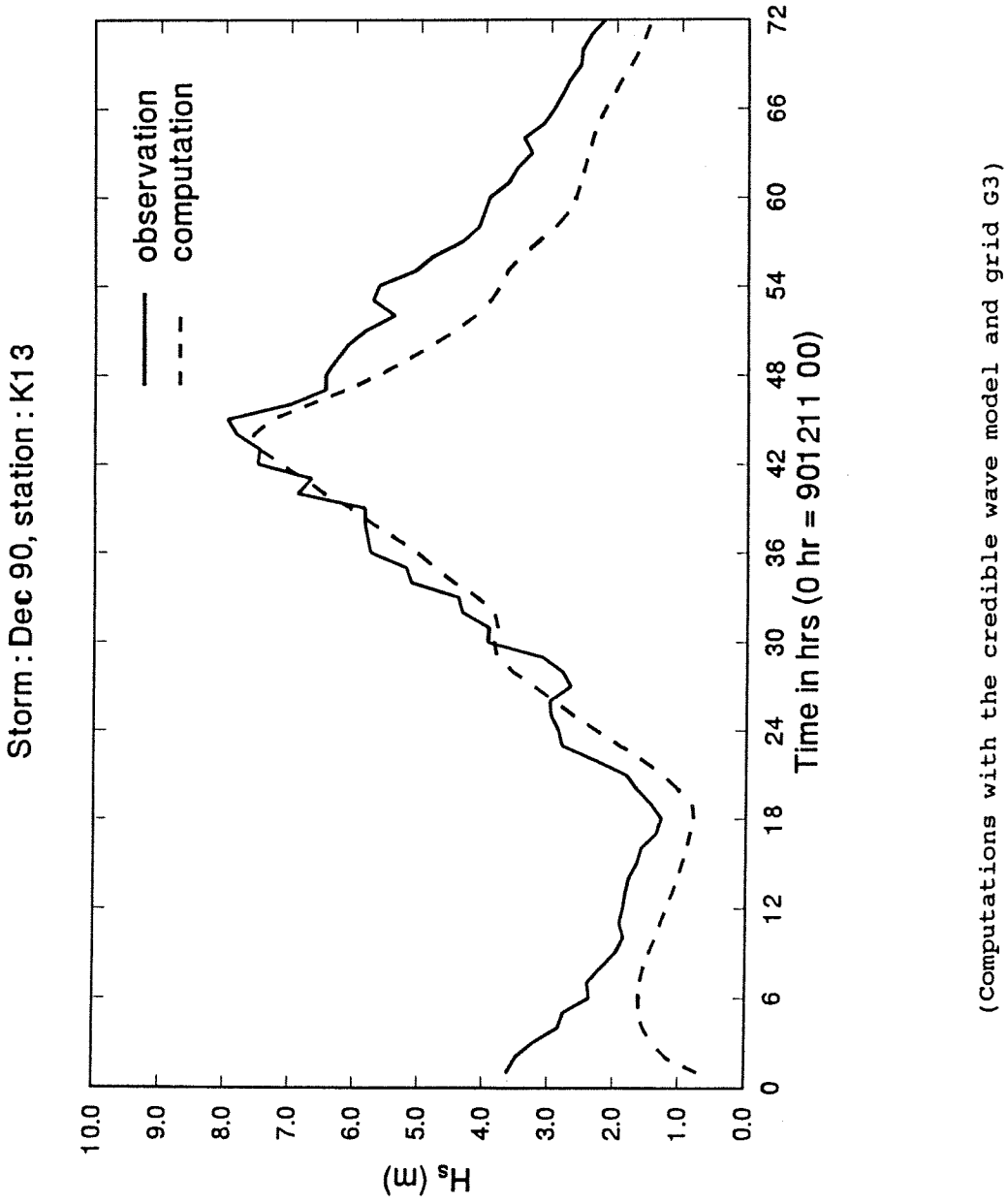


| | |
|---|---|
| Comparison between observed and computed significant wave height for Dec 90 storm at K13 | HSMAX |
| Delft University of Technology | Fig. 32 |

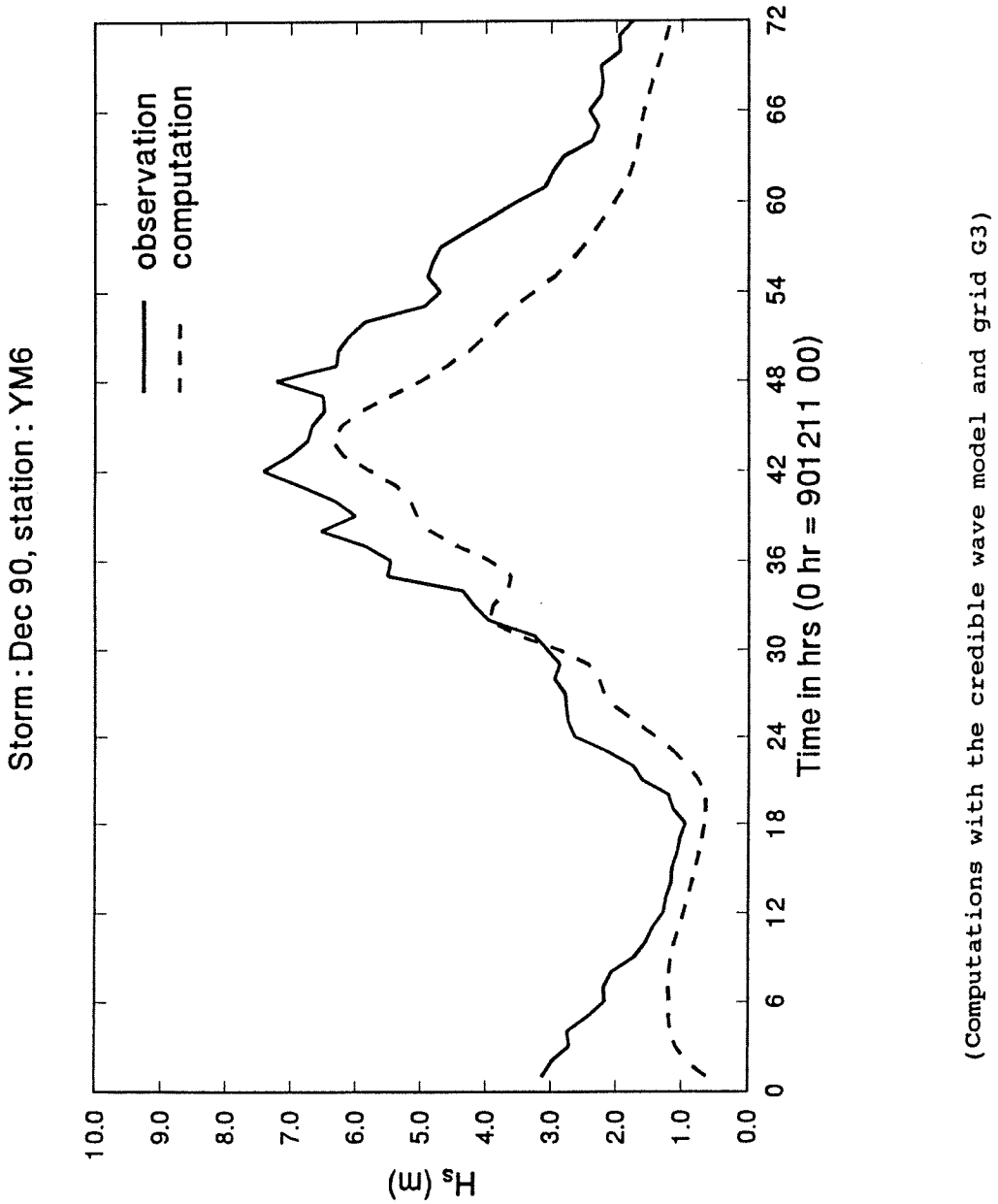


| | |
|---|---|
| Comparison between observed and computed significant wave height for Dec 90 storm at YM6 | HSMAX |
| Delft University of Technology | Fig. 33 |

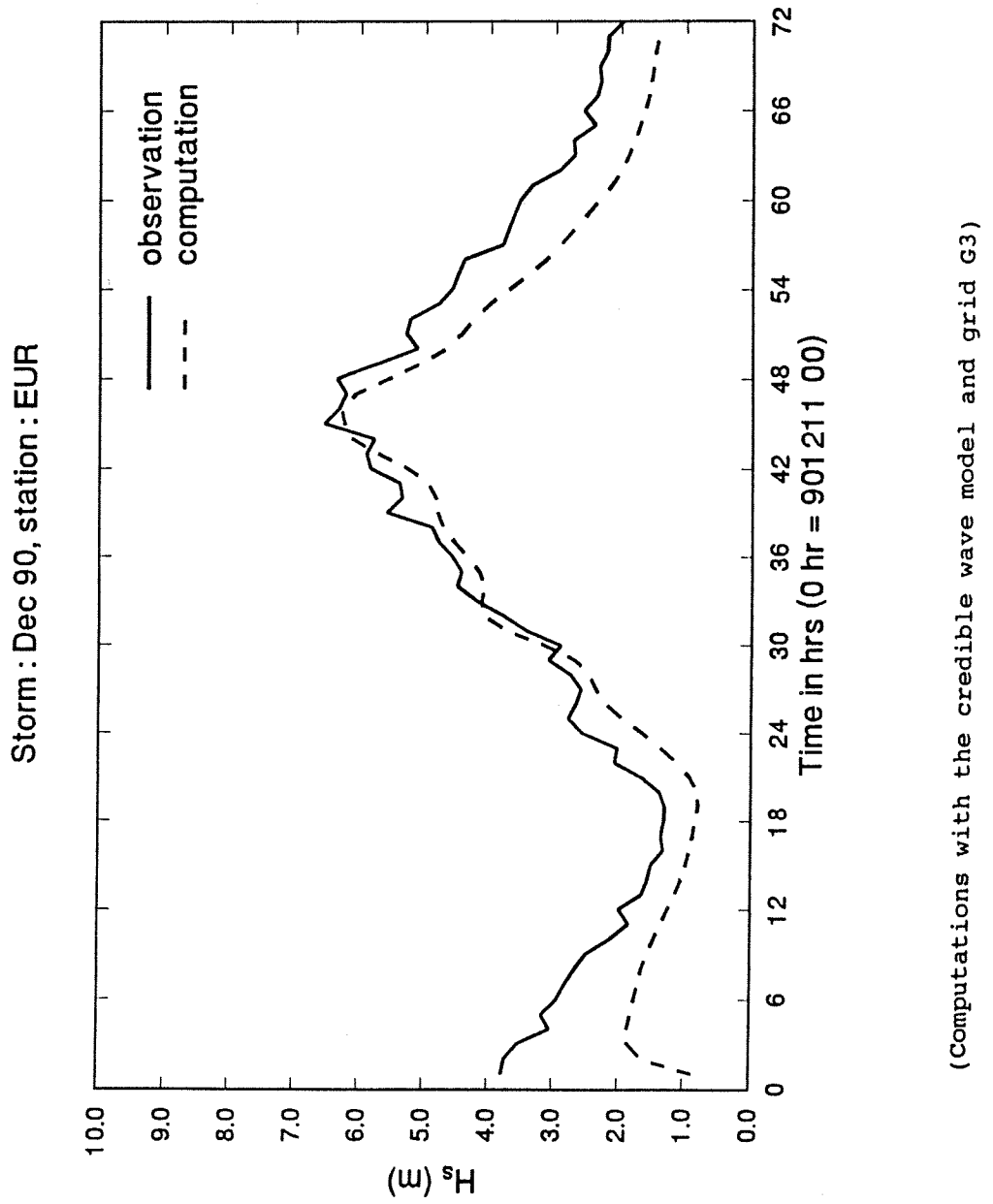


| | |
|---|---|
| Comparison between observed and computed significant wave height for Dec 90 storm at EUR | HSMAX |
| Delft University of Technology | Fig. 34 |

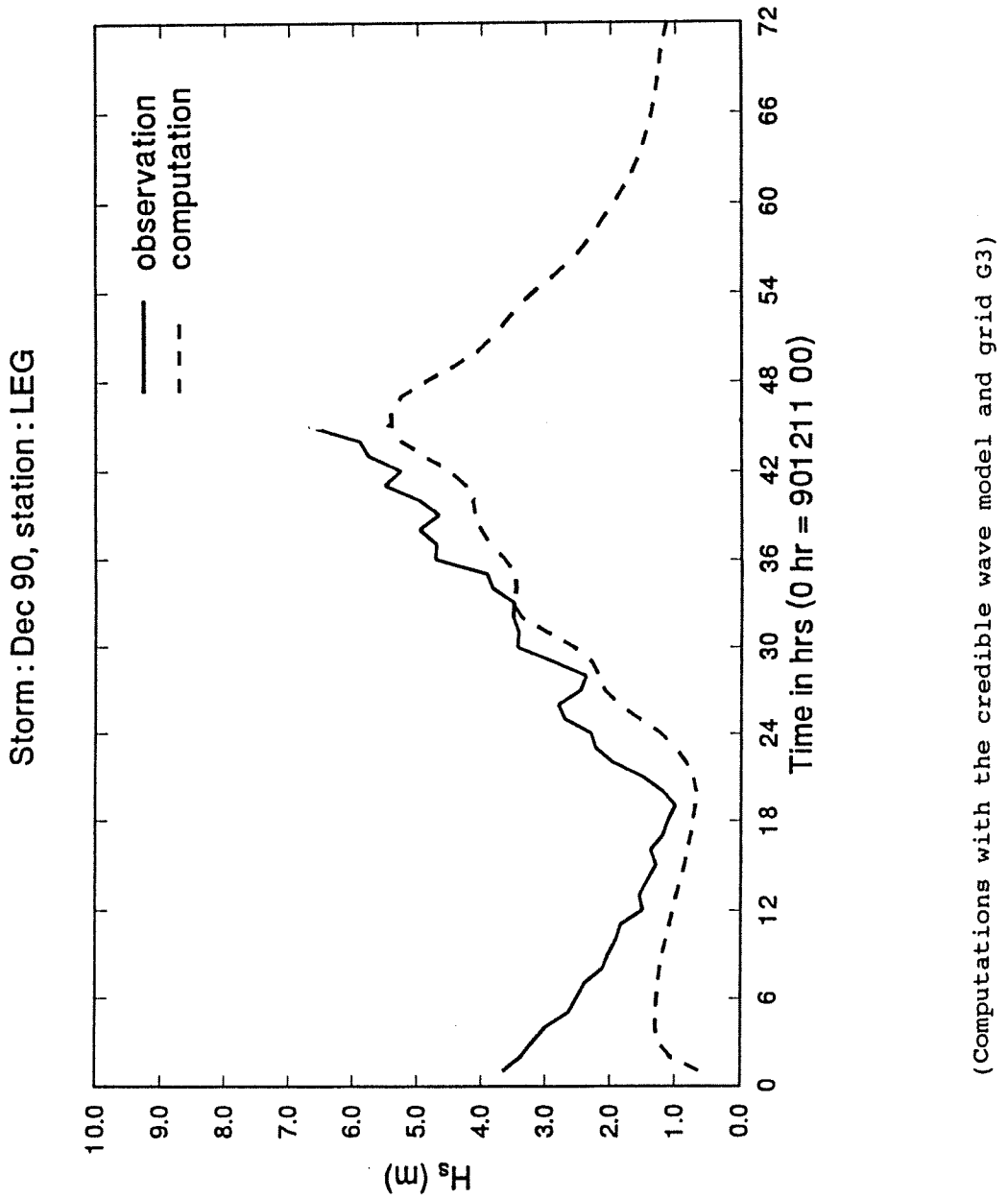


| | |
|---|---|
| Comparison between observed and computed significant wave height for Dec 90 storm at LEG | HSMAX |
| Delft University of Technology | Fig. 35 |

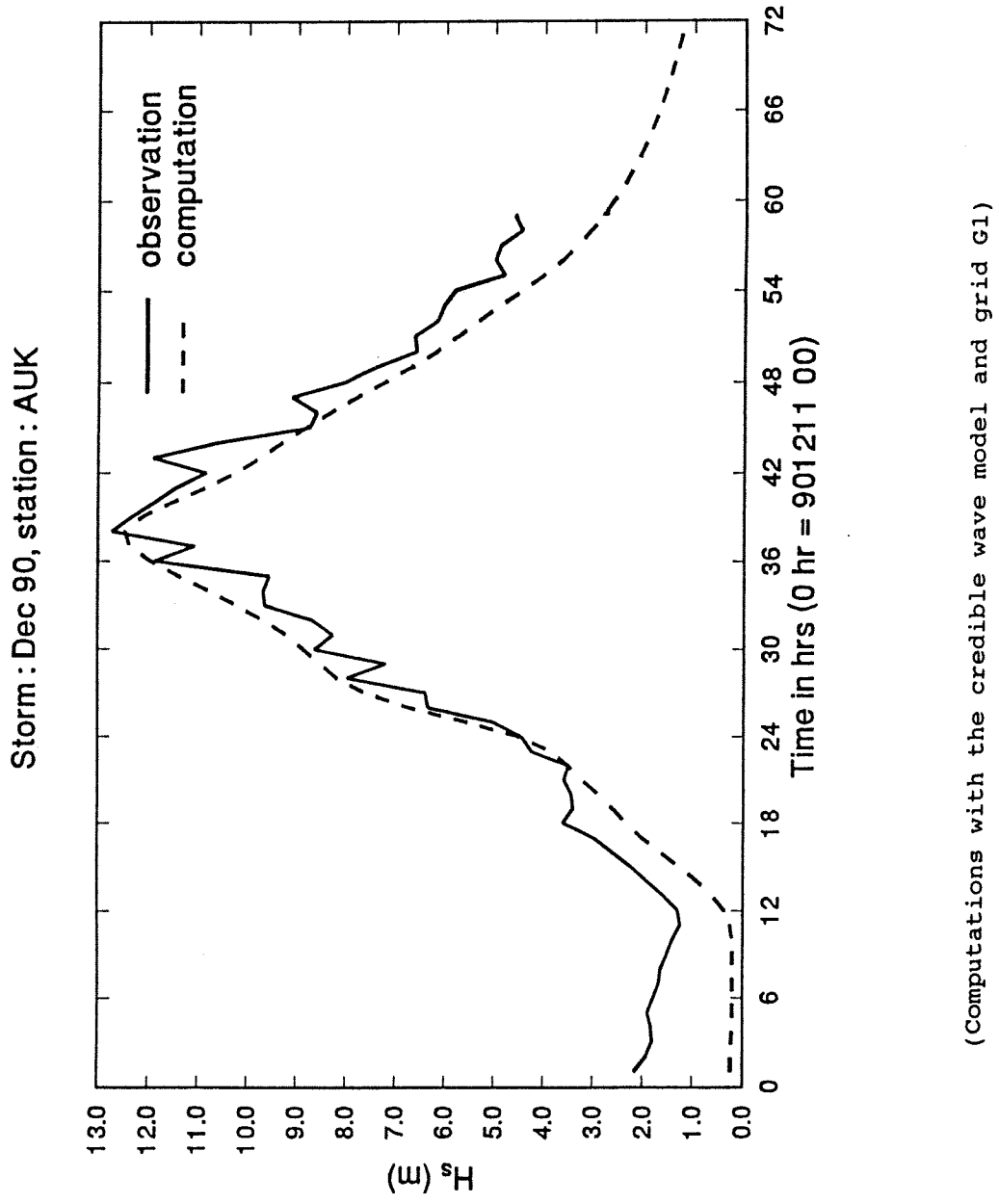


| | |
|---|---|
| Comparison between observed and computed significant wave height for Dec 90 storm at AUK | HSMAX |
| Delft University of Technology | Fig. 36 |

(a) energy spectrum

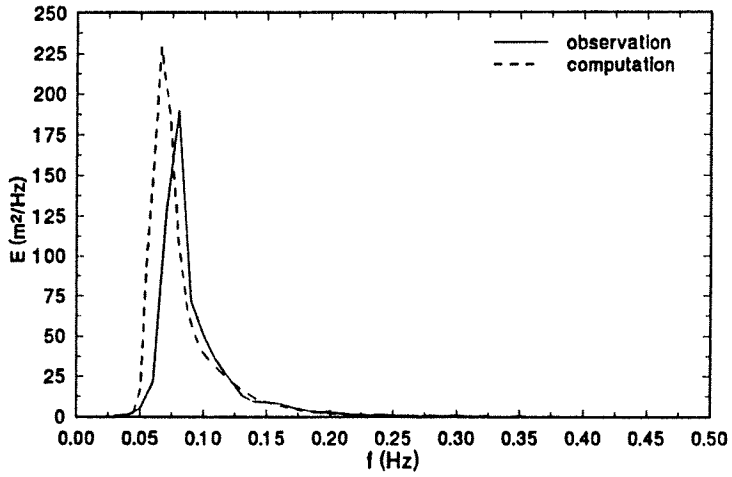


(b) direction

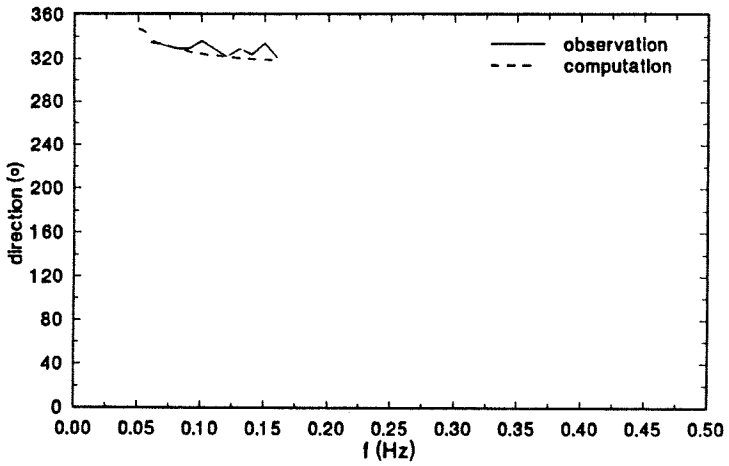


(c) spreading

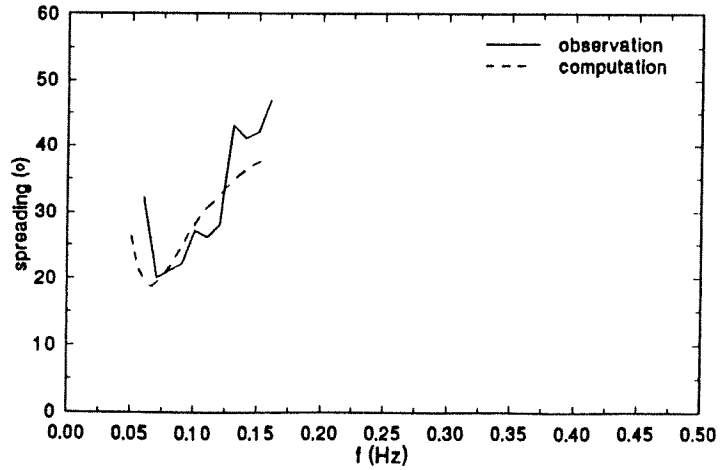


| | |
|---|---|
| Comparison between observed and computed spectra at AUK 3 hours before the peak of Dec 90 storm | HSMAX |
| Delft University of Technology | Fig. 37 |

AUK - 901212
(a) energy spectrum

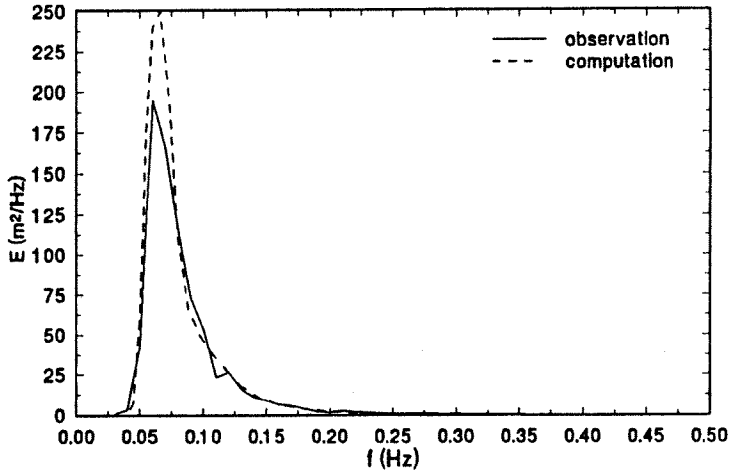


(b) direction

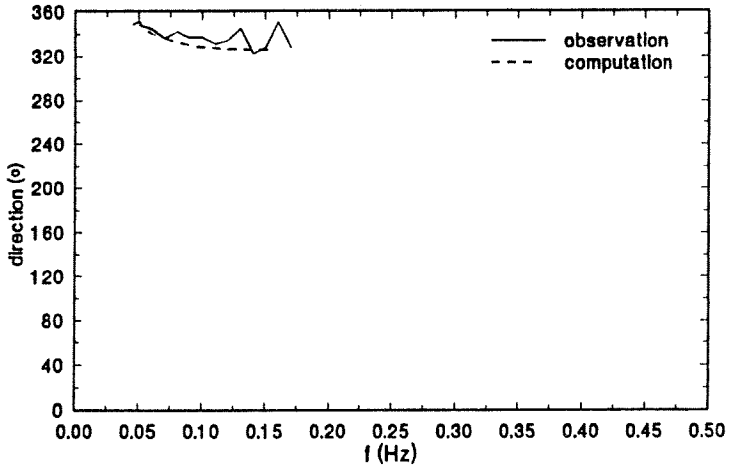


(c) spreading

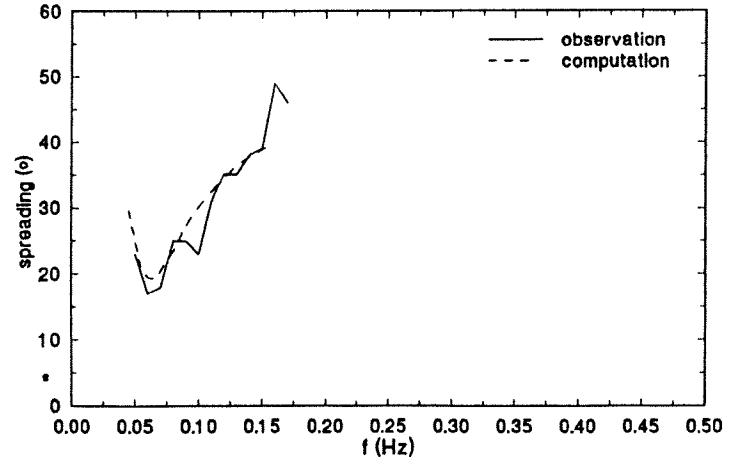


| | |
|---|---|
| Comparison between observed and computed spectra at AUK at the peak of Dec 90 storm | HSMAX |
| Delft University of Technology | Fig. 38 |

AUK - 901215
(a) energy spectrum

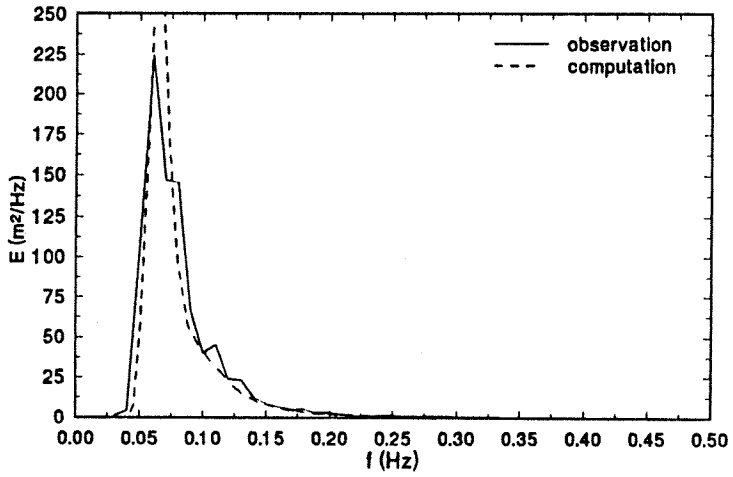


(b) direction

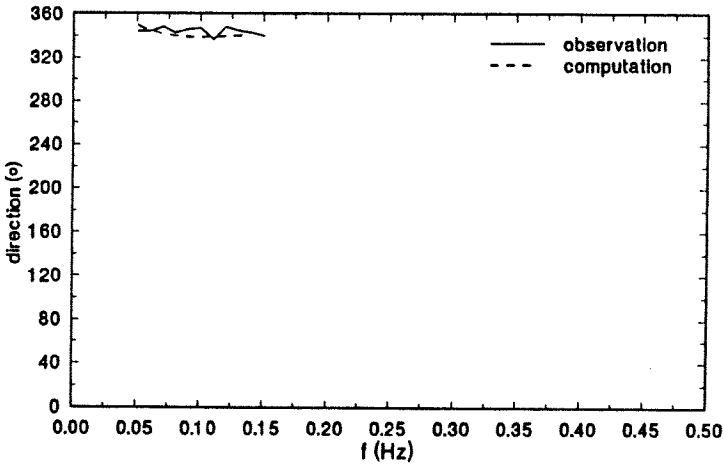


(c) spreading

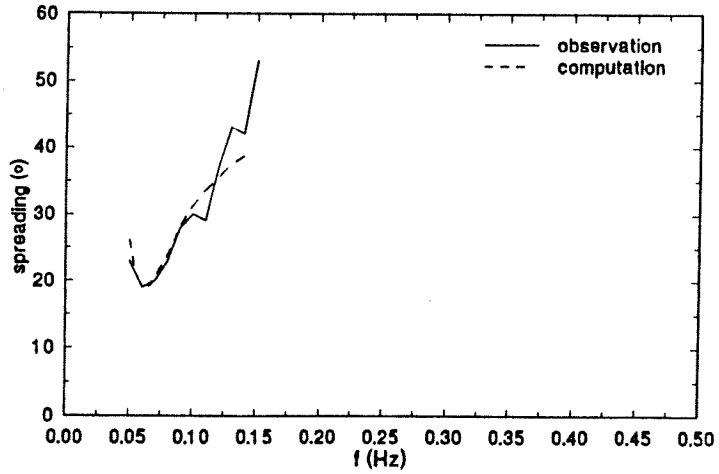


| | |
|---|---|
| Comparison between observed and computed spectra at AUK<br>3 hours after the peak of Dec 90 storm | HSMAX |
| Delft University of Technology | Fig. 39 |

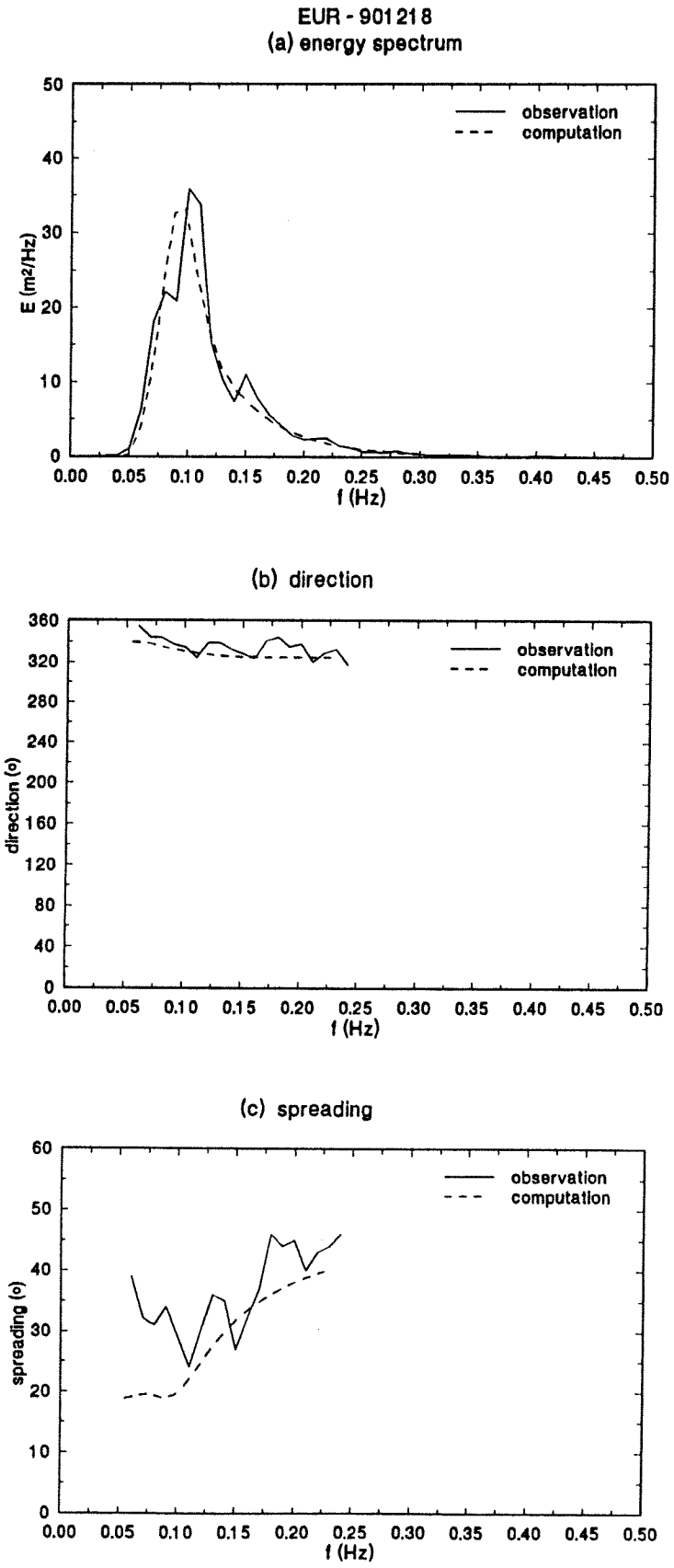


| | |
|---|---|
| Comparison between observed and computed spectra at EUR 3 hours before the peak of Dec 90 storm | HSMAX |
| Delft University of Technology | Fig. 40 |

EUR - 901221
(a) energy spectrum

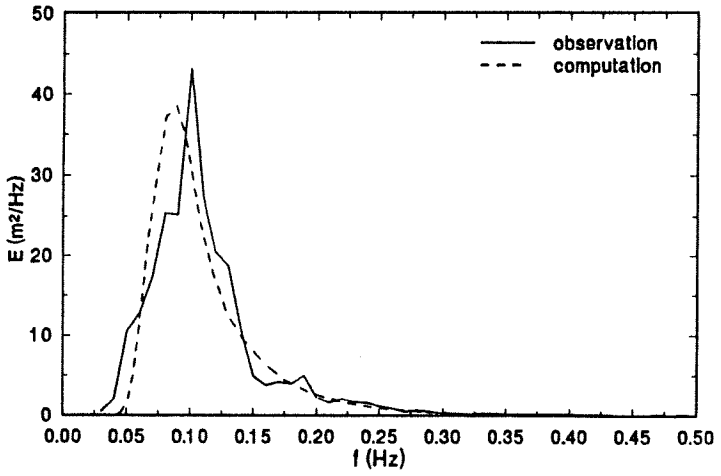


(b) direction

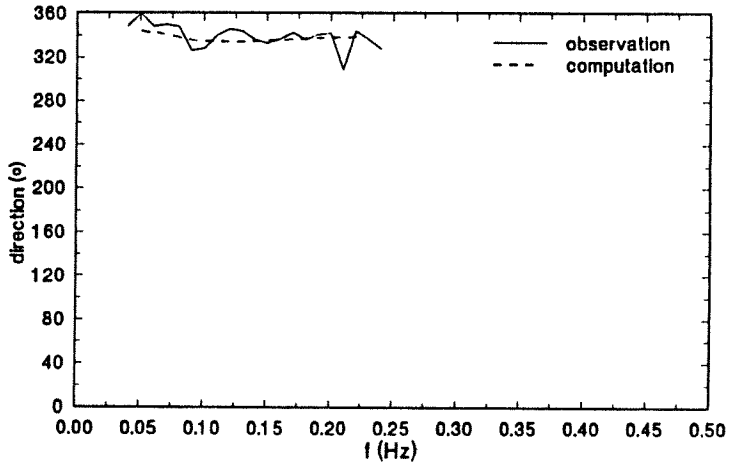


(c) spreading

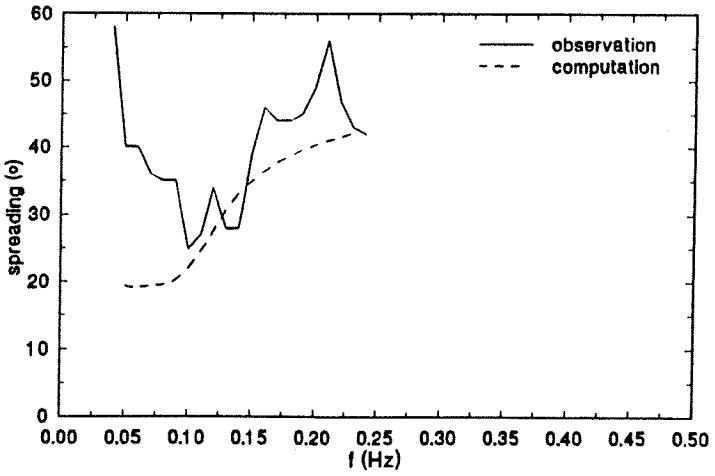


| | |
|---|---|
| Comparison between observed and computed spectra at EUR at the peak of Dec 90 storm | HSMAX |
| Delft University of Technology | Fig. 41 |

EUR - 901300
(a) energy spectrum

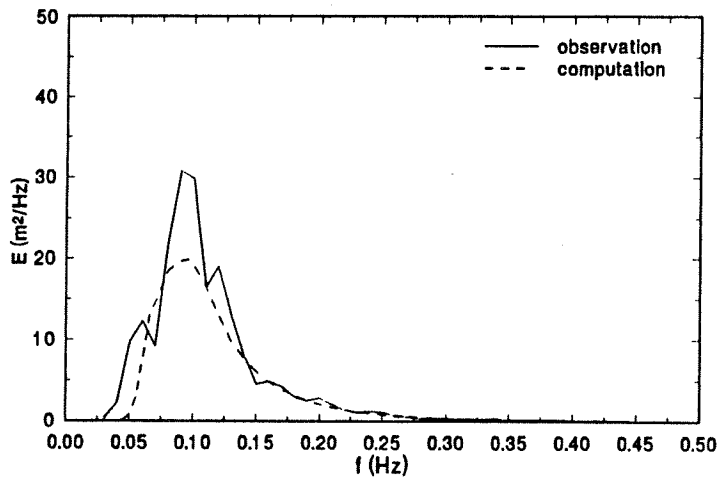


(b) direction

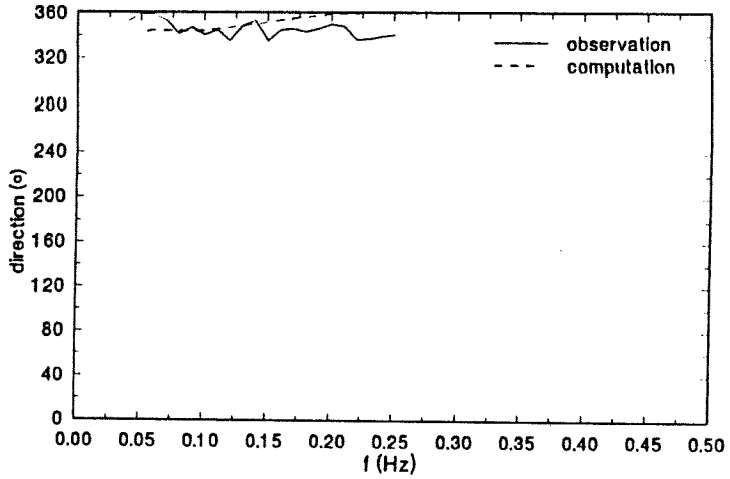


(c) spreading

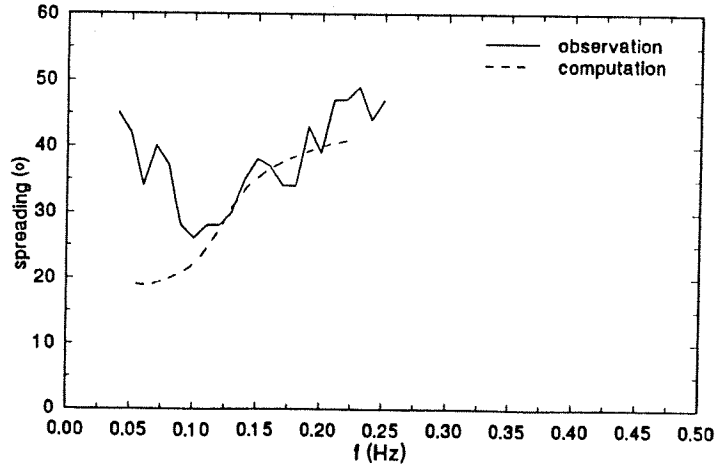


| | |
|---|---|
| Comparison between observed and computed spectra at EUR 3 hours after the peak of Dec 90 storm | HSMAX |
| Delft University of Technology | Fig. 42 |

K13 - 901215
(a) energy spectrum

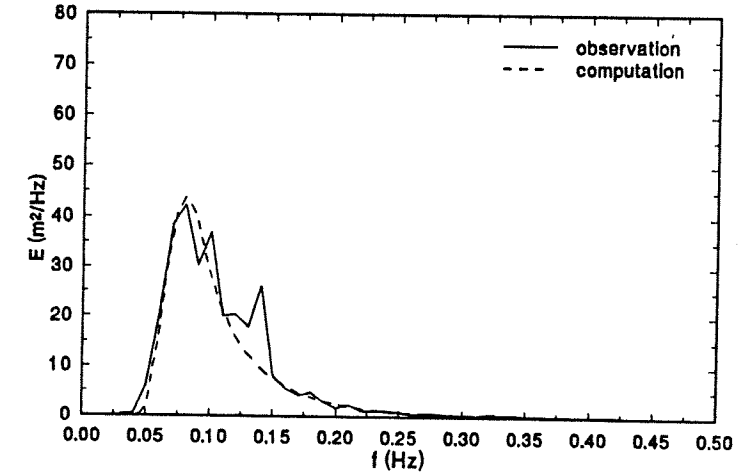


(b) direction

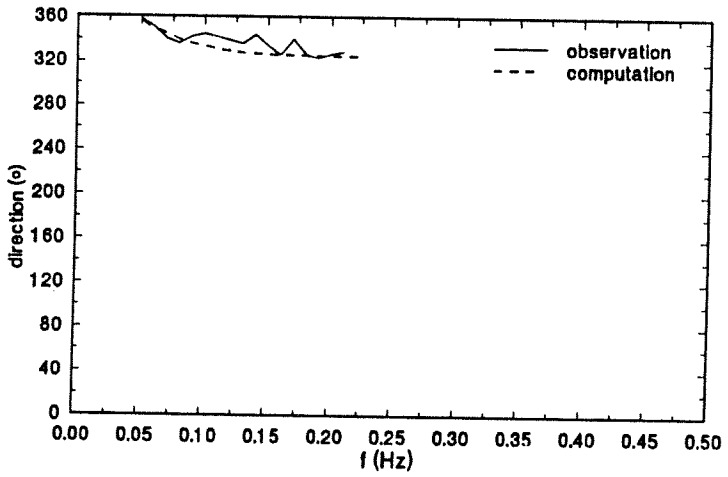


(c) spreading

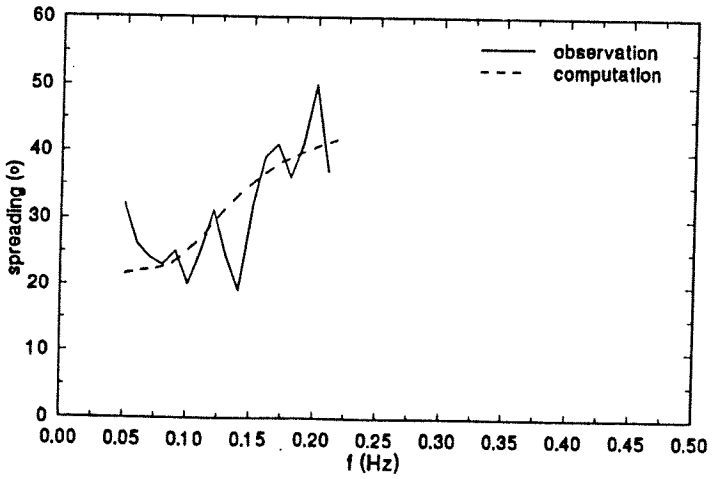


| | |
|---|---|
| Comparison between observed and computed spectra at K13<br>3 hours before the peak of Dec 90 storm | HSMAX |
| Delft University of Technology | Fig. 43 |

K13 - 901218
(a) energy spectrum

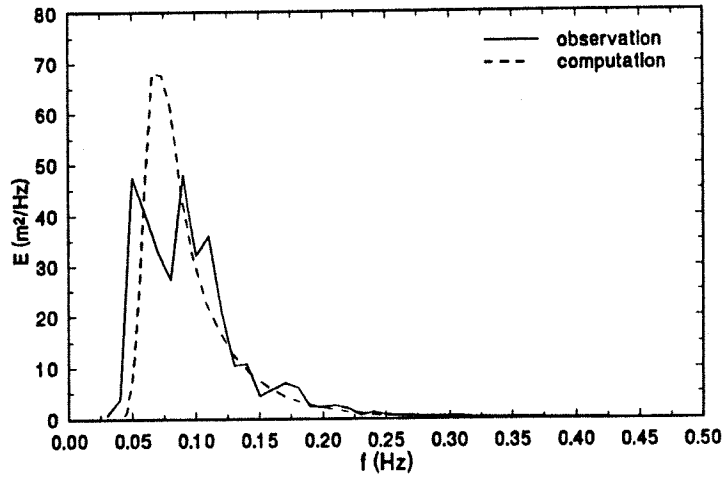


(b) direction

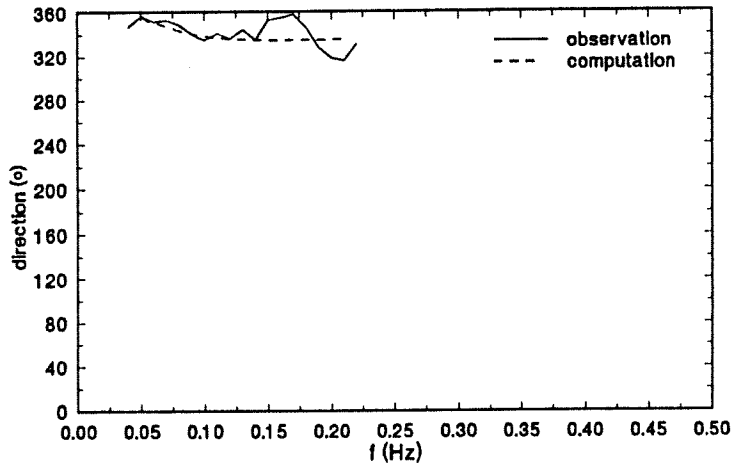


(c) spreading

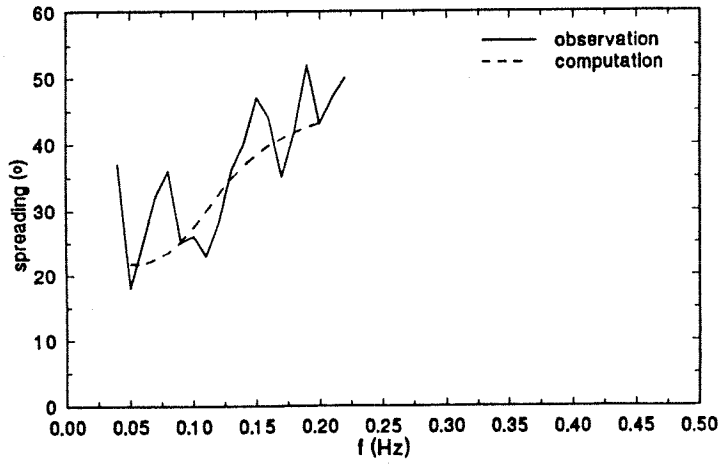


| | |
|---|---|
| Comparison between observed and computed spectra at K13 at the peak of Dec 90 storm | HSMAX |
| Delft University of Technology | Fig. 44 |

K13 - 901221
(a) energy spectrum

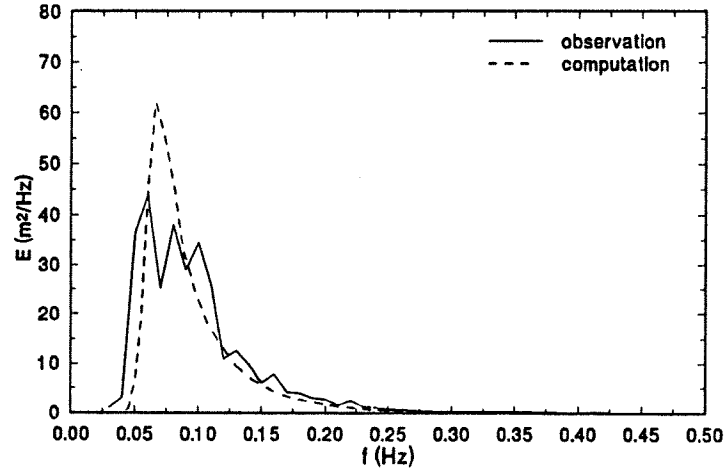


(b) direction

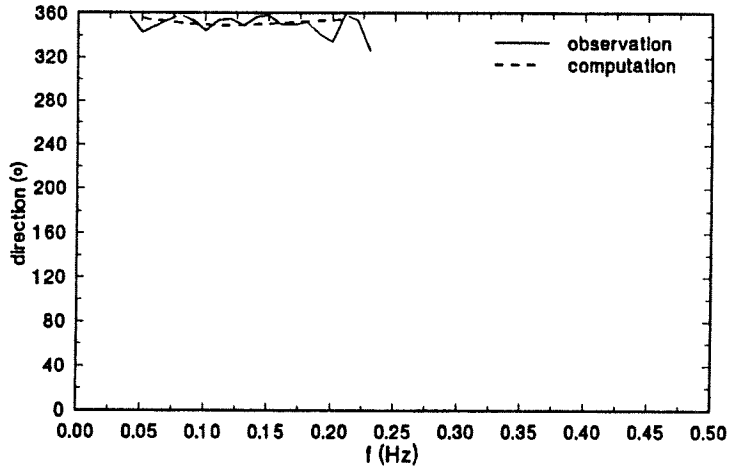


(c) spreading

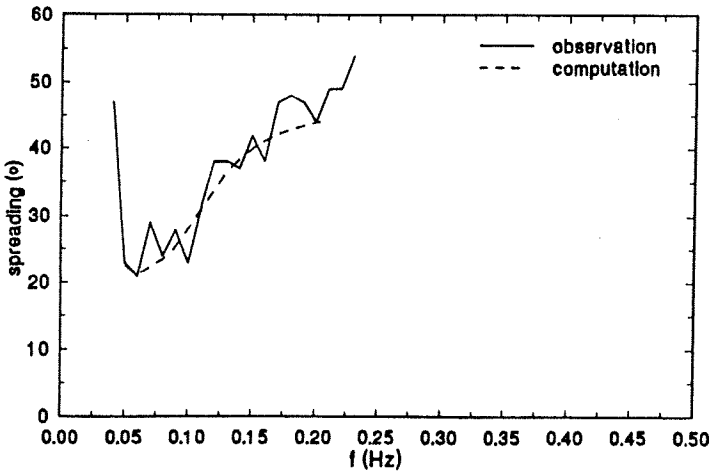


| | |
|---|---|
| Comparison between observed and computed spectra at K13<br>3 hours after the peak of Dec 90 storm | HSMAX |
| Delft University of Technology | Fig. 45 |

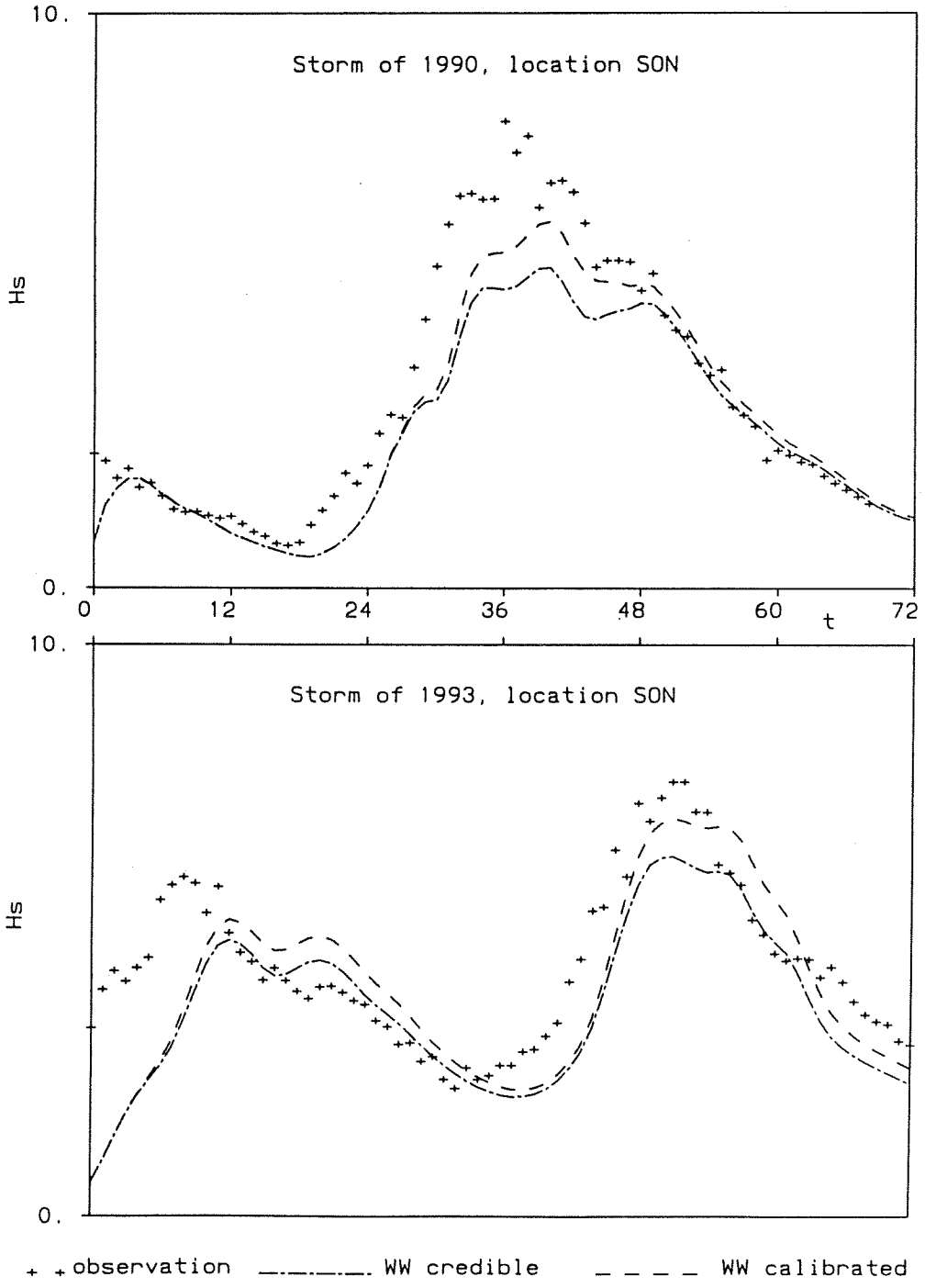


| | |
|---|---|
| Observed and computed significant wave height in historic storms at SON | HSMAX |
| Delft University of Technology | Fig. 46 |

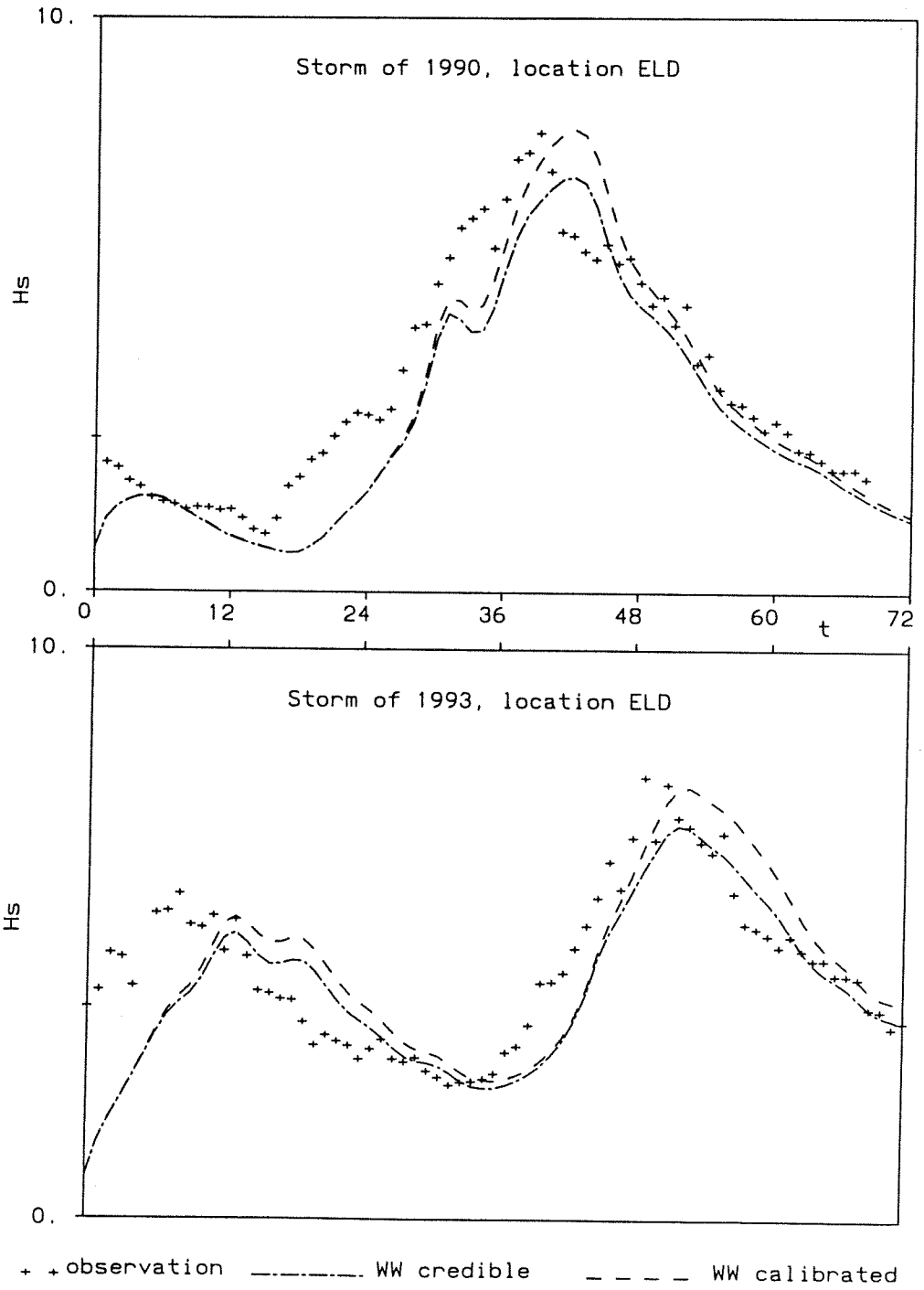


| | |
|---|---|
| Observed and computed significant wave height in historic storms at ELD | HSMAX |
| Delft University of Technology | Fig. 47 |

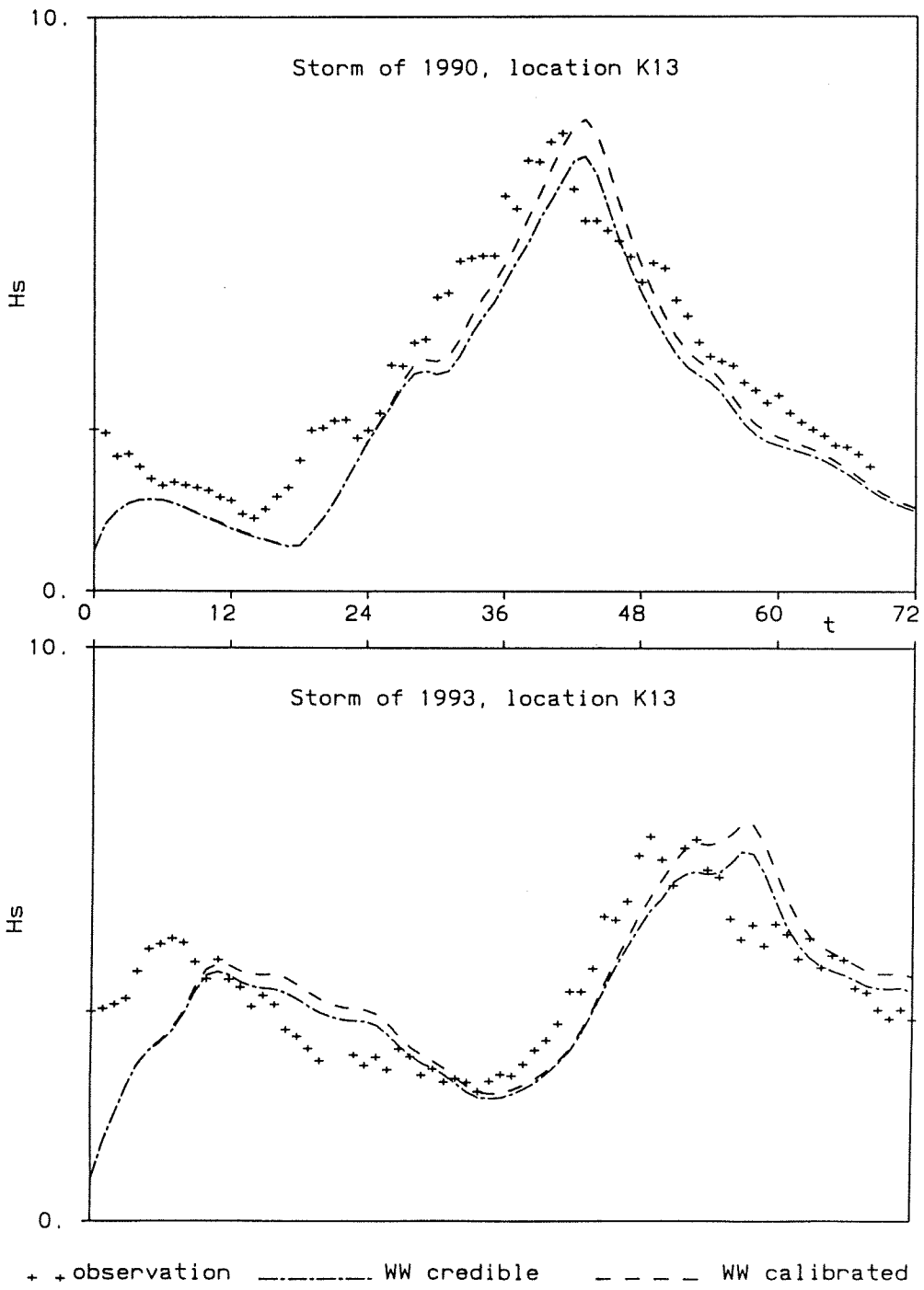


| | |
|---|---|
| Observed and computed significant wave height in historic storms at K13 | HSMAX |
| Delft University of Technology | Fig. 48 |

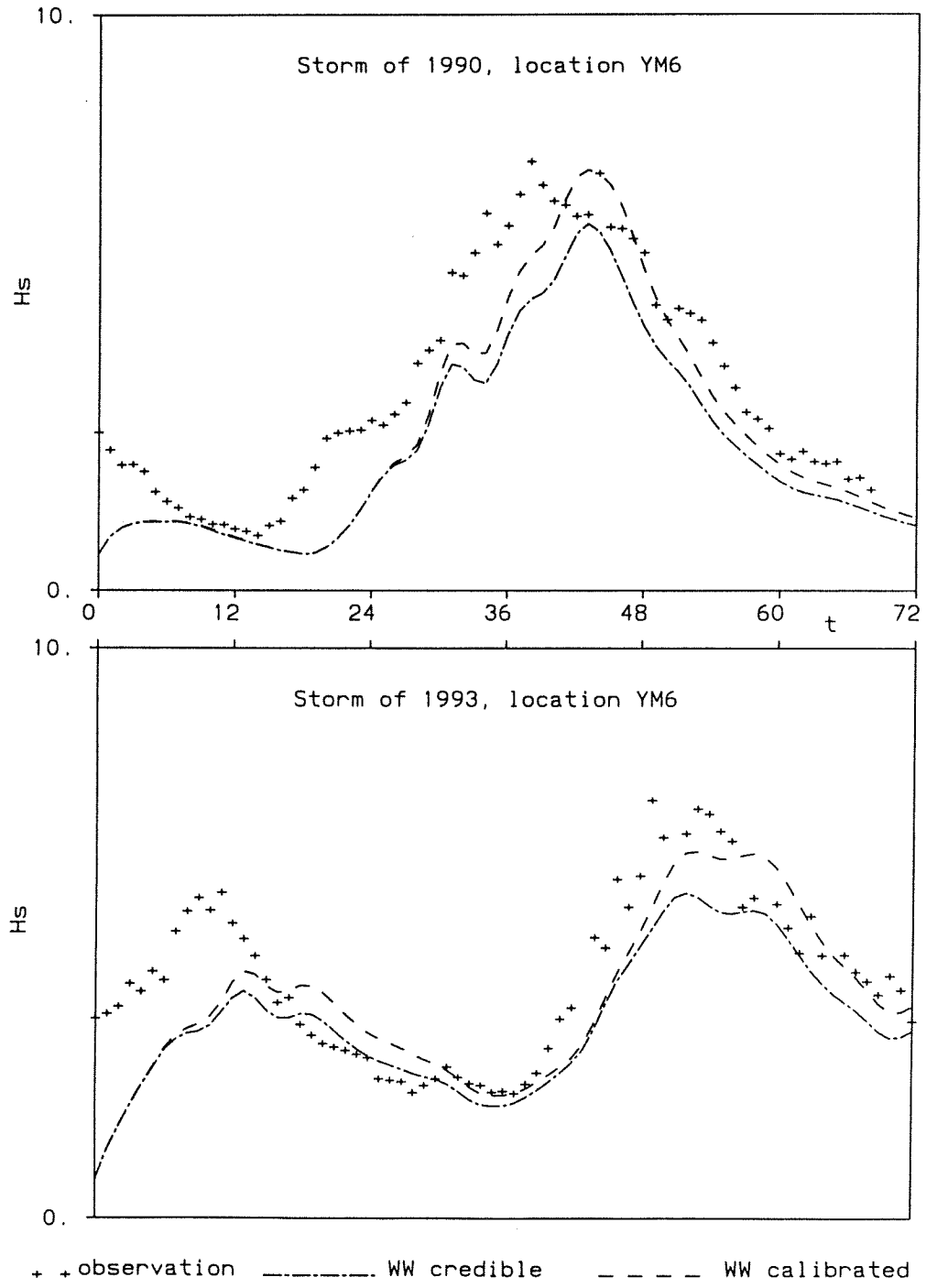


| | |
|---|---|
| Observed and computed significant wave height in historic storms at YM6 | HSMAX |
| Delft University of Technology | Fig. 49 |

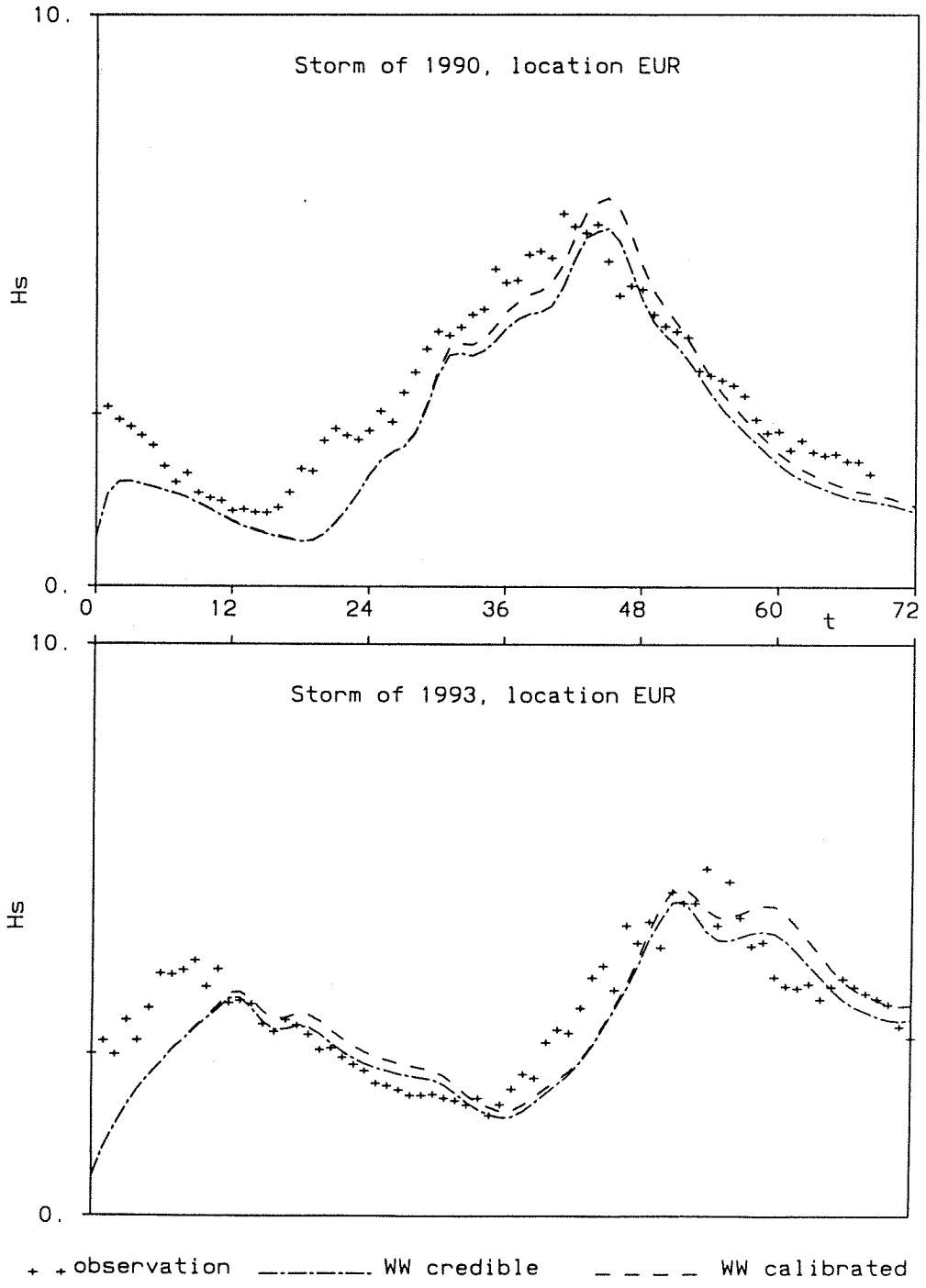


| | |
|---|---|
| Observed and computed significant wave height in historic storms at EUR | HSMAX |
| | |
| Delft University of Technology | Fig. 50 |

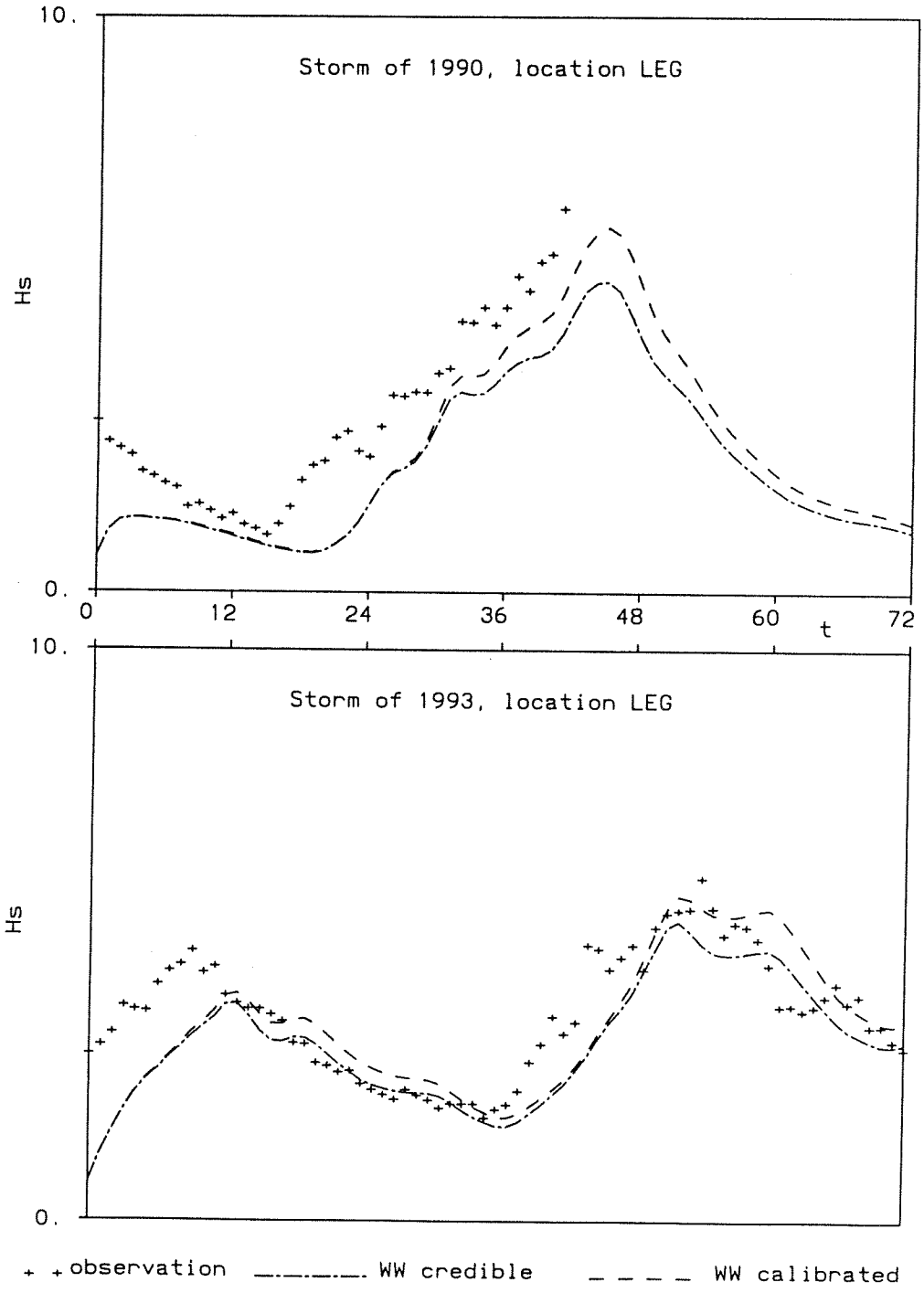


| | |
|---|---|
| Observed and computed significant wave height in historic storms at LEG | HSMAX |
| | |
| Delft University of Technology | Fig. 51 |

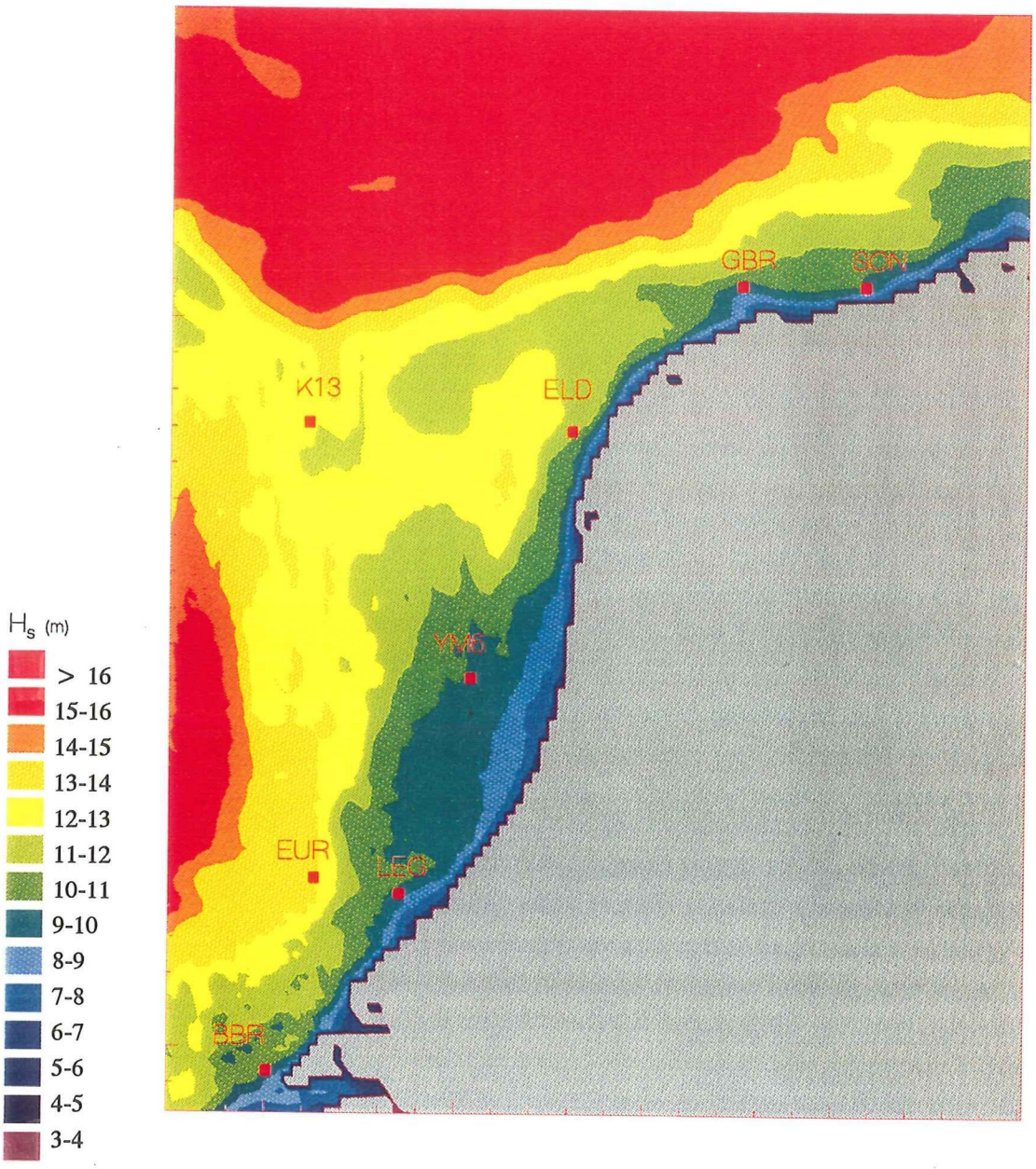


| | |
|---|---|
| Significant wave height in the extreme uniform wind (computation with the maximum calibrated model and grid G3) | HSMAX |
| Delft University of Technology | Fig. 52 |

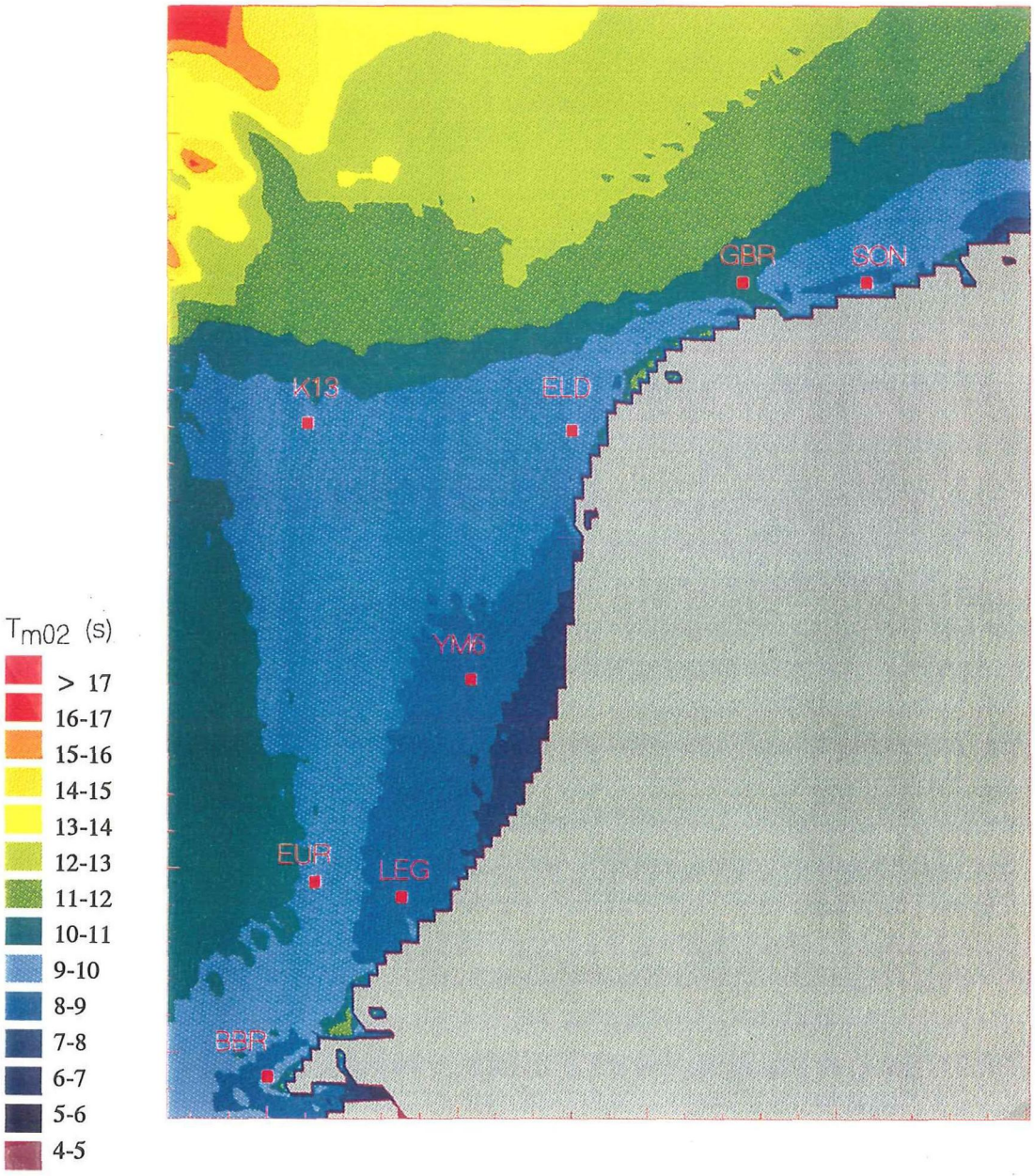


| | |
|---|---|
| Mean wave period in the extreme uniform wind (computation with the maximum calibrated model and grid G3) | HSMAX |
| Delft University of Technology | Fig. 53 |

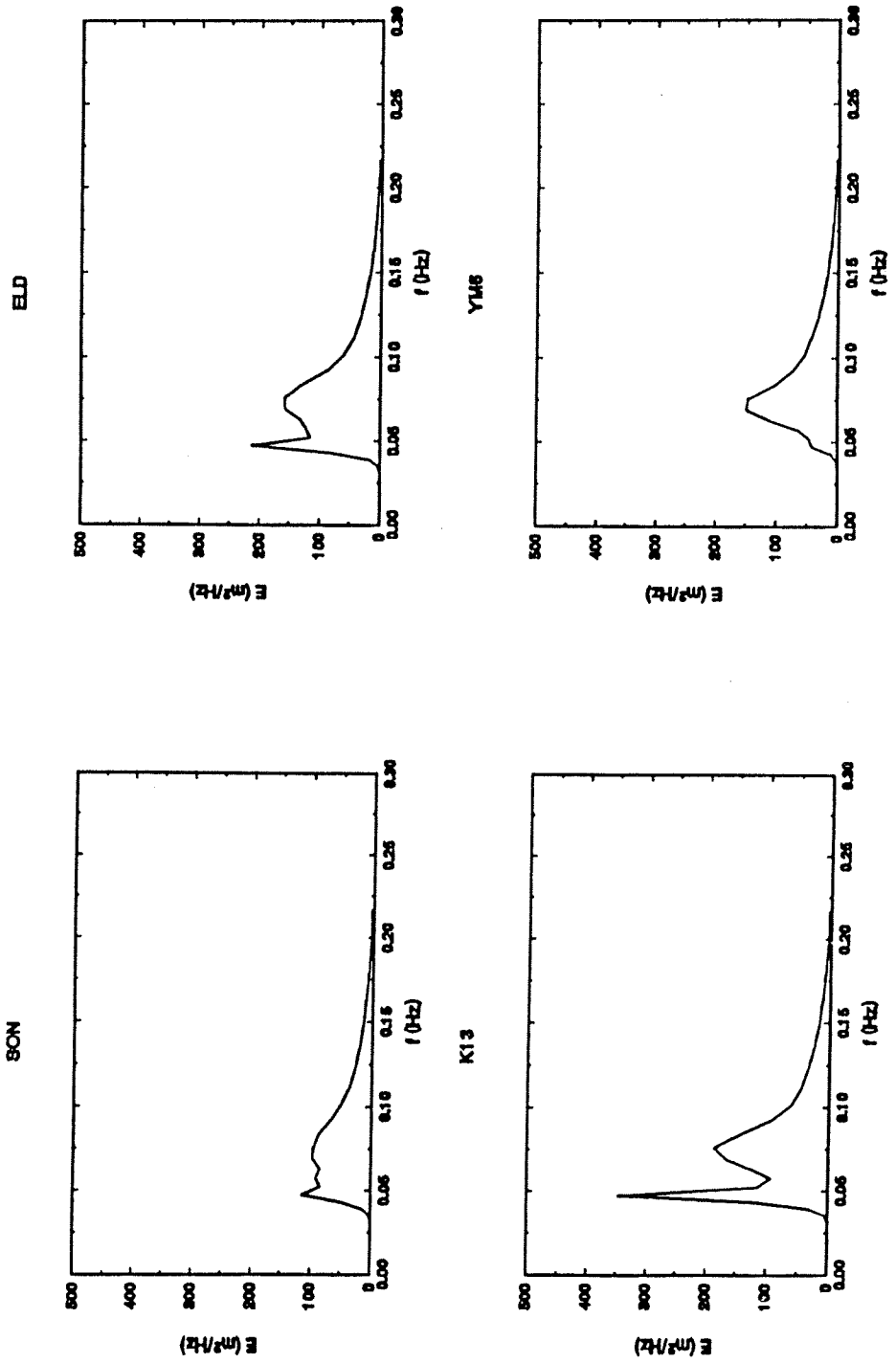


| Computed energy spectra at SON, ELD, K13, and YM6 in the extreme uniform wind using the maximum calibrated model | HSMAX |
|---|---|
| Delft University of Technology | Fig. 54 |

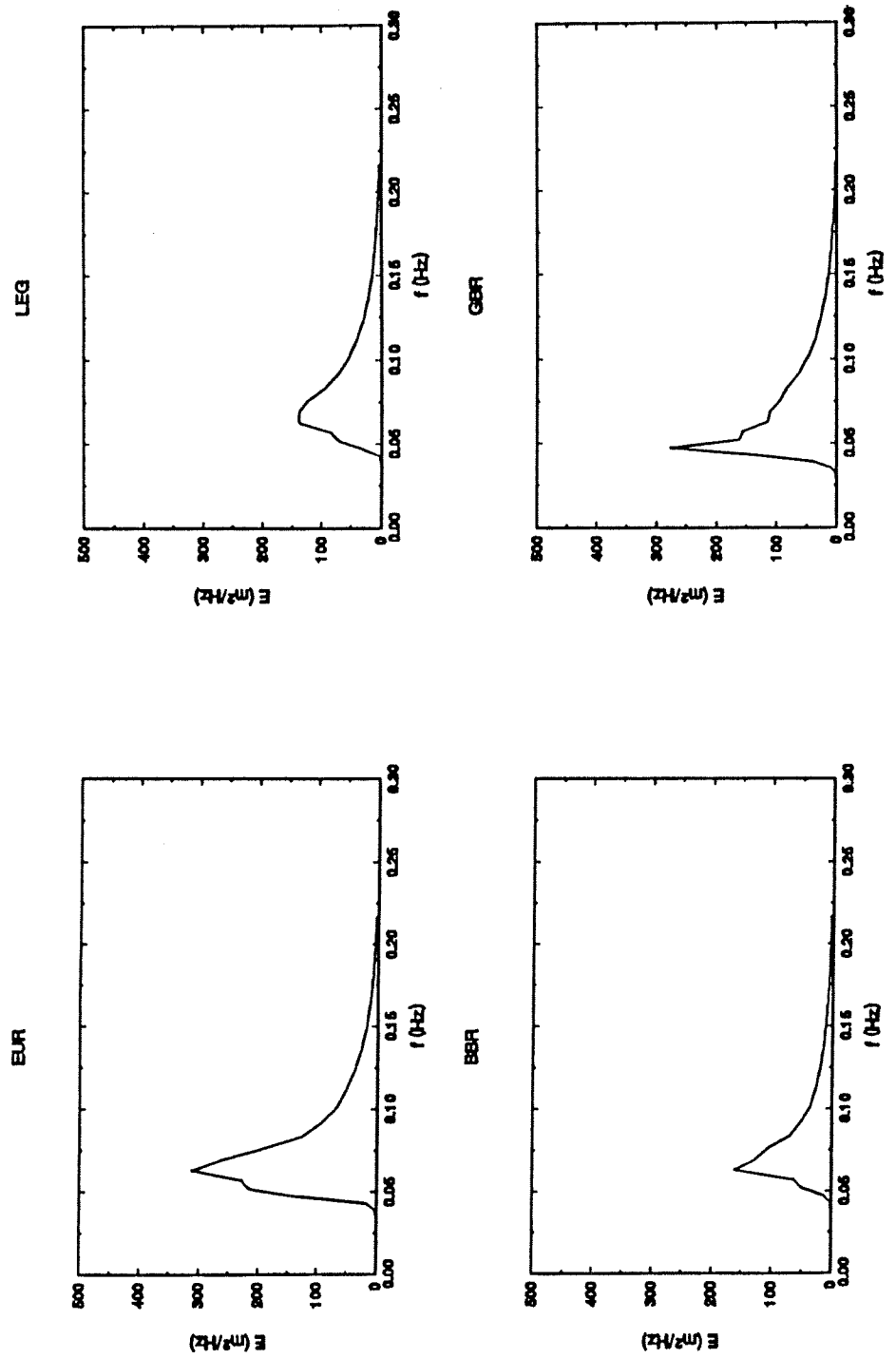


| | |
|---|---|
| Computed energy spectra at EUR, LEG, BBR, and GBR in the extreme uniform wind using the maximum calibrated model | HSMAX |
| Delft University of Technology | Fig. 55 |

Delft University of Technology

Time history of significant wave height for Feb 1953 storm and its manipulations at SON

HSMAX

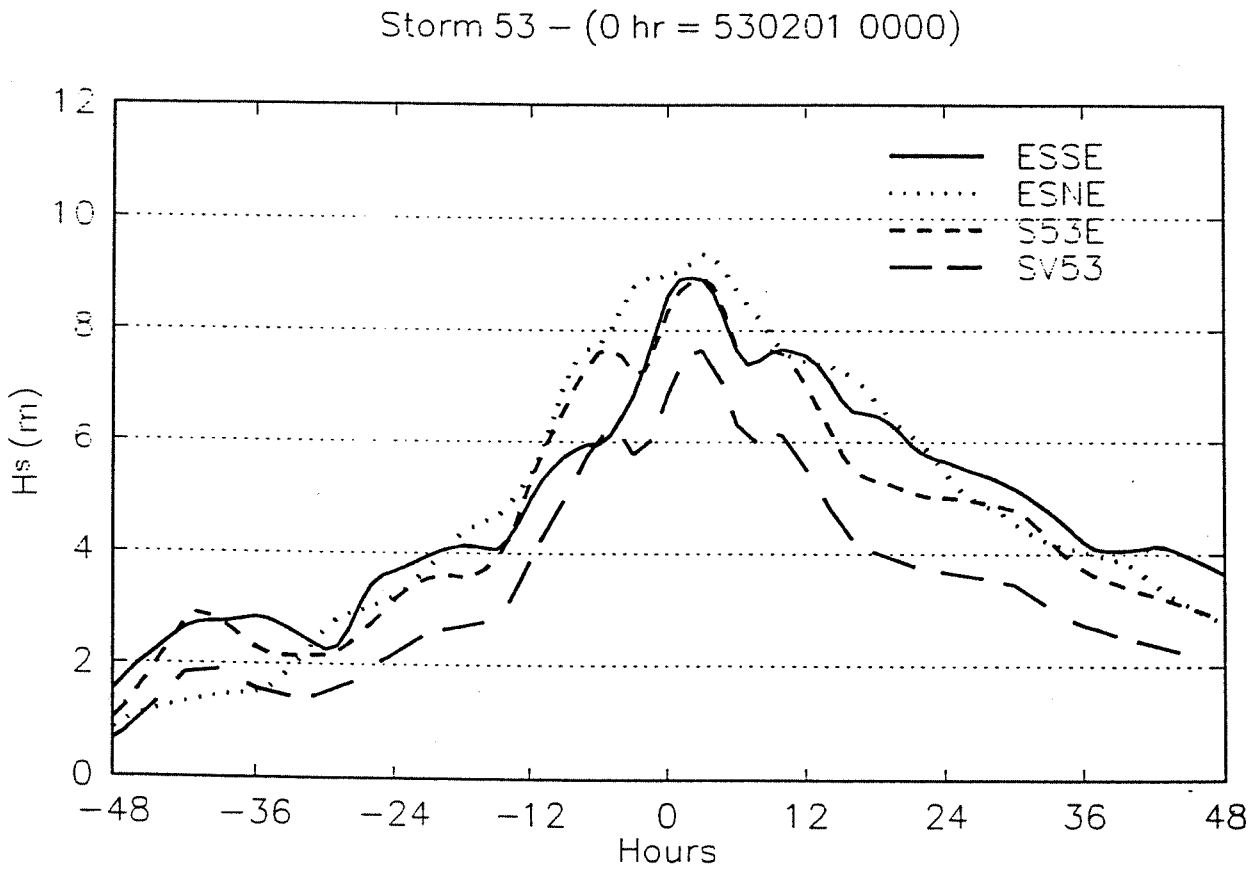


SV53 : '53 storm
S53E : enhanced '53 storm

ESSE : enhanced and shifted south east
ESNE : enhanced and shifted north east

Fig. A1

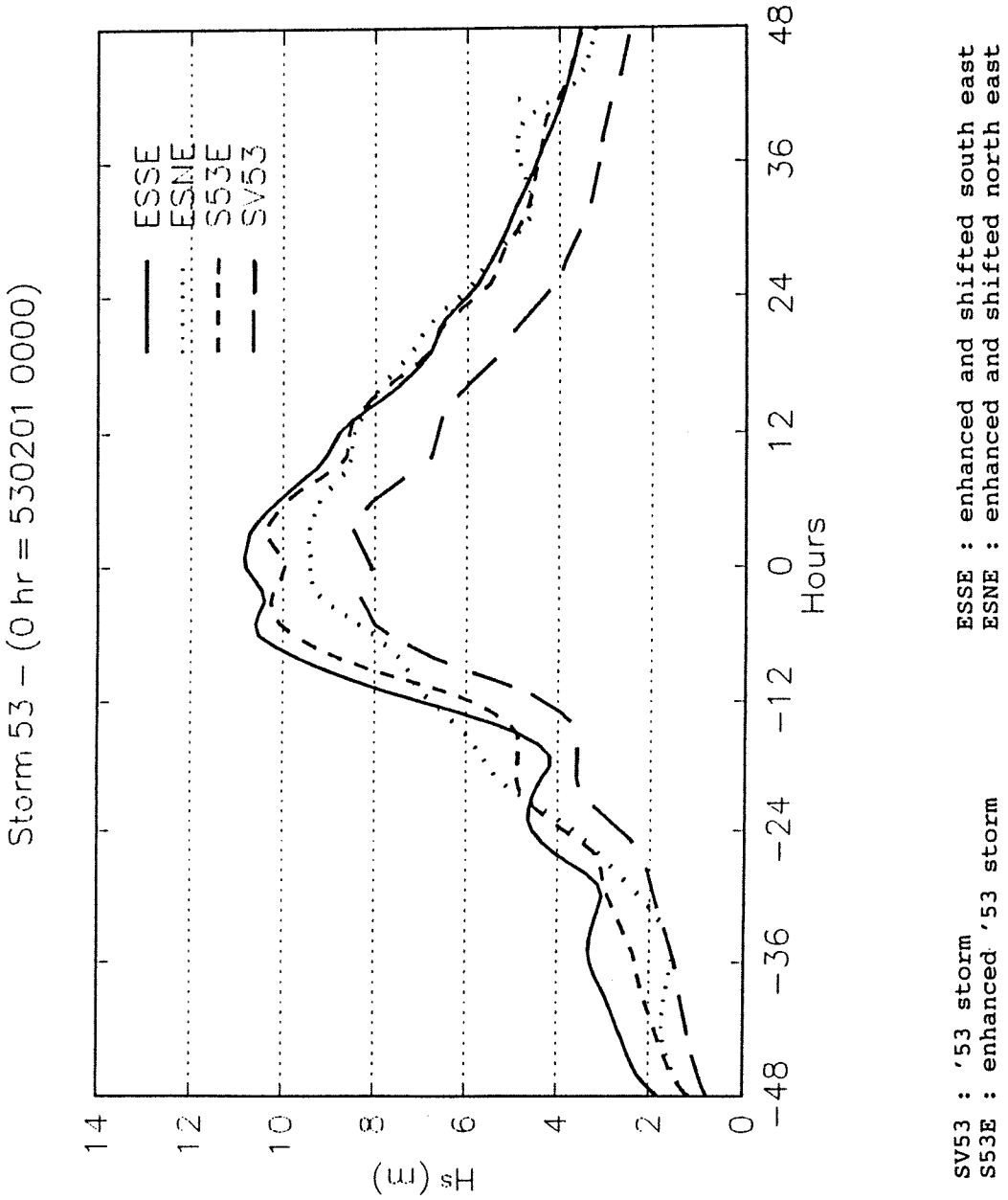


| | |
|---|---|
| Time history of significant wave height for Feb 1953 storm and its manipulations at ELD | HSMAX |
| Delft University of Technology | Fig. A2 |

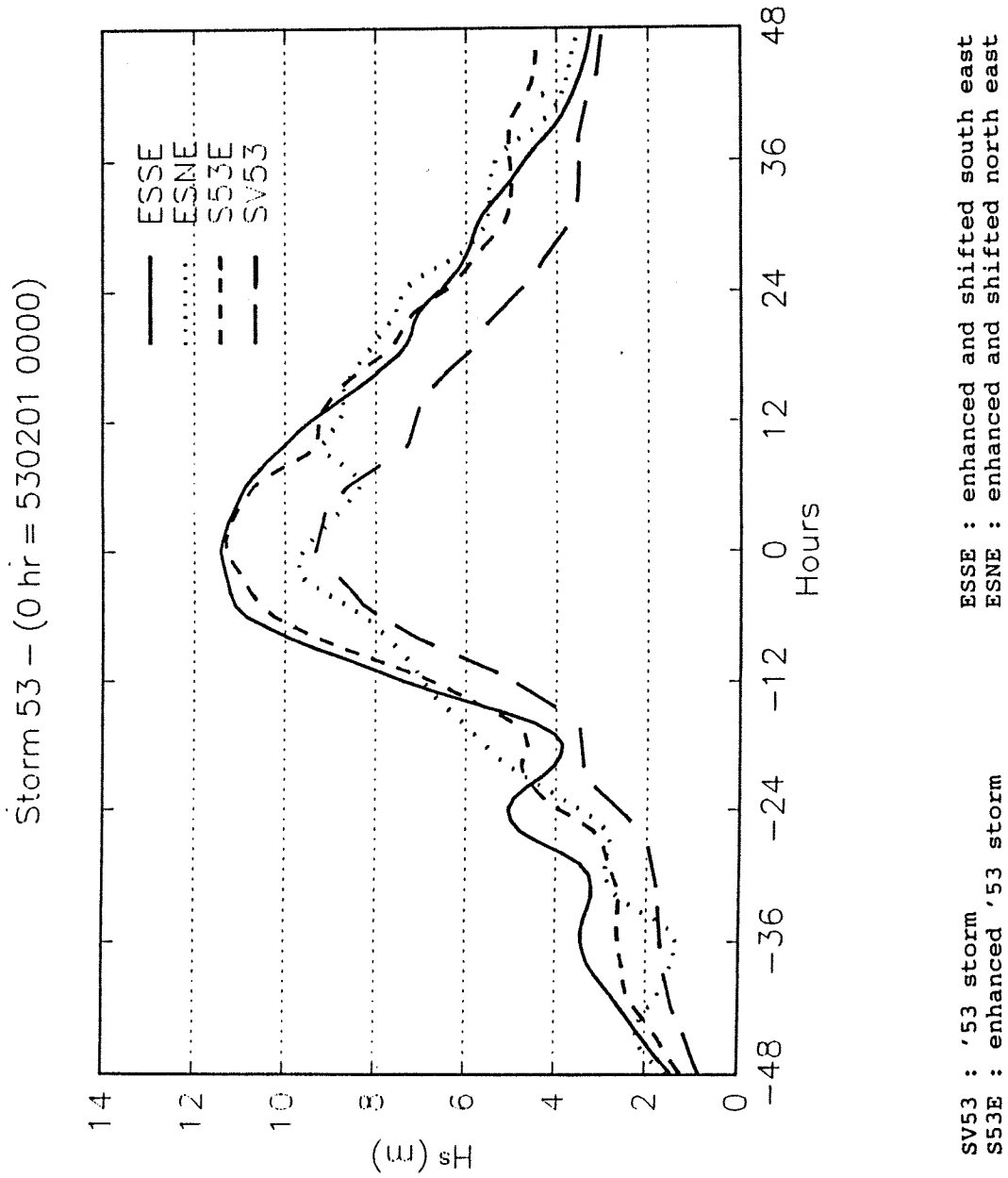


| | |
|---|---|
| Time history of significant wave height for Feb 1953 storm and its manipulations at K13 | HSMAX |
| | |
| Delft University of Technology | Fig. A3 |

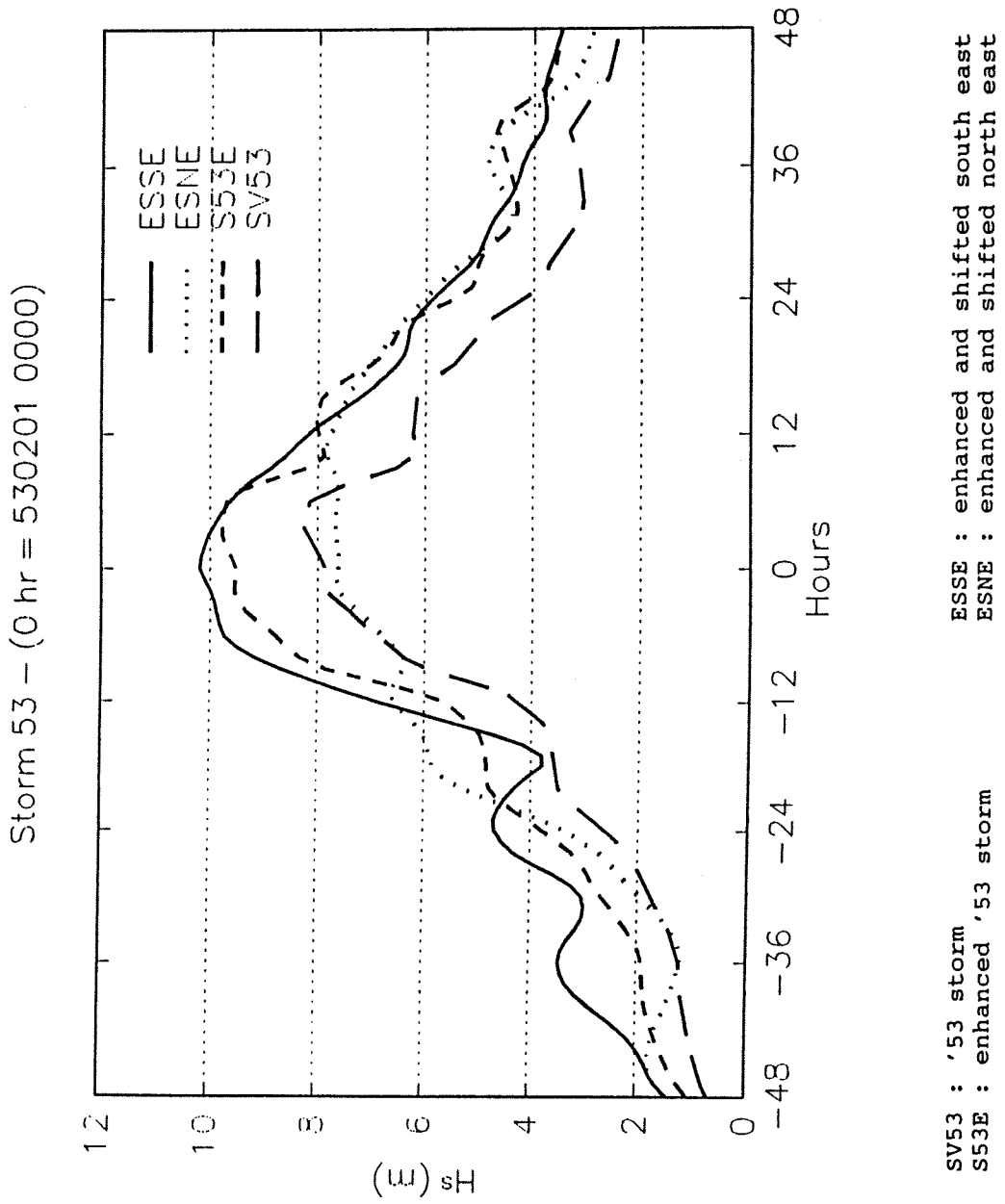


| | |
|---|---|
| Time history of significant wave height for Feb 1953 storm and its manipulations at YM6 | HSMAX |
| Delft University of Technology | Fig. A4 |

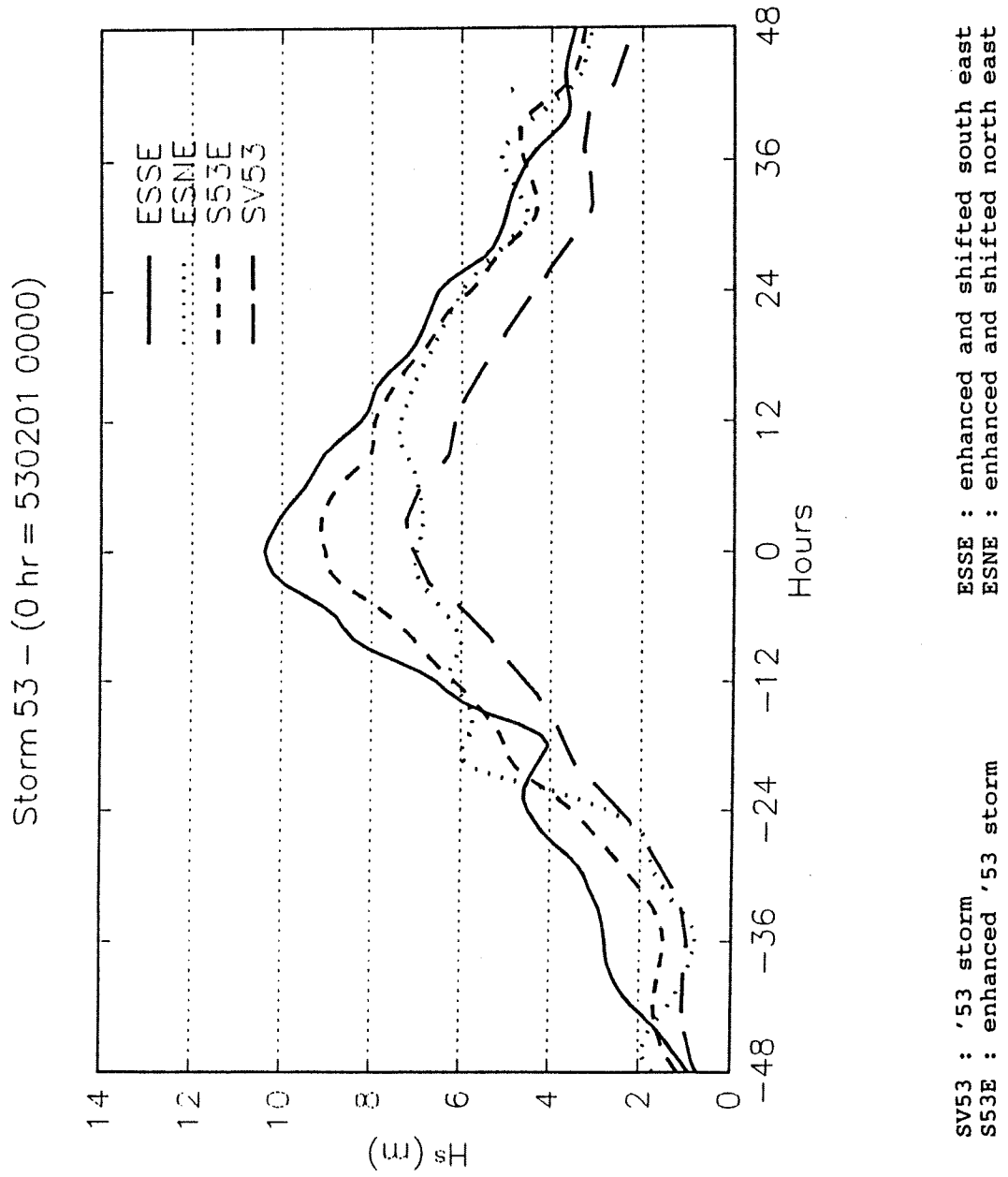


| | |
|---|---|
| Time history of significant wave height for Feb 1953 storm and its manipulations at EUR | HSMAX |
| Delft University of Technology | Fig. A5 |

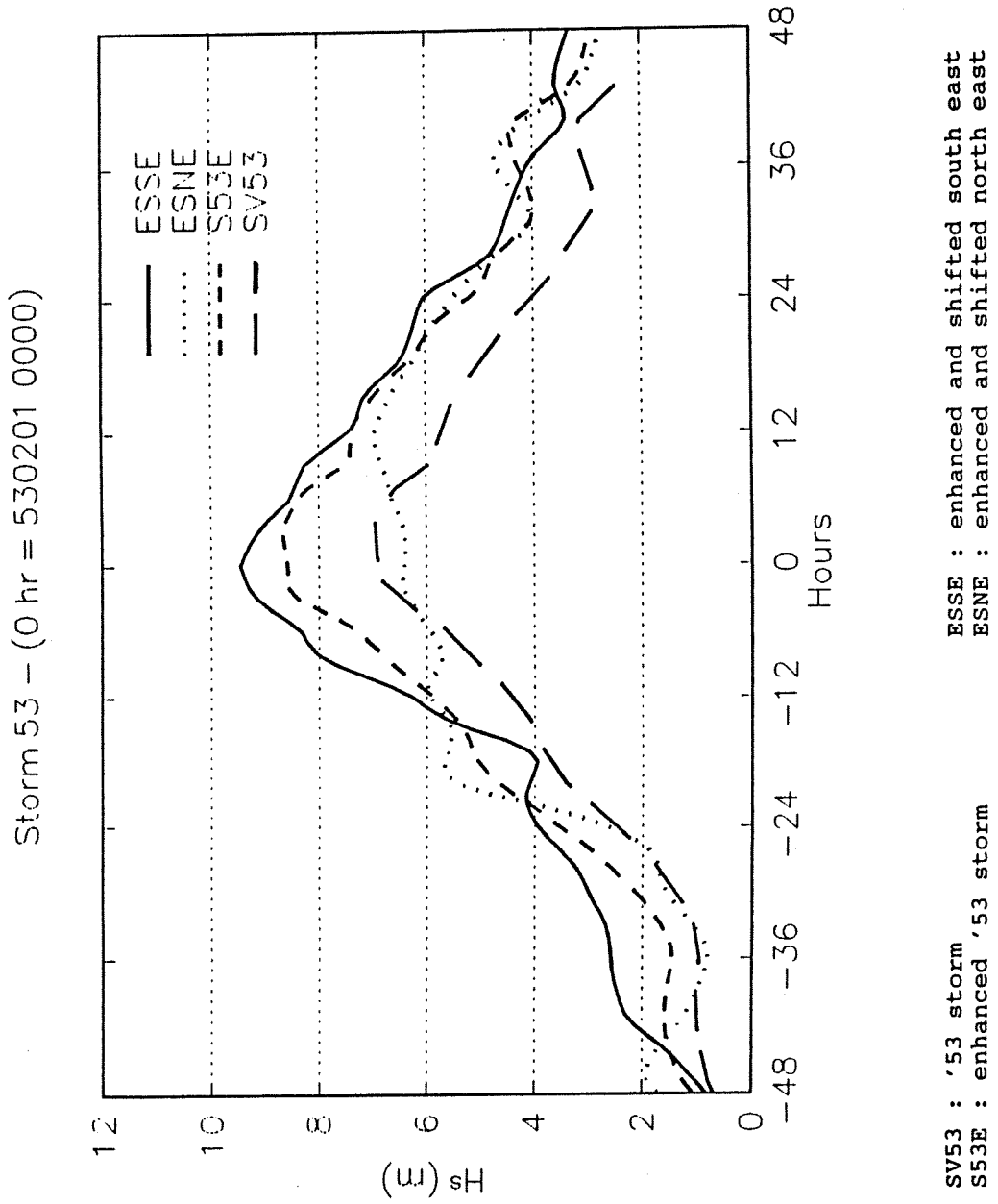


| | |
|---|---|
| Time history of significant wave height for Feb 1953 storm and its manipulations at LEG | HSMAX |
| Delft University of Technology | Fig. A6 |

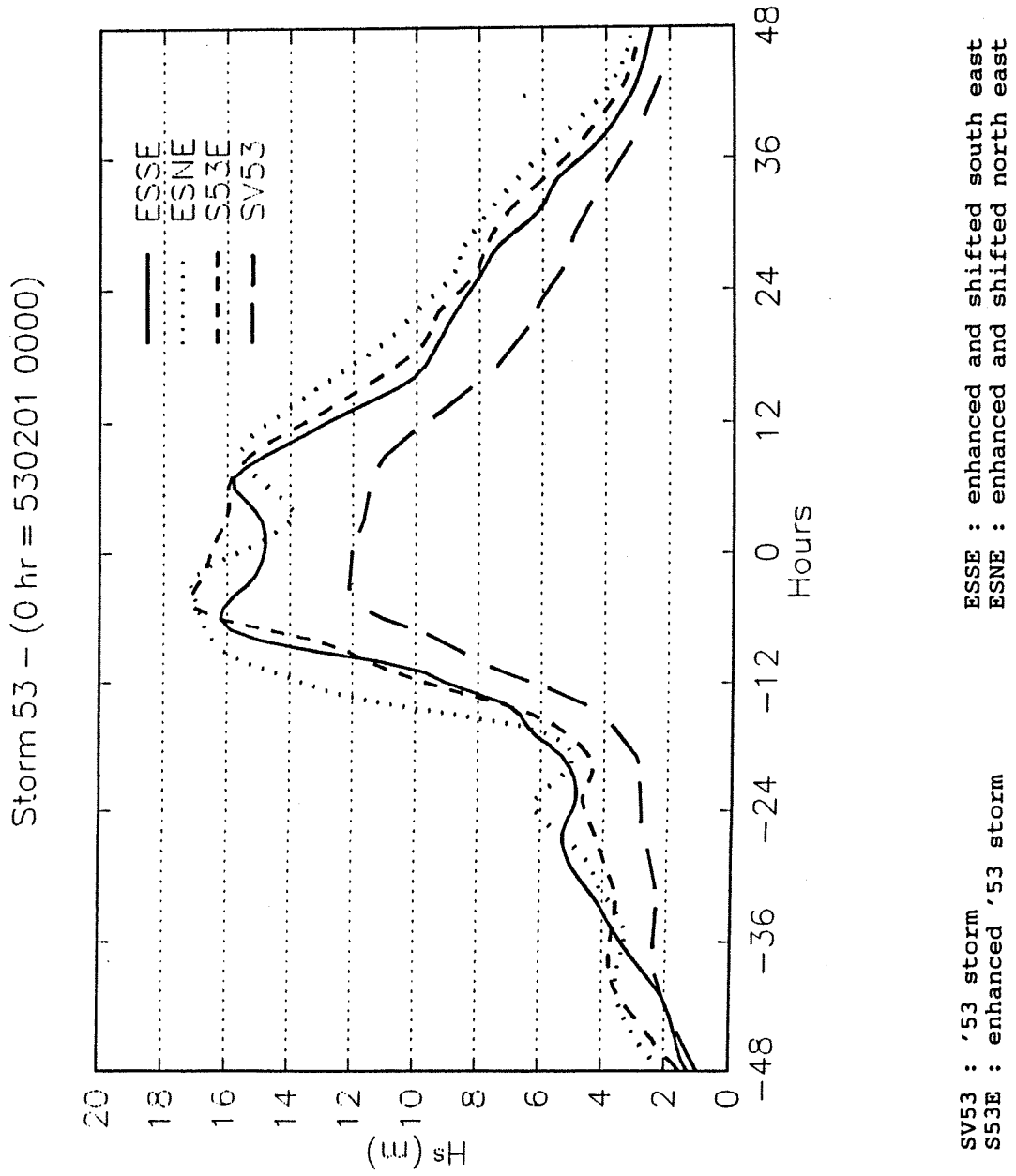


| | |
|---|---|
| Time history of significant wave height for Feb 1953 storm and its manipulations at AUK | HSMAX |
| | |
| Delft University of Technology | Fig. A7 |

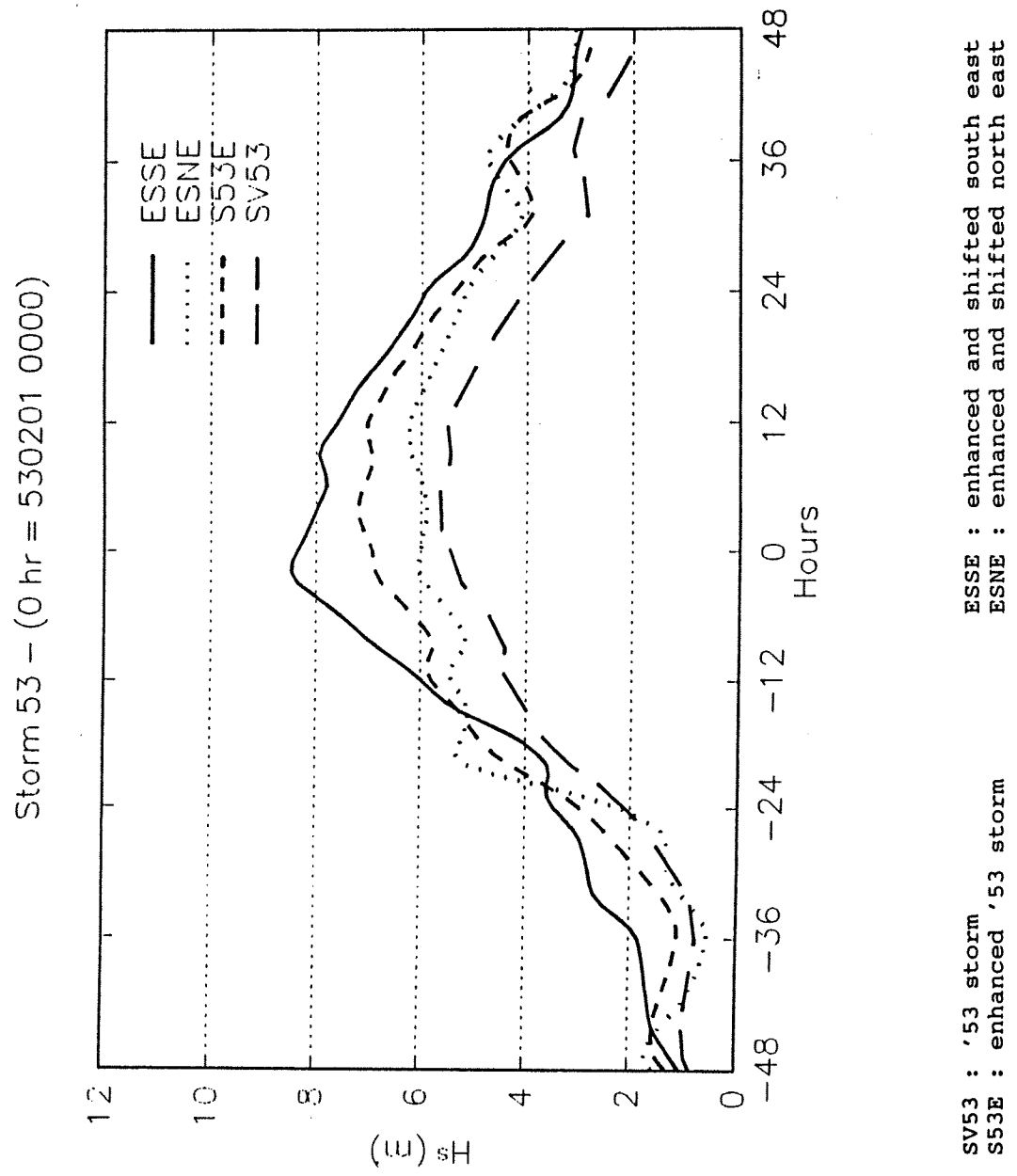


| | |
|---|---|
| Time history of significant wave height for Feb 1953 storm and its manipulations at BBR | HSMAX |
| | |
| Delft University of Technology | Fig. A8 |

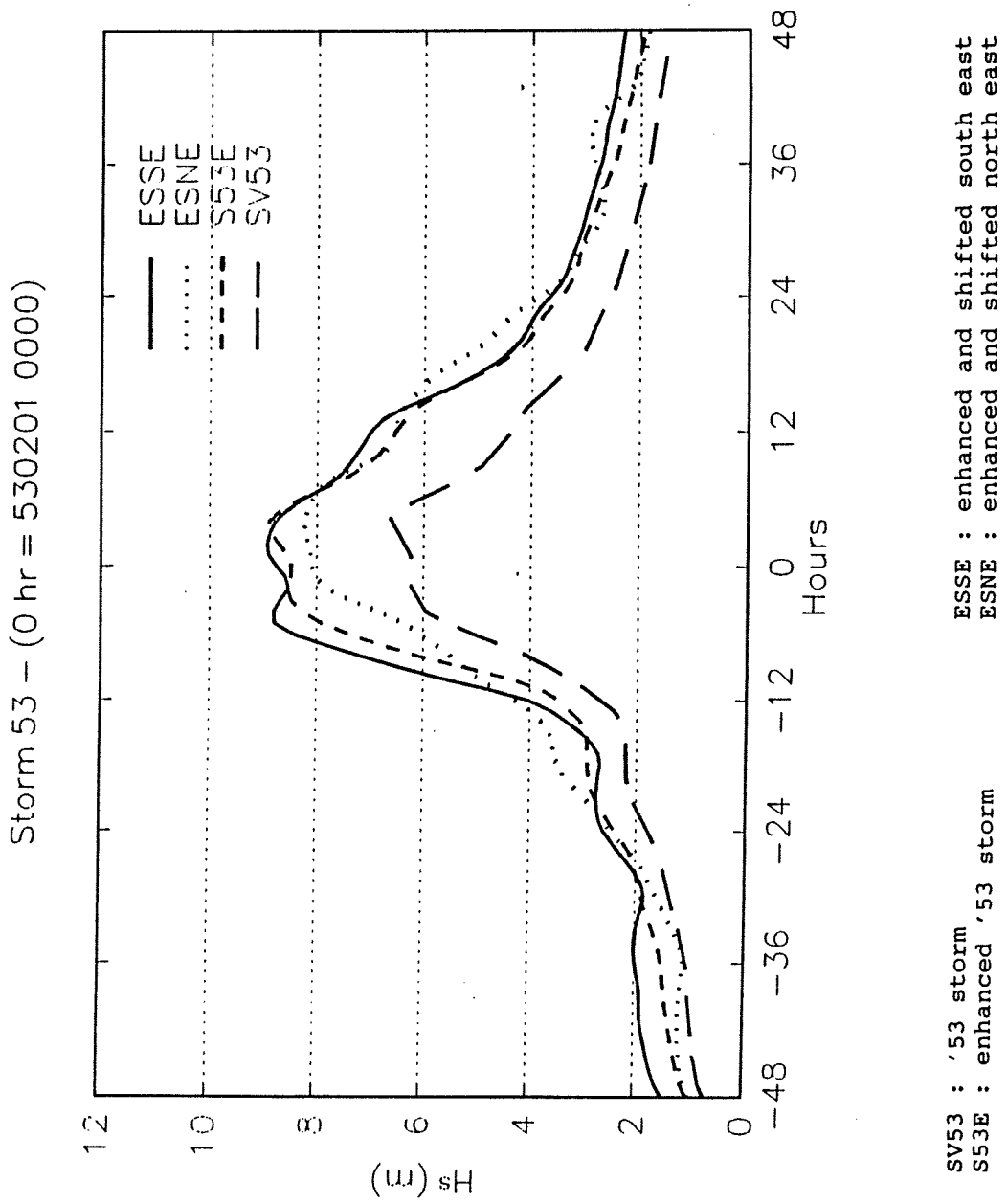


| | |
|---|---|
| Time history of significant wave height for Feb 1953 storm and its manipulations at GBR | HSMAX |
| | |
| Delft University of Technology | Fig. A9 |

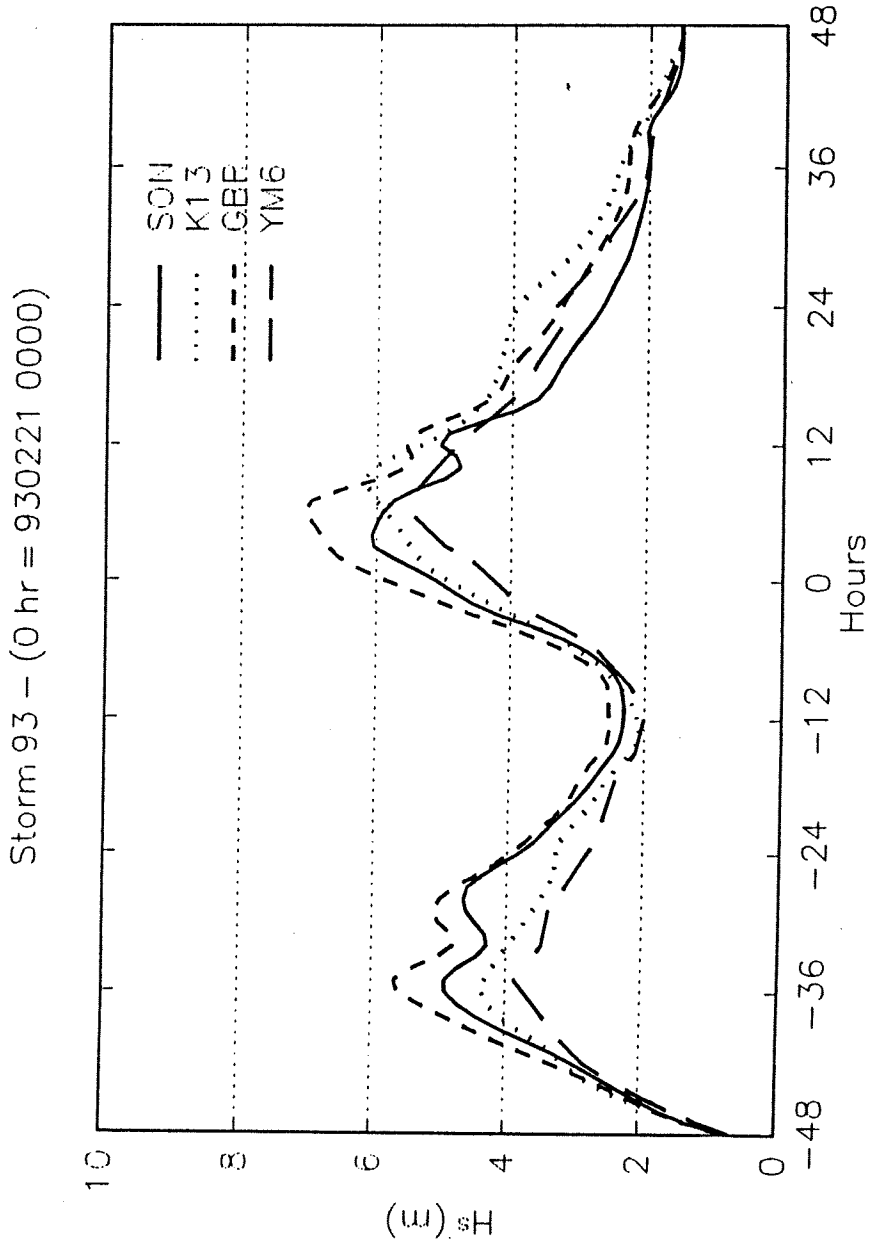


| | |
|---|---|
| Time history of significant wave height for Feb 1993 storm at SON, K13, GBR, and YM6 | HSMAX |
| Delft University of Technology | Fig. A10 |

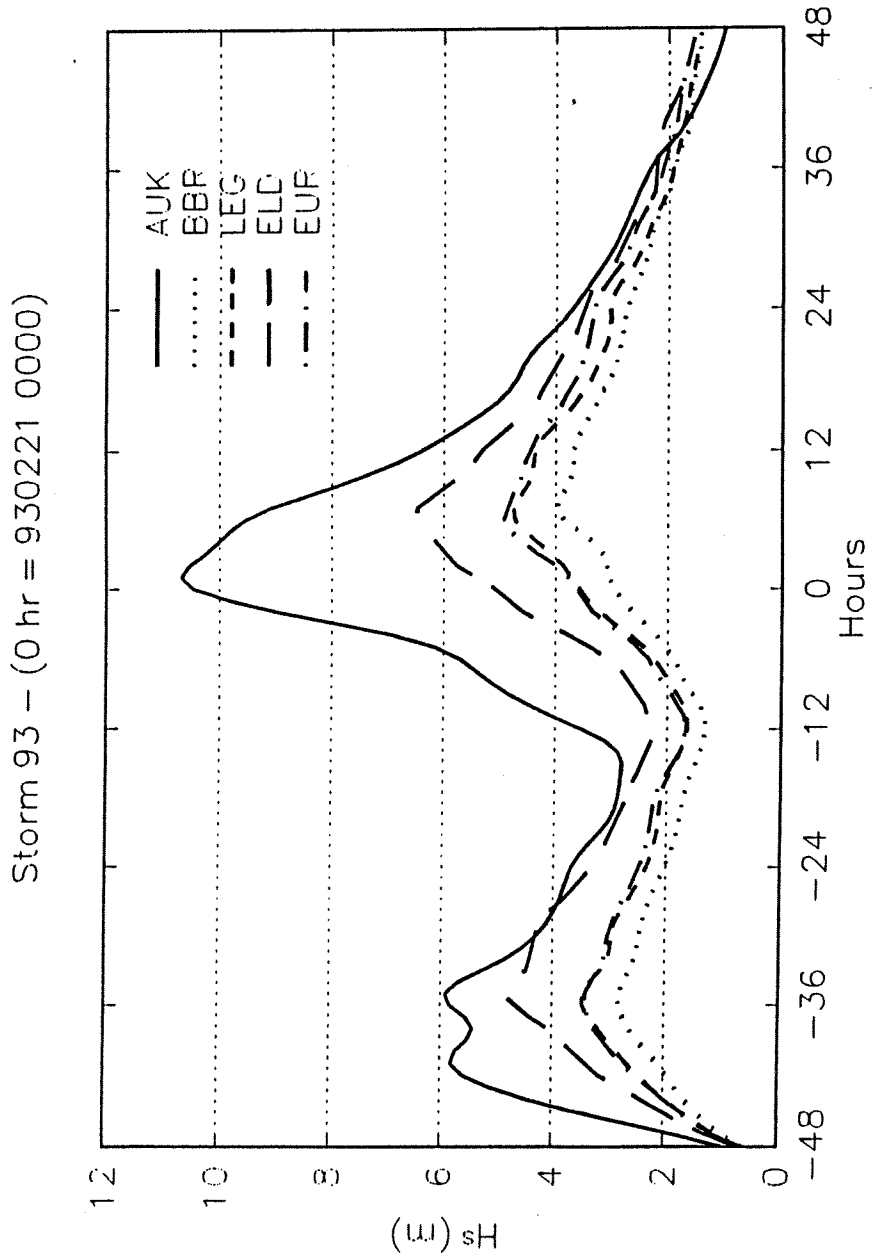


| | |
|---|---|
| Time history of significant wave height for Feb 1993 storm at AUK, BBR, LEG, ELD, and EUR | HSMAX |
| Delft University of Technology | Fig. A11 |

# TABLES

**Table 1**: Geogaphic locations of various stations and their water depths

| station | Latitude (degrees) | Longitude (degrees) | Depth(m) (CZM grid) | Depth(m) (ZUNBOL grid) |
|---|---|---|---|---|
| SON | 53 35 20 | 06 10 10 | 19.3 | 20.0 |
| GBR | 53 36 00 | 05 30 00 | 24.6 | 23.4 |
| ELD | 53 12 03 | 04 35 18 | 26.0 | 25.5 |
| K13 | 53 13 01 | 03 13 12 | 27.6 | 27.5 |
| YM6 | 52 33 00 | 04 04 00 | 22.5 | 21.5 |
| EUR | 51 59 55 | 03 16 35 | 26.9 | 30.6 |
| LEG | 51 55 05 | 03 40 02 | 22.1 | 21.6 |
| BBR | 51 25 00 | 03 00 00 | 19.6 | 17.4 |

**Table 2**: Description of the computational runs to setup the model.

| Run id | ΔX(km) | nf | $f_l$ (Hz) | $f_h$ (Hz) | $\gamma$ | $n\theta$ | $\Delta\theta$( o ) | I.C.(km) | Δt (s) |
|---|---|---|---|---|---|---|---|---|---|
| RREF | 16 | 34 | 0.031 | 0.792 | 1.1 | 24 | 15 | 2000 | 360 |
| RGR8 | 8 | 34 | 0.031 | 0.792 | 1.1 | 24 | 15 | 2000 | 180 |
| RF32 | 16 | 32 | 0.034 | 0.718 | 1.1 | 24 | 15 | 2000 | 360 |
| RT10 | 16 | 34 | 0.031 | 0.792 | 1.1 | 36 | 10 | 2000 | 360 |
| R108 | 16 | 42 | 0.031 | 0.786 | 1.08 | 24 | 15 | 2000 | 360 |
| RNFT | 16 | 34 | 0.031 | 0.792 | 1.1 | 24 | 15 | 16 | 360 |
| RBJO | 16 | 34 | 0.031 | 0.792 | 1.1 | 24 | 15 | 2000 | 360 |

Δx : spatial length step.
nf : number of discrete frequencies.
$f_l$ : lowest discrete frequency.
$f_h$ : highest discrete frequency.
$\gamma$ : parameter of the exponential frequency grid.
$n\theta$ : number of discrete directions.
$\Delta\theta$ : directional resolution.
I.C. : intitial condition expressed as fetch limited JONSWAP based on local wind speed.
Δt : propagation time step

**Table 3** : Wave parameters for run RREF using the standard model in wind speed of 30 m/s from 345° nautical direction.

| station | $H_s$ (m) | $T_m$ (s) | $\theta_m$ (°) |
|---|---|---|---|
| SON | 8.37 | 11.69 | 348.8 |
| ELD | 9.24 | 11.22 | 348.9 |
| K13 | 10.16 | 11.46 | 0.0 |
| YM6 | 8.67 | 10.55 | 352.8 |
| EUR | 8.94 | 10.30 | 352.3 |
| LEG | 8.02 | 9.93 | 348.1 |
| AUK | 17.83 | 15.63 | 352.5 |

**Table 4** : Wave parameters for run RGR8 using the standard model in wind speed of 30 m/s from 345° nautical direction.

| station | $H_s$ (m) | $T_m$ (s) | $\theta_m$ (°) |
|---|---|---|---|
| SON | 8.59 | 11.57 | 349.1 |
| ELD | 9.28 | 11.36 | 348.8 |
| K13 | 10.11 | 11.46 | 1.0 |
| YM6 | 8.61 | 10.51 | 353.8 |
| EUR | 8.99 | 10.29 | 353.3 |
| LEG | 8.12 | 9.91 | 349.8 |
| AUK | 17.57 | 15.43 | 352.5 |

**Table 5** : Wave parameters for run RF32 using the standard model in wind speed of 30 m/s from 345° nautical direction.

| station | $H_s$ (m) | $T_m$ (s) | $\theta_m$ (°) |
|---|---|---|---|
| SON | 8.39 | 11.65 | 349.0 |
| ELD | 9.26 | 11.16 | 348.9 |
| K13 | 10.14 | 11.45 | 359.9 |
| YM6 | 8.67 | 10.54 | 352.9 |
| EUR | 8.94 | 10.27 | 352.4 |
| LEG | 8.03 | 9.87 | 348.3 |
| AUK | 17.72 | 15.50 | 352.6 |

**Table 6** : Wave parameters for run RT10 using the standard model in wind speed of 30 m/s from 345° nautical direction.

| station | $H_s$ (m) | $T_m$ (s) | $\theta_m$ (°) |
|---|---|---|---|
| SON | 8.45 | 11.78 | 348.4 |
| ELD | 9.32 | 11.28 | 348.4 |
| K13 | 10.24 | 11.58 | 359.5 |
| YM6 | 8.72 | 10.63 | 352.3 |
| EUR | 9.00 | 10.41 | 351.4 |
| LEG | 8.11 | 9.98 | 347.1 |
| AUK | 18.00 | 15.73 | 352.2 |

**Table 7** : Wave parameters for run R108 using the standard model in wind speed of 30 m/s from 345° nautical direction.

| station | $H_s$ (m) | $T_m$ (s) | $\theta_m$ (°) |
|---|---|---|---|
| SON | 8.38 | 11.70 | 348.9 |
| ELD | 9.26 | 11.18 | 348.9 |
| K13 | 10.16 | 11.45 | 0.00 |
| YM6 | 8.66 | 10.57 | 352.5 |
| EUR | 8.95 | 10.29 | 352.1 |
| LEG | 8.03 | 9.92 | 347.8 |
| AUK | 17.83 | 15.63 | 352.5 |

**Table 8** : Wave parameters for run RNFT using the standard model in wind speed of 30 m/s from 345° nautical direction.

| station | $H_s$ (m) | $T_m$ (s) | $\theta_m$ (°) |
|---|---|---|---|
| SON | 8.29 | 11.25 | 349.0 |
| ELD | 9.10 | 10.77 | 349.1 |
| K13 | 9.90 | 11.10 | 359.9 |
| YM6 | 8.54 | 10.28 | 353.0 |
| EUR | 8.88 | 10.09 | 352.7 |
| LEG | 7.97 | 9.75 | 348.4 |
| AUK | 15.04 | 13.18 | 354.7 |

**Table 9** : Wave parameters for run RBJO using the standard model in wind speed of 30 m/s from 345° nautical direction.

| station | $H_s$ (m) | $T_m$ (s) | $\theta_m$ (°) |
|---|---|---|---|
| SON | 9.13 | 11.46 | 349.3 |
| ELD | 9.38 | 11.28 | 348.9 |
| K13 | 10.29 | 11.60 | 359.7 |
| YM6 | 8.76 | 10.63 | 353.0 |
| EUR | 8.98 | 10.32 | 352.2 |
| LEG | 8.10 | 9.95 | 348.5 |
| AUK | 17.84 | 15.65 | 352.4 |

**Table 10** : Significant wave height at various locations in 50 m/s wind speed from different directions (Computations with the standard wave model and grid G1).

| Station | 240° | 270° | 300° | 330° | 360° | 30° |
|---|---|---|---|---|---|---|
| SON | 9.01 | 9.47 | 9.85 | 10.11 | 10.35 | 10.15 |
| ELD | 11.65 | 11.75 | 11.85 | 11.95 | 11.80 | 11.61 |
| K13 | 11.91 | 12.02 | 12.22 | 12.43 | 12.31 | 12.30 |
| YM6 | 10.51 | 10.71 | 10.69 | 10.61 | 10.60 | 10.54 |
| EUR | 11.70 | 11.74 | 11.84 | 11.97 | 11.81 | 11.70 |
| LEG | 10.15 | 10.30 | 10.25 | 10.20 | 10.10 | 9.90 |
| BBR | 9.37 | 9.90 | 10.30 | 10.38 | 10.32 | 10.02 |
| GBR | 11.28 | 11.61 | 11.85 | 11.82 | 11.80 | 11.65 |

**Table 11** : Significant wave height at various locations for different wind speed from 330° nautical direction (Computations with the standard wave model and grid G1).

| Station | 20 (m/s) | 30 (m/s) | 40 (m/s) | 50 (m/s) | 60 (m/s) |
|---|---|---|---|---|---|
| SON | 5.62 | 8.52 | 9.64 | 10.11 | 10.32 |
| ELD | 5.91 | 9.42 | 11.11 | 11.95 | 12.31 |
| K13 | 6.20 | 10.11 | 11.78 | 12.43 | 12.83 |
| YM6 | 5.58 | 8.79 | 10.11 | 10.61 | 11.03 |
| EUR | 5.63 | 9.02 | 11.18 | 11.97 | 12.45 |
| LEG | 5.24 | 8.22 | 9.60 | 10.20 | 10.54 |
| BBR | 5.35 | 8.65 | 9.89 | 10.38 | 10.62 |
| GBR | 5.84 | 9.31 | 11.01 | 11.82 | 12.18 |

**Table 12**: Computed significant wave height with different formulations of wave physics at various locations in the extreme uniform wind (computational grid G1).

| station | WW-std | $S_{bot}$ | $S_{inp}$,$S_{ds}$ | $S_{br}$ | WW-max |
|---|---|---|---|---|---|
| SON | 10.11 | 10.95 | 10.89 | 7.51 | 11.19 |
| ELD | 11.95 | 12.81 | 12.54 | 8.54 | 12.86 |
| K13 | 12.43 | 13.15 | 12.92 | 9.09 | 13.18 |
| YM6 | 10.61 | 11.18 | 11.03 | 7.98 | 11.41 |
| EUR | 11.97 | 12.51 | 12.42 | 8.77 | 12.69 |
| LEG | 10.20 | 10.64 | 10.59 | 7.74 | 10.72 |
| BBR | 10.38 | 10.89 | 10.92 | 7.66 | 11.16 |
| GBR | 11.82 | 12.32 | 12.19 | 8.20 | 12.48 |

WW-std : standard settings of WAVEWATCH-II
$S_{bot}$ : Perturbation of bottom friction source term (Madsen et al to JONSWAP)
$S_{inp}$, $S_{ds}$ : Perturbation of wind input and white capping source terms (snyder et al and Komen et al to Janssen)
$S_{br}$ : Perturbation of depth breaking source term (Battjes-Janssen to Roelvink)
WW-max: maximum formulation of wave physics

**Table 13** : Wave parameters in the extreme uniform wind at various locations using the maximum wave model and computational grid G3.

| Station | $H_s$ (m) | $T_{m02}$ (s) | $\theta_m$ (deg.) |
|---|---|---|---|
| SON | 10.49 | 9.43 | 333.1 |
| ELD | 12.50 | 10.33 | 330.3 |
| K13 | 13.16 | 10.46 | 335.5 |
| YM6 | 10.83 | 9.41 | 328.5 |
| EUR | 14.02 | 10.79 | 328.1 |
| LEG | 10.81 | 9.52 | 324.2 |
| BBR | 9.70 | 9.67 | 332.6 |
| GBR | 11.84 | 10.91 | 331.8 |

**Table 14** : Wave parameters in extreme synthetic storm at various locations using the maximum wave model and computational grid G3.

| Station | $H_s$ (m) | $T_{m02}$ (s) | $\theta_m$ (deg.) |
|---|---|---|---|
| SON | 10.41 | 9.46 | 11.9 |
| ELD | 12.19 | 9.93 | 3.1 |
| K13 | 13.05 | 10.27 | 7.8 |
| YM6 | 10.64 | 9.33 | 359.3 |
| EUR | 13.57 | 10.60 | 352.2 |
| LEG | 10.57 | 9.43 | 351.4 |
| BBR | 9.38 | 9.88 | 347.8 |
| GBR | 11.88 | 9.9 | 11.7 |

**Table 15** : Sensitivity of $H_s$ for variation in source term coefficients at various locations in the extreme uniform wind using the maximum wave model and computational grid G1.

| col. | 1 | 2 | 3 | 4 | 5 | 6 | 7 | 8 |
|---|---|---|---|---|---|---|---|---|
| stat. | REF16 | NLI16 | FR16-DN | FR16-UP | INP16-DN | INP16-UP | WC16 | BR16-UP |
| SON | 11.19 | 11.06 | 11.18 | 11.24 | 10.08 | 11.35 | 11.23 | 11.89 |
| ELD | 12.86 | 12.85 | 12.72 | 12.94 | 11.12 | 12.91 | 12.92 | 13.34 |
| K13 | 13.18 | 13.12 | 13.07 | 13.33 | 11.73 | 13.34 | 13.17 | 13.63 |
| YM6 | 11.41 | 11.40 | 11.27 | 11.49 | 10.27 | 11.42 | 11.46 | 11.89 |
| EUR | 12.69 | 12.71 | 12.58 | 12.77 | 11.24 | 12.70 | 12.57 | 13.06 |
| LEG | 10.72 | 10.86 | 10.71 | 10.81 | 9.86 | 10.77 | 10.75 | 11.19 |
| BBR | 11.16 | 11.20 | 11.11 | 11.24 | 9.91 | 11.18 | 11.11 | 11.65 |
| GBR | 12.48 | 12.49 | 12.45 | 12.56 | 11.60 | 12.73 | 12.58 | 13.18 |

REF16 : reference run, maximum wave model with standard coefficients (16 km grid res.)
NLI16 : quadruplet interactions, $\lambda$=0.26 (standard=0.25)
FR16-DN : bottom friction, $\Gamma$=-0.097 (standard=-0.067)
FR16-UP : bottom friction, $\Gamma$=-0.047 (standard=-0.067)
INP16-DN : wind input, $\beta$=0.65 (standard=1.2)
INP16-UP : wind input, $\beta$=1.35 (standard=1.2)
WC16 : white capping , $\alpha$=-1.9 (standard=-2.25)
BR16-UP : depth induced breaking, $\gamma$=0.83 (standard=0.8)

**Table 16** : Sensitivity of $H_s$ for variation in source term coefficients at various locations in the extreme uniform wind using the maximum wave model and computational grid G3.

| station | REF3 | INP3-DN | INP3-UP | INP-BR3-DN | INP-BR3-UP |
|---|---|---|---|---|---|
| SON | 10.49 | 9.87 | 10.41 | 7.46 | 10.92 |
| ELD | 12.50 | 11.38 | 12.45 | 8.88 | 12.86 |
| K13 | 13.16 | 11.99 | 13.07 | 9.27 | 13.52 |
| YM6 | 10.83 | 10.00 | 10.80 | 7.72 | 11.23 |
| EUR | 14.02 | 12.06 | 14.00 | 9.83 | 14.43 |
| LEG | 10.81 | 9.95 | 10.91 | 7.74 | 11.28 |
| BBR | 9.70 | 8.97 | 9.65 | 6.79 | 10.13 |
| GBR | 11.84 | 11.16 | 12.08 | 8.41 | 12.46 |

REF3 : reference run, maximum wave model with standard coefficients (3 km grid res.)
INP3-DN : wind input, $\beta$=0.65 (standard=1.2), 3 km grid resolution
INP3-UP : wind input, $\beta$=1.35 (standard=1.2), 3 km grid resolution
INP-BR3-DN : wind input $\beta$=0.65, breaking coefficient $\gamma$=0.60, 3 km grid resolution
INP-BR3-UP : wind input $\beta$=1.35, breaking coefficient $\gamma$=0.83, 3 km grid resolution

**Table 17** : The uncertainty in the computed significant wave height using the maximum wave model, extreme uniform wind and computational grid G3.

| station | REF3 | DHS-DN | DHS-UP | %DHS-DN | %DHS-UP |
|---|---|---|---|---|---|
| SON | 10.49 | 2.65 | 0.54 | 25.3 | 5.1 |
| ELD | 12.49 | 3.05 | 0.41 | 24.4 | 3.3 |
| K13 | 13.16 | 3.08 | 0.48 | 23.4 | 3.7 |
| YM6 | 10.82 | 2.55 | 0.43 | 23.6 | 4.0 |
| EUR | 14.02 | 2.66 | 0.43 | 19.0 | 3.1 |
| LEG | 10.81 | 2.37 | 0.37 | 21.9 | 3.5 |
| BBR | 9.70 | 2.51 | 0.48 | 25.9 | 5.0 |
| GBR | 11.84 | 2.89 | 0.45 | 24.4 | 3.8 |

**Table 18** : The upper and lower limits of the maximum significant wave height due to uncertainty in the model coefficients.

| station | REF3 | HS-DN | HS-UP | INP-BR3-DN | INP-BR3-UP |
|---|---|---|---|---|---|
| SON | 10.49 | 7.84 | 11.03 | 7.46 | 10.92 |
| ELD | 12.49 | 9.44 | 12.90 | 8.88 | 12.86 |
| K13 | 13.16 | 10.08 | 13.64 | 9.27 | 13.52 |
| YM6 | 10.82 | 8.27 | 11.25 | 7.72 | 11.23 |
| EUR | 14.02 | 11.36 | 14.45 | 9.83 | 14.43 |
| LEG | 10.81 | 8.44 | 11.18 | 7.74 | 11.28 |
| BBR | 9.70 | 7.19 | 10.18 | 6.79 | 10.13 |
| GBR | 11.84 | 8.95 | 12.29 | 8.41 | 12.49 |

REF3 : reference run, maximum wave model with standard coefficients (3 km grid res.)
DHS-DN : $\Delta H_s$ down
DHS-UP : $\Delta H_s$ up
%DHS-DN : percentage of $\Delta H_s$ down w.r.t reference value
%DHS-UP : percentage of $\Delta H_s$ up w.r.t reference value

HS-DN : $H_s$ down
HS-UP : $H_s$ up
INP-BR3-DN : wind input $\beta=0.65$, breaking coefficient $\gamma=0.60$, 3 km grid resolution
INP-BR3-UP : wind input $\beta=1.35$, breaking coefficient $\gamma=0.83$, 3 km grid resolution

**Table 19** : Influence of storm surge level on the computed significant wave height in the extreme synthetic storm using the maximum wave model and computational grid G1.

| station | $H_s$ (5 m SSL) | $H_s$ (6 m SSL) | $\Delta H_s$ | d(CSM) | $H_s/h$ (5 m SSL) | $H_s/h$ (6 m SSL) |
|---|---|---|---|---|---|---|
| SON | 10.08 | 10.40 | 0.32 | 19.3 | 0.415 | 0.411 |
| ELD | 12.26 | 12.69 | 0.43 | 26.0 | 0.396 | 0.397 |
| K13 | 13.32 | 13.55 | 0.23 | 27.6 | 0.409 | 0.403 |
| YM6 | 11.26 | 11.53 | 0.27 | 22.5 | 0.409 | 0.405 |
| EUR | 12.47 | 12.83 | 0.36 | 26.9 | 0.391 | 0.390 |
| LEG | 10.57 | 10.99 | 0.42 | 22.1 | 0.390 | 0.391 |
| BBR | 10.23 | 10.57 | 0.33 | 19.6 | 0.416 | 0.413 |
| GBR | 12.48 | 12.82 | 0.34 | 24.6 | 0.421 | 0.419 |

$H_s$ (+5m) : significant wave height for the case with 5 m extra water level
$H_s$ (+6m) : significant wave height for the case with 6 m extra water level
$\Delta H_s$ : difference in $H_s$ between the computation with 5 and 6 m extra water level.
d (CSM) : water depth measured from 0 NAP from CSM grid
$H_s/h$ : ratio of $H_s$ to total water depth h (= d + water level)

**Table 20** : Comparison between the computed significant wave height by WAVEWATCH-II and HISWA in the extreme uniform wind using computational grid G1 (both models are used with their standard settings).

| station | WW-II | HISWA |
|---|---|---|
| SON | 10.11 | 7.67 |
| ELD | 11.95 | 8.76 |
| K13 | 12.43 | 9.11 |
| YM6 | 10.61 | 7.66 |
| EUR | 11.97 | 8.67 |
| LEG | 10.20 | 7.51 |
| BBR | 10.38 | 7.67 |
| GBR | 11.82 | 9.04 |

**Table 21** : The computed and measured significant wave height in the storm of Dec 1990 at various locations (computations using the credible model).

| station | observations | computations | difference |
|---|---|---|---|
| AUK | 12.20 | 12.47 | -0.27 (2%) |
| SON | 7.70 | 5.60 | +2.10 (26%) |
| ELD | 7.70 | 7.25 | +0.45 (6%) |
| K13 | 7.70 | 7.60 | +0.10 (1%) |
| YM6 | 6.70 | 6.40 | +0.30 (4%) |
| EUR | 6.25 | 6.30 | -0.05 (1%) |
| LEG | 6.00 | 5.42 | +0.58 (10%) |

**Table 22** : Comparison between computed and measured wave parameters in the storm of Dec 1990 at station AUK

| time | result | $H_{mo}$ | $T_{m02}$ | $\theta_o$ | $S_o^*$ | $f_{peak}$ | $\theta_{peak}$ |
|---|---|---|---|---|---|---|---|
| 901212 09 | meas. | 9.71 | 10.0 | 330 | 27 | .08 | 329 |
| | comp | 10.81 | 10.9 | 331.2 | 23.6 | .068 | 334.0 |
| 901212 12 | meas. | 11.08 | 10.9 | 340 | 25 | .06 | 345 |
| | comp. | 12.37 | 11.6 | 336.6 | 23.9 | .065 | 337.0 |
| 901212 15 | meas. | 11.88 | 11.3 | 345 | 26 | .06 | 344 |
| | comp. | 11.51 | 11.59 | 342.6 | 23.7 | .065 | 343.0 |

meas : measurements
comp : computations

* Defined accoding to:
measurements : Kuik et al., 1988
computation : Yamartino, 1984

**Table 23** : Comparison between computed and measured wave parameters in the storm of Dec 1990 at station EUR

| time | result | $H_{mo}$ | $T_{m02}$ | $\theta_o$ | $S_o$ | $f_{peak}$ | $\theta_{peak}$ |
|---|---|---|---|---|---|---|---|
| 901212 18 | meas. | 5.90 | 7.8 | 335 | 33 | .10 | 335 |
| | comp | 5.75 | 7.64 | 330.2 | 24.3 | .094 | 331.0 |
| 901212 21 | meas. | 6.33 | 8.2 | 339 | 36 | .10 | 328 |
| | comp. | 6.29 | 8.2 | 336.9 | 25.0 | .087 | 336.1 |
| 901213 00 | meas. | 5.73 | 8.2 | 346 | 34 | .10 | 347 |
| | comp. | 5.05 | 7.7 | 347.2 | 26.5 | .094 | 343.8 |

**Table 24** : Comparison between computed and measured wave parameters in the storm of Dec 1990 at station K13

| time | result | $H_{mo}$ | $T_{m02}$ | $\theta_o$ | $S_o$ | $f_{peak}$ | $\theta_{peak}$ |
|---|---|---|---|---|---|---|---|
| 901212 15 | meas. | 6.90 | 8.5 | 341 | 28 | .08 | 336 |
| | comp | 6.50 | 8.5 | 336.0 | 27.2 | .081 | 339.9 |
| 901212 18 | meas. | 7.49 | 9.2 | 346 | 31 | .09 | 340 |
| | comp. | 7.50 | 9.4 | 346.3 | 26.8 | .070 | 349.2 |
| 901212 21 | meas. | 7.02 | 9.2 | 351 | 31 | .06 | 348 |
| | comp. | 6.73 | 9.6 | 352.1 | 26.7 | .068 | 357.3 |

meas : measurements
comp : computations

* Defined accoding to:
measurements : Kuik et al., 1988
computation : Yamartino, 1984

**Table 25** : Wave parameters in the extreme uniform wind field at various locations using the maximum calibrated model and computational grid G3.

| station | $H_{m0}$ (m) | $T_{m02}$ (s) | $L_m$ (m) | $\theta_m$ (°) | $S_o$ (°) | $f_p$ (Hz) | $\theta_p$ (°) |
|---|---|---|---|---|---|---|---|
| SON | 10.58 | 9.89 | 184.1 | 333.1 | 22.9 | 0.048 | 334.4 |
| ELD | 12.64 | 10.43 | 208.1 | 330.4 | 24.5 | 0.048 | 335.2 |
| K13 | 13.29 | 10.82 | 223.0 | 336.3 | 27.5 | 0.047 | 343.4 |
| YM6 | 10.99 | 9.47 | 169.3 | 328.6 | 26.2 | 0.072 | 327.1 |
| EUR | 14.22 | 10.94 | 221.8 | 328.0 | 23.7 | 0.064 | 327.5 |
| LEG | 10.88 | 9.62 | 173.6 | 324.0 | 24.4 | 0.066 | 321.3 |
| BBR | 9.71 | 9.78 | 166.4 | 332.7 | 21.5 | 0.065 | 334.7 |
| GBR | 11.92 | 11.22 | 227.5 | 331.9 | 21.6 | 0.048 | 332.3 |